NOVEL METHODS FOR MICELLAR ELECTROKINETIC CHROMATOGRAPHY AND PRECONCENTRATION ON TRADITIONAL MICROFLUIDIC DEVICES AND THE FABRICATION AND CHARACTERIZATION OF PAPER MICROFLUIDIC DEVICES

by

KURT W. HOEMAN

B.S., Truman State University, 2003.

AN ABSTRACT OF A DISSERTATION

submitted in partial fulfillment of the requirements for the degree

DOCTOR OF PHILOSOPHY

Department of Chemistry
College of Arts and Sciences

KANSAS STATE UNIVERSITY
Manhattan, Kansas

2009

Abstract

Chemical separations are a necessary component in many scientific analyses. Microfluidics, the use of micron-sized fluidic channels defined in glass or polymer blends, is a powerful branch of separation science that is developing rapidly. Miniaturized analytical devices offer important advantages compared to traditional bench-top techniques, most notably capillary electrophoresis (CE).

This dissertation was focused on developing several novel methods to improve microfluidic based separations and techniques. The electrophoretic separation of small similarly charged analytes can be very difficult. Chapter 2 discusses a new buffer that has been developed for fast, high efficiency separations of amino acids by micellar electrokinetic chromatography (MEKC). This buffer is more environmentally friendly than the most commonly used surfactant containing buffers for MEKC separations. It uses a commercially available dish washing soap by Seventh Generation™ Inc. that contains three micelle forming agents; sodium lauryl ether sulfate (anionic), cocamidopropyl betaine (zwitterionic), and cocamide monoethanolamine (MEA) (non-ionic), and is completely void of organic solvents.

Many biological samples contain analytes below the limit of detection of traditional detection systems; therefore, chapter 3 reports the fabrication of nanoporous membranes on microfluidic devices that are capable of analyte concentration enrichment. Donnan exclusion is responsible for the preconcentration of fluorescent dyes near a

charged, porous titania membrane. The level of analyte enrichment was monitored, and enrichment factors greater than 4000 in 400 s were obtained for 2,7-Dichlorofluorescein.

Chapter 4 describes the fabrication and characterization of paper based microfluidic devices. Mixtures of acrylate modified photocurable polymers were used to photolithographically define channels on multiple paper substrates. Flow characteristics are described and their use for monitoring complications associated with type 1 diabetes is demonstrated. Finally in Chapter 5, Sol-gel modified gold surfaces for preventing protein adsorption during surface plasmon resonance (SPR) detection are also presented.

NOVEL METHODS FOR MICELLAR ELECTROKINETIC CHROMATOGRAPHY AND PRECONCENTRATION ON TRADITIONAL MICROFLUIDIC DEVICES AND THE FABRICATION AND CHARACTERIZATION OF PAPER MICROFLUIDIC DEVICES

by

KURT W. HOEMAN

B.S., Truman State University, 2003.

A DISSERTATION

submitted in partial fulfillment of the requirements for the degree

DOCTOR OF PHILOSOPHY

Department of Chemistry
College of Arts and Sciences

KANSAS STATE UNIVERSITY
Manhattan, Kansas

2009

Approved by:

Major Professor
Christopher T. Culbertson

Copyright

KURT W. HOEMAN

2009

Abstract

Chemical separations are a necessary component in many scientific analyses. Microfluidics, the use of micron-sized fluidic channels defined in glass or polymer blends, is a powerful branch of separation science that is developing rapidly. Miniaturized analytical devices offer important advantages compared to traditional bench-top techniques, most notably capillary electrophoresis (CE).

This dissertation was focused on developing several novel methods to improve microfluidic based separations and techniques. The electrophoretic separation of small similarly charged analytes can be very difficult. Chapter 2 discusses a new buffer that has been developed for fast, high efficiency separations of amino acids by micellar electrokinetic chromatography (MEKC). This buffer is more environmentally friendly than the most commonly used surfactant containing buffers for MEKC separations. It uses a commercially available dish washing soap by Seventh Generation™ Inc. that contains three micelle forming agents; sodium lauryl ether sulfate (anionic), cocamidopropyl betaine (zwitterionic), and cocamide monoethanolamine (MEA) (non-ionic), and is completely void of organic solvents.

Many biological samples contain analytes below the limit of detection of traditional detection systems; therefore, chapter 3 reports the fabrication of nanoporous membranes on microfluidic devices that are capable of analyte concentration enrichment. Donnan exclusion is responsible for the preconcentration of fluorescent dyes near a

charged, porous titania membrane. The level of analyte enrichment was monitored, and enrichment factors greater than 4000 in 400 s were obtained for 2,7-Dichlorofluorescein.

Chapter 4 describes the fabrication and characterization of paper based microfluidic devices. Mixtures of acrylate modified photocurable polymers were used to photolithographically define channels on multiple paper substrates. Flow characteristics are described and their use for monitoring complications associated with type 1 diabetes is demonstrated. Finally in Chapter 5, Sol-gel modified gold surfaces for preventing protein adsorption during surface plasmon resonance (SPR) detection are also presented.

Table of Contents

List of Figures

List of Tables

Acknowledgements

I would like to take this opportunity to thank everyone who helped me in the completion of my graduate degree. Everyone's help and encouragement made this goal attainable.

Chris, thank you for all the help and knowledge you passed along throughout the years. I really enjoyed being a part of your research group and learning much more than just chemistry during my time in your group.

The Culbertson Group…. Wow, the times we've had, I have enjoyed working with all of you. I am a firm believer that "a happy workplace is a safe and productive work place." Thanks for making my time here enjoyable but also generating an environment for success.

My friends, Scott, Karch, Nate, Jeff, Tom and Alex…. We've had some good times; graduate school would have been very different without all of you.

To the faculty and staff of the chemistry department, thanks for your time and friendship. Especially, the chemistry department support staff; Jim Hodgson, Tobe Eggers, Ron Jackson, Richard Bachamp, thanks for helping create and design the necessary tools for my research, and for fixing them when I broke them. The office staff; Donna Wright, Connie Cusimano, and Kim Ross, you helped me more than you know during my time here.

I would also like to thank my committee members, Dr. Daniel Higgins, Dr. Stefan Bossmann, Dr. Mary Rezac, and Dr. Kevin Lease.

Finally, I would like to thank my family. To my parents, Mom, Dad and Sally, thanks for pushing me and always believing in me. You have taught me many life lessons that help me every day. Thanks for everything you do to make me a better person. To my siblings, Brent, Erin, Maureen, and Leah, thanks for showing interest in what I have been doing here at KSU, even though we all know it was just to humor me. To my wife Kate and your family, thanks for being such an important part of my life.

Dedication

To Kate: thank you for your love, support, and sacrifices

CHAPTER 1 - **Introduction**

1.1 Chemical Separations

The ability to separate mixtures of analytes into their principle components, detect and quantify them is critically important for a wide variety of scientific disciplines. There are many different separation methods available today, including high performance liquid chromatography (HPLC), capillary electrophoresis (CE), field flow fractionation (FFF), and gas chromatography (GC). Each of these methods has its own advantages and limitations. In this dissertation I will report results from research that sought to 1) improve the selectivity of electrokinetic based separations, 2) increase analyte concentration prior to separation, and 3) develop paper microfluidic devices that might prove useful for performing very low cost analysis in resource poor situations. In this introductory chapter the mechanisms that underlie these separation and fluidic transport methods will be discussed.

Chapter 2 will discuss the development of a new method to increase the resolving power and selectivity of an already developed separation technique. After a separation, a method of detection is required with the ability to quantitate each analyte independently. There are many well developed detection mechanisms; however, there are many samples that cannot be detected because their concentrations are below the limit of detection (LOD). Chapter 3 will discuss a novel method for sample preconcentration. Capillary Electrophoresis (CE) is one of many methods for separating analytes from a mixture and can easily be coupled with many different detectors for analysis, such as laser induced fluorescence (LIF), mass spectrometry, UV-Visible absorption, conductivity, and

refractive index. CE is one of the youngest separation mechanisms, still being optimized today. This separation technique is widely used because it requires very small sample sizes, as small as a single mammalian cell, and also consumes drastically reduced reagent volumes. Previously developed separation techniques, i.e. chromatography, relied on the use of a mobile phase and a stationary phase. The mobile phase is typically an aqueous unbuffered solution or an aqueous/organic mixture. The stationary phase can come in many forms, from a thin silica layer on glass to a tube packed with small, potentially porous particles. The analytes being separated interact with each phase and depending upon their relative interaction times with each phase, the analytes are separated. CE differs from other commonly used separation mechanisms in that it typically employs the use of an open unpacked tube and a chemically buffered mobile phase and is limited to separation of ions. As such, modifications to CE have been made to allow the separation of neutral compounds. Some of these modifications to traditional CE use pseudo-stationary phases, such as micellar electrokinetic chromatography (MEKC) and microemulsion electrokinetic chromatography. However, capillary electrochromatography employs a traditional stationary phase. These methods separate analytes based on their hydrophobicities. There are also methods that use discontinuous buffer systems such as capillary isoelectric focusing and capillary isotachophoresis, but the original use, capillary zone electrophoresis (CZE), employs no stationary phase and separates the analytes exclusively by their respective electrophoretic mobilities induced by an electric field in a background electrolyte solution (BGE). All of the separation techniques listed above have similar separation mechanisms but are all extensions of CZE.[1-5]

1.1.1 Capillary Electrophoresis

1.1.1.1 Electrophoretic Mobility

When an electric field is applied axially along an aqueous capillary channel, ions migrate at a velocity proportional to the field strength. This electrostatic force can be represented by the following equation where F is the force, q is the charge on the ion, and E is the applied field strength.

(1.1) $$F = qE$$

The field strength is defined as:

(1.2) $$E = \frac{V}{L}$$

where V is the applied voltage and L is the length of the capillary. This force is countered by the viscous forces that are inherent in the electrolyte solution. Stoke's law gives the viscous force felt by a spherical particle as:

(1.3) $$F = 6\pi\eta r \upsilon_{ep}$$

where η is the solution viscosity, r is particle radius and υ_{ep} is the electrophoretic velocity of the particle. These two forces reach a steady state quickly after the voltage is applied. Equations 1.4 and 1.5 can be combined and solved to give the electrophoretic velocity of a charged particle relative to the solution velocity:

(1.4) $$\upsilon_{ep} = \frac{qE}{6\pi\eta r}$$

An electrophoretic mobility (μ_{ep}) is further defined as:

(1.5) $$\mu_{ep} = \frac{\upsilon_{ep}}{E} = \frac{q}{6\pi\eta r}$$

From the electrophoretic mobility we can see that the charge and the size of an analyte are the major factors in defining electrophoretic mobility, and for analytes of similar sizes their mobilities are greatly dependant on their relative charges. Therefore, analytes are separated by their effective charge to size ratios. The actual velocity and mobility of a particle is also affected by an additional attribute, the electroosmotic mobility (μ_{eo}) and velocity (υ_{eo}), coming from the movement of the bulk fluid in the channel, i.e. electroosmotic flow (EOF).[1, 2, 4-6]

1.1.1.2 Electroosmotic Flow

EOF is a phenomenon that arises in capillary channels filled with an electrolyte solution where upon the application of a voltage along the length of the channel bulk fluid movement is generated. This fluid flow is generated in glass devices because the surfaces of these devices are negatively charged above a pH of 3 due to the ionized silanol groups on the glass surface. These negative charges attract solvated cations (counterions) creating an electric double layer (EDL). The EDL can be broken down into three components according to the Gouy-Chapman model. Directly adjacent to the wall is an adsorbed layer of cations. An imaginary plane through the center of these adsorbed cations is called the inner Helmholtz plane. Beyond the inner Helmholtz plane is the Stern layer, which is the region between the inner and outer Helmholtz planes, a region comprised of a higher concentration of solvated counterions. Finally, there exists the diffuse layer. The diffuse layer decays rapidly towards the bulk solution where electroneutrality laws are again observed. In the diffuse layer an imaginary plane, the slip plane, separates the mobile ions in solution from the immobile ions near the surface.

There is an electrical potential at this boundary, called the zeta potential (ζ). A Gouy-Chapman model of the EDL is shown in Figure 1.1.

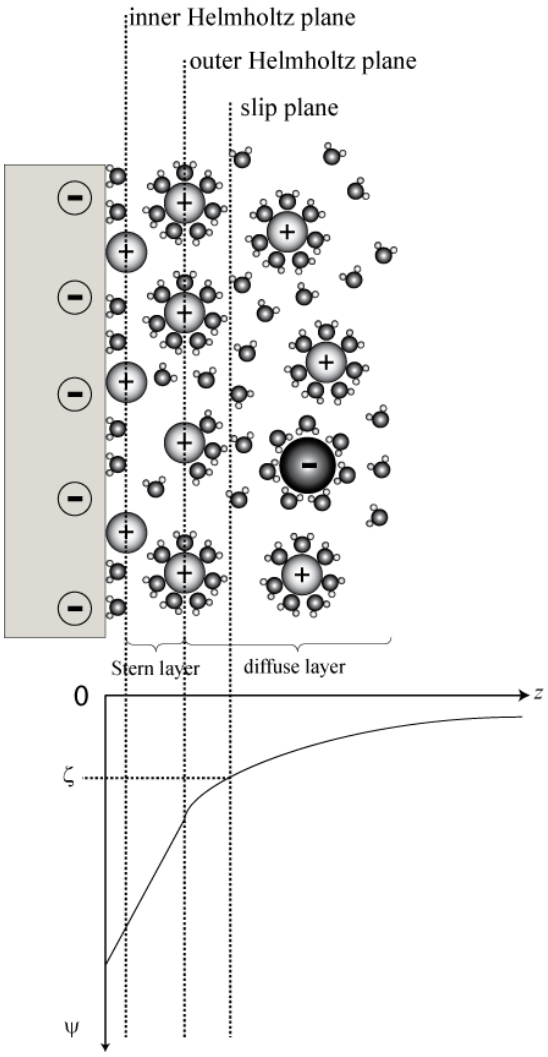

Figure 1.1 - Gouy-Chapman model of the EDL, where ψ is the electrical potential due to the surface charge density

Generally the thickness of the diffuse layer for typical buffer concentrations is between 1 and 100 nm. This thickness is not important for typical microfluidic applications as the EDL thickness is much smaller than the minimum channel dimension. However, as channel dimensions approach the EDL, thickness does play a role, i.e. nanochannels. The thickness of the diffuse layer, also known as the Debye length (λ_D) at 25 ^{o}C is:

(1.6) $$\lambda_D = \frac{3.04 \times 10^{-10}}{z_i \sqrt{c_i}} = \frac{2.15 \times 10^{-10}}{\sqrt{I_s}}$$

where z_i is the valency of the ion, c_i is the electrolyte concentration and I_s is the ionic strength.

(1.7) $$I_s = \frac{1}{2} \sum c_i z_i^2$$

The effect of λ_D will be discussed later in this chapter.[7]

When a voltage is applied axially to the surface of the channels there is bulk fluid movement. For the purposes herein, the surfaces of the channels are negatively charged and after the application of a positive voltage, the excess cations in the diffuse layer will migrate towards the anode. Bulk fluid movement occurs due to the viscous drag created by these cations. There is no movement at the surface, but the velocity increases rapidly in the diffuse part of the double layer and remains constant across the majority of the channel width, giving a flat flow profile. This flow profile is one of the major advantages of CE compared to other separation mechanisms, as it helps reduce band broadening. The Smoluchowski equation describes the electroosmotic velocity of the bulk liquid:

(1.8) $$\upsilon_{eo} = -\frac{\varepsilon_0 k \varsigma}{\eta} E = \mu_{eo} E$$

where ε_0 is the permittivity of free space, k is the dielectric constant, and μ_{eo} is the electroosmotic mobility. Therefore, the total (electrokinetic) velocity or mobility of an analyte is given by:

(1.9) $$\upsilon_{ek} = (\mu_{eo} + \mu_{ep}) E$$

An advantage of CE is that $\upsilon_{eo} > \upsilon_{ep\ anion}$, therefore, all analytes have an overall migration towards the cathode and detector.

In CE, in order to separate analytes from one another they must be charged. All neutral analytes move with the EOF and are detected at the same time. CZE is employed in Chapter 2 for the separation of amino acids. These analytes are negatively charged and have negative mobilities. Many amino acids have similar charges and similar sizes, and so from equation 1.5, should have similar electrophoretic mobilities. This is a common problem with CZE and so a second orthogonal separation mechanism such as hydrophobicity must be employed to completely separate the analytes, as will be discussed further below.[1, 2, 4-6]

Another major advantage of CE deals with the flow of fluid through the capillary or microfluidic channel. In other separation methods where fluid transport is accomplished with pressure driven flow, there exists a parabolic flow profile. This originates from the viscous drag forces that are higher at the fluid channel interface. This parabolic flow profile leads to higher solution velocities at the center of the channel, leading to the broadening of analyte bands thus decreasing the efficiency of the separation. Electroosmotic flow profiles on the other hand have a relatively flat flow profile. The flow profile decreases rapidly from the slip plane towards the surface which is proportional to the electrical potential as shown in Figure 1.1. A comparison of the flow profiles is shown in Figure 1.2.

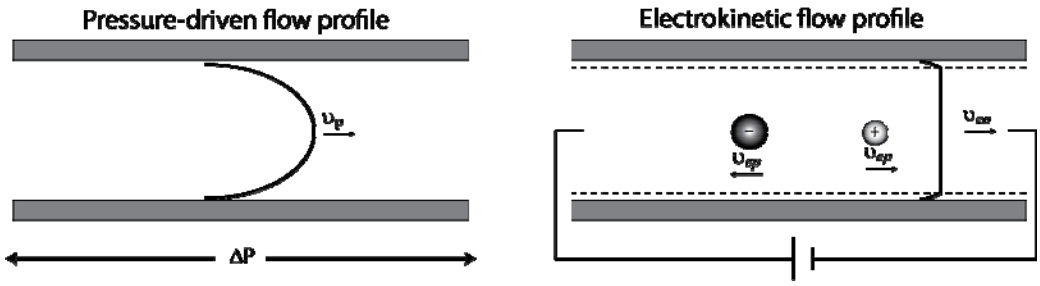

Figure 1.2 - Velocity profiles for pressure-driven and electrokinetic flow through a capillary or microfluidic channel

1.1.2 Separation Parameters

There exists a set of analytical parameters that allow separations to be qualified as "good" or "bad". The most important of these parameters is the efficiency (number of theoretical plates, N), which is directly related to the plate height (H). In CE, most of the band broadening mechanisms are stochastic in nature and so a peak can be represented as a Gaussian distribution. For a Gaussian peak, σ, is the standard deviation of the peak and σ^2 is referred to as the peak variance. A sample chromatogram, Figure 1.3, shows the common analytical parameters used to describe a peak.

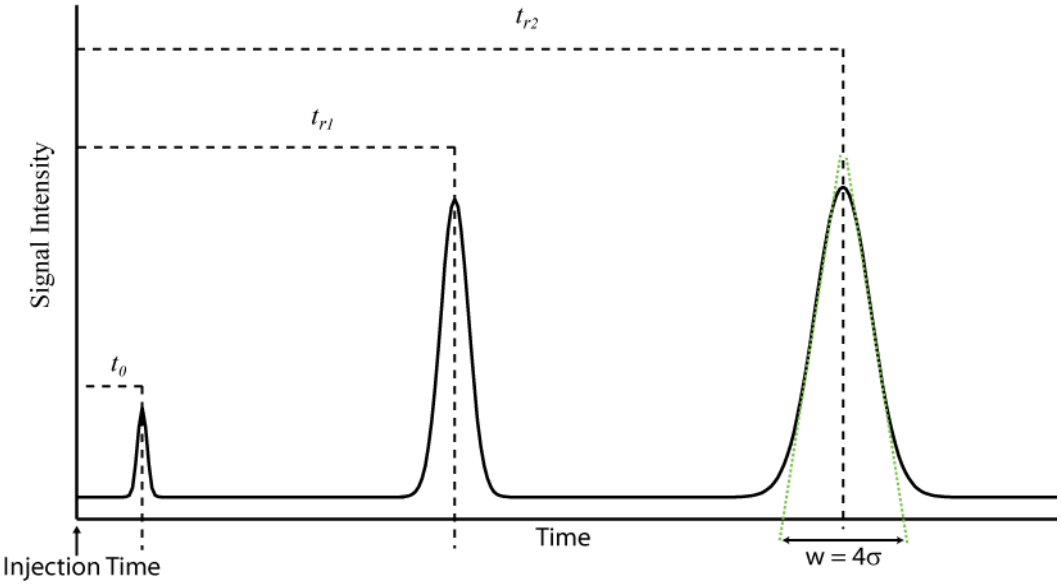

Figure 1.3 - Sample chromatogram displaying common analytical parameters.

The variance is defined as:

$$\sigma^2 = 2Dt \tag{1.10}$$

where D is the diffusion coefficient of the analyte and t is time. The peak standard deviation approximately one fourth of the peak width at the base and this along with the separation distance (l) can be used to calculate the efficiency of the separation.

$$N = \left(\frac{l}{\sigma}\right)^2 \tag{1.11}$$

Separation efficiency can be directly related to the plate height:

$$H = \frac{l}{N}. \tag{1.12}$$

Since separation efficiency is used to quantify the quality of the separation we can see from equation 1.10 that the easiest way to increase separation efficiency is to decrease the peak variance. There are many factors that lead to increasing the variance such as diffusion, detection, adsorption, temperature (Joule heating), detection, injection, and electrodispersion. The total variance (σ_t^2) can be defined as the sum of the contributions from each individual factor.

$$\sigma_{\text{total}}^2 = \sigma_{\text{diff}}^2 + \sigma_{\text{inj}}^2 + \sigma_{\text{det}}^2 + \sigma_{\text{flow}}^2 + \sigma_{\text{Joule}}^2 + \sigma_{\text{edisp}}^2 + \sigma_{\text{ads}}^2 \tag{1.13}$$

Therefore, if they can be decreased or eliminated the separation efficiency is increased. Most of these factors can be easily eliminated or drastically reduced depending on experimental setup. Contribution from electrodispersion is eliminated by using a constant ionic strength buffer. Injection variance for a gated injection, the injection used in this work, is defined as

$$\sigma_{\text{inj}}^2 = \frac{l_{inj}^2}{12} \tag{1.14}$$

Injection variance is a function of injection plug length. Decreasing the plug size decreases the associated variance. For laser-induced fluorescence detection the variance is defined as spatial filter size divided by the collection objective magnification. Since the spatial filter in the optical set-up defines the detection spot size, the same top hat equation for injection can be used here. For LIF with proper filters and optics this is insignificant and can be ignored. Variance with respect to fluid flow rises with the occurrence of parabolic flow profiles, typically generated from pressure difference, defined in equation 1.15 for a rectangular microfluidic channel.

$$\sigma_{\text{flow}}^2 = 4\frac{(\Delta P)^2 d^6}{105 D \eta^2 L^2}\left[\frac{1}{12} - \frac{16d}{\pi^5 w}\tanh\left(\frac{\pi w}{2d}\right)\right]^2 t \tag{1.15}$$

Where d and w are the channel depth and width, and $\Delta P/L$ is the pressure drop along the channel. Electrokinetic transport with appropriate field strengths has flat flow profiles as shown in figure 1.2. Parabolic flow profiles can also be generated from Joule heating or pressure differentials across the channels. Pressure differentials can be eliminated by keeping fluid reservoir levels the same to prevent hydrodynamic flow and Joule heating only occurs at extremely high field strengths. With the proper detection setup, buffer, field strength, and fluidic reservoir heights; all of the terms in equation 1.13 can be drastically reduced or ignored except for diffusion, so a high efficiency separation is said to be diffusion limited.

It is important to reduce all of the contributions to dispersion; however, it is most important to fully resolve the peaks. Resolution (R_s) is the measure of how well two peaks are separated from one another. It is defined as:

$$R_s = \frac{2(t_2 - t_1)}{(w_1 + w_2)} = \frac{\Delta t}{4\sigma} \tag{1.16}$$

where (t) is the peak time and (w) is the peak width. It can be further related to the efficiency of the separation by:

$$R_s = \frac{\sqrt{N}}{4}\frac{\Delta\mu}{\overline{\mu}} \tag{1.17}$$

where $\Delta\mu$ is the difference between the mobilities of the neighboring analytes and $\overline{\mu}$ is the mean of the mobilities. Generally a resolution of 1.5 is desired as this indicates the peaks are base line resolved.[1, 2, 4-6]

1.1.3 Micellar Electrokinetic Chromatography

MEKC is a powerful technique for separating uncharged analytes and/or analytes with similar electrophoretic mobilities. Micelle forming agents are added to the BGE above their critical micelle concentration (cmc). Micelles are molecules with charged hydrophilic head groups and hydrophobic "tails". When in aqueous solution above the cmc, they form spherical colloids with the head groups on the outside of the sphere and the tails extending inwards towards the core of the micelle. These micelles act as a pseudo-stationary phase and interact with the analytes during the separation. The micelles have their own electrophoretic mobility based on their charge and size. Typically anionic surfactants are used because their electrophoretic mobilities are in the opposite direction of the electroosmotic flow. In the experiments in Chapter 2 both anionic surfactants are used as well as mixed surfactant systems with anionic, cationic and zwitterionic surfactants. The mixed micelle system is predominated by an anionic component and, therefore, should have an overall negative electrophoretic mobility. Micelles increase the resolving power by adding a second separation mechanism that increases the selectivity of the buffer solution. As the analytes travel towards the detector

they partition into and out of the micelles at different rates. Since the micelles are moving slower than the bulk fluid flow the amount of time that the analyte spends in the micelle will increase the time it takes for the analyte to reach the detector. Analytes with similar electrophoretic mobilities will interact differently with the micelles depending on their hydrophobicities and each analyte will have its own partition coefficient K:

$$K = \frac{c_{PS}}{c_M} \tag{1.18}$$

where c_{PS} is the molar concentration of analyte in the pseudo-stationary phase and c_M is the concentration in the mobile phase. The partition coefficient can also be used to define the retention factor (k') of an analyte, which is a ratio of the amount of time the analyte spends in the stationary phase compared to the mobile phase:

$$k' = K\left(\frac{V_s}{V_M}\right) = \left(\frac{(t_r - t_0)}{t_0\left(1 - \frac{t_r}{t_m}\right)}\right) \tag{1.19}$$

where V_S, V_M, t_r, t_0, and t_m, are the volume of the stationary, mobile phase, retention times of an analyte, unretained analyte (rate of EOF), and the micelles, respectively. A ratio of the retention factor for multiple analytes in a separation is the separation selectivity (α) is defined as:

$$\alpha = \frac{K_B}{K_A} = \frac{k'_B}{k'_A} = \frac{(t_r)_B - t_M}{(t_r)_A - t_M} \tag{1.20}$$

The selectivity is always defined such that $\alpha > 1$.

Resolution of analytes in a CE separation have already been discussed in this chapter, however, there are additional contributions to resolution when considering

MEKC. Resolution for typical CZE separations is defined in equation 1.16 and 1.17, resolution for chromatography with traditional mobile and stationary phase is defined as:

$$R_s = \frac{\sqrt{N}}{4}\left(\frac{\alpha - 1}{\alpha}\right)\left(\frac{k'_B}{1 + k'_B}\right) \tag{1.21}$$

However, for MEKC there is an additional term. For MEKC of neutral analytes there is a specific time window where all peaks will elute. This window is defined as the time between t_0 and t_M, i.e. for neutral analytes with no electrophoretic mobility, they cannot elute before the dead time and analytes that do not interact with micelles will have a velocity equal to the υ_{eo}, and completely retained analytes will have velocity equal to the velocity of the micelle (υ_{mc}). Because of this extra consideration the resolution for MEKC can be defined as:

$$R_s = \frac{\sqrt{N}}{4}\left(\frac{\alpha - 1}{\alpha}\right)\left(\frac{k'_B}{1 + k'_B}\right)\left(\frac{1 - \frac{t_0}{t_M}}{1 + \left(\frac{t_0}{t_M}\right)k'_A}\right) \tag{1.22}$$

The additional term at the end results from the limited elution window. In order to increase the elution window and also increase the peak capacity of a separation it is common to add organic solvents. These solvents will alter the partition coefficient by changing the hydrophobicity of the mobile phase. These solvents also suppress EOF which increases the separation time, but also increases the interaction between the analytes and micelles, which can increase the resolving power of the buffer.[1, 2, 4-6]

1.2 Preconcentration and Double Layer Overlap

Electrokinetic transport has already been described in this chapter; however, all of the previous theory and discussion included one major assumption, that the Debye length (λ_D) is much less than the smallest channel/pore dimension (h). If $h/\lambda_D < 5$ or even closer to 1, the previous rules of fluid transport no longer apply. When $h/\lambda_D < 5$ ion transport through these small channels is dominated by an electrochemical equilibrium, Donnan equilibrium. This equilibrium theory has been developed to explain the electrochemical equilibrium that exists when charge selective nanochannels or nanopores are in contact with a bulk electrolyte solution. The phenomenon occurs when localized ionic concentrations change to compensate for the electrochemical potential difference between two regions separated by a charge selective membrane. These rules do follow some assumptions as well; however, these fit our application explained in Chapter 3. Here a microchannel and nanoporous membrane fit the criteria, because the limiting dimensions of the microfluidic channel are much greater than the porous membrane. For this explanation, the microfluidic channel will be treated as a bulk solution. In a nanoporous membrane that is negatively charged, the EDL theory remains appropriate to the extent that an adsorbed layer and Stern layer exist, however, the diffuse layers from opposing sides can either overlap or come in close proximity to one another. The electrochemical equilibrium associated with Donnan equilibrium is a result of the difference in electrochemical potential inside the nanopore versus the bulk solution outside. This potential change is compensated by differences in ionic concentrations. The electrochemical potential ($\widetilde{\widetilde{\mu}}_i$) of an ion at constant temperature and pressure can be defined as:

$$\tilde{\tilde{\mu}}_i = \tilde{\mu}_i + z_i F\psi = \tilde{\mu}_i^0 + RT\ln\left(\gamma_a \frac{c_i}{c^0}\right) + z_i F\psi \tag{1.23}$$

where $\tilde{\mu}_i$ is the chemical potential, F is the Faraday constant, ψ is the electric potential due to the surface charge, $\tilde{\mu}_i^0$ is the standard chemical potential of ion i at constant temperature and pressure, R is the gas constant, T is the temperature, γ_a is the activity coefficient, and c^0 is the standard molarity of 1 M. In the nanopore, the wall is negatively charged; therefore, there is higher concentration of free cations than anions due to the charge on the walls of the pore. The electrochemical potential of these cations are equal inside (II) the nanopores and in the bulk (I) solution, and can be described by the following equation:

$$RT\ln(c_i^{\mathrm{I}}/c^0) + z_i F\Phi^{\mathrm{I}} = RT\ln(c_i^{\mathrm{II}}/c^0) + z_i F\Phi^{\mathrm{II}} \tag{1.24}$$

where Φ represents the electric potential. The Donnan potential (Φ_D) is the electric potential difference between the two sides, i.e. $\Phi_D = \Phi^{\mathrm{II}} - \Phi^{\mathrm{I}}$:

$$\Phi_D = \frac{RT}{z_i F}\ln\left(\frac{c_i^{\mathrm{I}}}{c_i^{\mathrm{II}}}\right) \tag{1.25}$$

which results in the Donnan ratio (r_D) of cations and anions:

$$r_D = \left(\frac{c_i^{\mathrm{I}}}{c_i^{\mathrm{II}}}\right)^{1/z_i} = \frac{c_{\mathrm{ca}}^{\mathrm{I}}}{c_{\mathrm{ca}}^{\mathrm{II}}} = \frac{c_{\mathrm{an}}^{\mathrm{II}}}{c_{\mathrm{an}}^{\mathrm{I}}} \tag{1.26}$$

with a valency of 1 and -1, respectively. The Donnan ratio shows that a negatively charged nanopore adjacent to a bulk electrolyte will result in a cation selective pore which excludes anions. This interaction is called the exclusion-enrichment effect (EEE). The EEE can be explained by considering the anionic permeability of the pore as the Debye length increases. When $\lambda_D << h$ the ionic flux (φ^*) is proportional to the

geometric cross section (S^*) of the channel. When the Debye length becomes similar to the effective pore height the new effective flux (φ_{eff}) is proportional to the effective geometric cross section (S_{eff}), which for the case of $h/\lambda_D = 5$ or less, is drastically reduced effectively excluding anions from the pore. The ion flux is proportional to the concentration of ions along the longitudinal axis (x) of the pore, so the exclusion-enrichment coefficient (β) can be define as:

$$\beta = \frac{c_{\text{eff}}(x)}{c^*(x)} = \frac{P_{\text{eff}}}{P^*} \tag{1.27}$$

where P is the permeability of the ions. Coefficients less than 1 would indicate exclusion of anions from a negatively charged pore. All of the above theory is derived under the assumption of no external field, where all of the fluidic movement is based on diffusion.[7, 8]

Upon application of an external field electrokinetic transport occurs along with diffusion. However, the transport of ions through nanopores can create large forces and large irregularities in fluidic movement at the junction creating complex flow circulations. Analyte concentration enrichment does occur, as seen in Chapter 3, but the current electrokinetic theory cannot completely explain the mechanics at the junction. When the external field is applied the concentration enrichment does occur due to the generation of concentration gradients of ionic species adjacent to the ion selective membrane. On the anodic side of the porous region an anodic diffusion boundary layer (DBL) develops. This DBL has lower ionic concentration levels when compared to the bulk solution, and the anions move away from this region. In order to observe electroneutrality the surrounding cations not transported through the membrane also vacate the DBL creating a charge depletion zone. Since the anions cannot traverse the

membrane they will begin to increase in concentration on the anodic side of the membrane at the anodic border of the DBL. Conversely, on the cathodic side of the membrane, an additional DBL will develop due to the increase of cations that are transported through the membrane and in order to obey electroneutrality there will be an increase in the local ionic concentration. These regions of ionic depletion and enrichment are called concentration polarization zones. Figure 1.4 demonstrates the effect of concentration at both the anodic and cathodic side of a membrane with an applied external field.

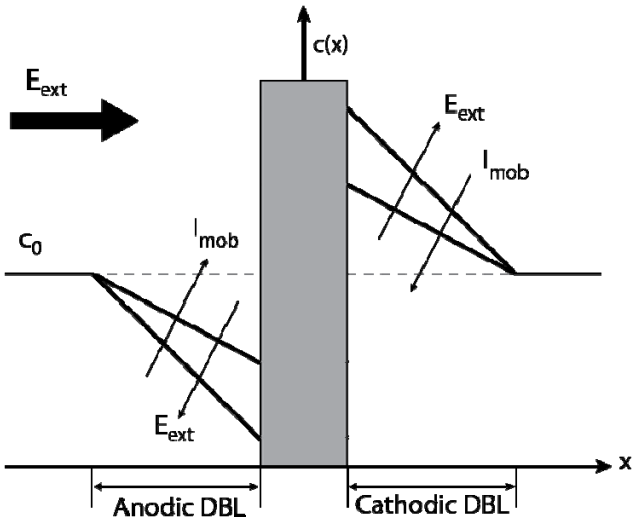

Figure 1.4 - Concentration polarization zones at an ion selective membrane, where I_{mob} is the ionic strength of the mobile phase

The degree of ion depletion and enrichment in the DBL is directly proportional to the applied electric field. This attribute of ion selective membranes can be used to enrich the concentration of analytes at a microfluidic/nanofluidic junction.[7, 8]

The creation of the ion depletion zones also has an effect on the current flow through the membrane. The ionic concentration on the anodic side of the membrane can decrease to the point where the current through the membrane reaches a limit due to

insufficient ions to transport the current across the membrane. The limiting current (I_{lim}) is defined as:

$$I_{\text{lim}} = nFAD\frac{c_b}{\delta} \tag{1.28}$$

where n is the number of electrons transferred per molecule, A is the surface area of the membrane, c_b is the concentration of the bulk solution and δ is the DBL thickness. Therefore, the current through the membrane is directly proportional to the surface area of the membrane.[7, 8]

1.3 Microfluidics

The advantages that microfluidic devices have over conventional separation techniques potentially have the power to alter how chemical analysis is performed. These devices are capable of performing multiple analytical processes rapidly, in a parallel manner, and with reduced sample and solvent consumption. Microfluidics is a relatively young field in the separation sciences. It differs from traditional separation devices in that the devices consist of multiple intersecting channels on a single solid substrate. The ability to design a variety of channel layouts allows the microchips to perform many different analytical procedures on one fluidic platform. There are three basic channel variations, "T" junctions, cross intersections, and straight channels. The "T" junctions can easily be used to bring into contact two different analytes for mixing purposes, the cross intersections can be used for valving and fluidic switching, and the straight channels are typically used to perform chromatographic or electrokinetic separations. These channel structures can be combined in many different combinations to tailor the

device for each individual application. The most common application combines a cross intersection and a straight channel. Using electrokinetic transport, a sample and separation buffer can be brought in contact at the intersection, upon fast switching of the voltages a small sample plug can be injected into the separation channel where the analytes are separated and detected. An injection is shown in Figure 1.5. With the application of different voltages at each channel reservoir, additional considerations are necessary to calculate the electric field. Using a combination of Ohm's Law (1.29) and Kirchhoff's Law (1.30) the voltage at the intersection of multiple channels can be calculated.

(1.29) $$V = IR$$

(1.30) $$\sum_{k=1}^{n} I_k = 0$$

Kirchhoff's current law states that the current into an intersection is equal the current out of the intersection. Using this along with measured channel resistances the voltage at the intersection can be calculated. The electric field of the separation channel can be calculated using the voltage drop from the channel intersection to end of the separation channel and the length of the separation channel using equation 1.2. An increase in electric field strength is another advantage of microchips. Microfluidic devices can typically operate at higher electric fields because as the channel dimensions decrease the surface area to volume ration increases giving better heat dissipation. Also, as the lengths decrease, the voltages necessary to reach high field strengths also decrease. The increased field strength decreases the separation times from minutes to seconds. These

rapid separations can be easily automated and sequential separations are possible. Solvent and sample requirements are also decreased with these devices. The ability to manipulate small volumes especially through decreased sample injection is another advantage, as it decreases the variance of the separation, as outlined in section 1.1.2.

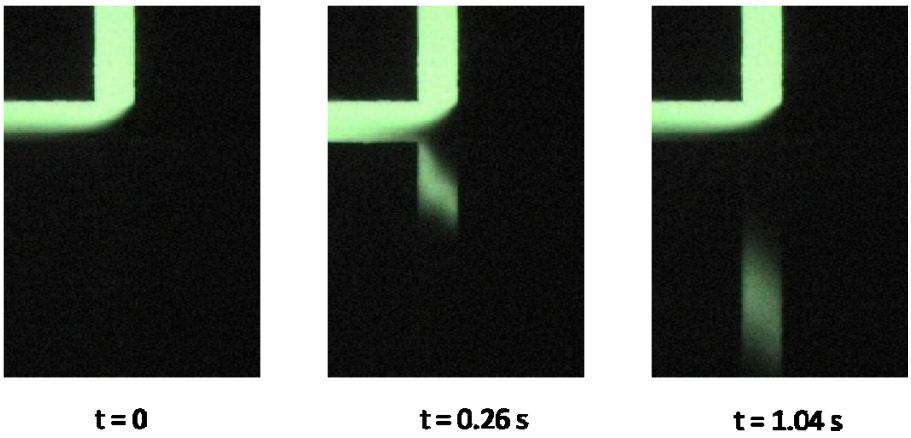

Figure 1.5 - Injections on a microfluidic device at a cross intersection

1.3.1 Laminar Flow

In other separation methods turbulent flow is often generated. Turbulent flow is characterized as chaotic flow which can cause mixing, also decreasing the separation efficiency. The Reynolds number is a measure of the flow characteristics of a contained fluidic stream, laminar or turbulent, given as:

$$\mathrm{Re} = \frac{d_c \rho \upsilon}{\eta} \tag{1.31}$$

where d_c is the tube diameter, ρ is the fluid density and η is the viscosity of the fluid. Turbulent flow is generally not desired for microfluidic applications as it increases mixing and band broadening. Laminar flow is defined as flow that moves in expected paths, Reynolds numbers below 2300. Laminar flow is possible with both electrokinetic and hydrodynamic transport.[9] This allows two streams that come in contact at a junction

on a microfluidic device to not readily mix. Any mixing will be diffusion related. For fluids in microfluidic devices the Reynolds number is often less than 1.

1.4 Conclusions

In the subsequent chapters I will examine multiple applications of microfluidic devices. Chapter 2 will discuss MEKC and the creation of a new separation buffer using a mixed micelle system that alters the selectivity and enhances the separation efficiency of amino acids. Chapter 3 will utilize multiple properties outlined in this chapter including laminar flow to create a titania nanoporous membrane at the intersection of multiple microfluidic channels, and using double layer overlap and Donnan equilibrium to increase the concentration of analytes on microfluidic devices. In Chapter 4, an exciting new field of paper based microfluidic devices capable of performing biologically relevant assays is reported. Chapter 5 describes the fabrication of protein resistant surfaces for surface plasmon resonance detection of proteins. Finally, Chapter 6 discusses the future outlook for these projects.

CHAPTER 2 - A Novel, Environmentally Friendly Sodium Lauryl Ether Sulfate, Cocamidopropyl Betaine, Cocamide MEA Containing Buffer for Micellar Electrokinetic Chromatography on Microfluidic Devices

The majority of this chapter is published as: Hoeman, Kurt W., Culbertson, Christopher T., *Electrophoresis*, **2008**, 29(24), 4900-5

2.1 Introduction

Micellar electrokinetic chromatography (MEKC) is a very powerful separation technique, developed by Terabe et al.[10], and has been used to study a wide variety of analytes. While MEKC initially focused upon the separation of neutral analytes, it has also been used to improve the separation of charged analytes that have hydrophobic functional groups.[11-17] One particularly important class of charged analytes whose separations have been improved by MEKC are amino acids. While amino acids are charged, 15 of the 20 have very similar mass to charge ratios and this makes them difficult to separate by free solution electrophoresis. In order to improve such separations, one can add a second, orthogonal separation mechanism such as hydrophobicity through the addition of micelle forming agents in the separation buffer. There are multiple reports of both native and fluorescently labeled amino acids [18-24] being separated using MEKC[20, 25]. Most of the MEKC separations of amino acids reported thus far have, however, used sodium dodecyl sulfate (SDS) as the micelle forming reagent.

While SDS is by far the most commonly used micelle forming agent, it does have some selectivity limitations. To overcome some of these limitations, additives are used to modify the selectivity of the surfactant. Organic solvents, in particular are regularly added to MEKC buffers. These additives are especially useful to improve the separation of exceedingly hydrophobic analytes, as they shift the partition equilibrium towards the mobile phase. Methanol, ethanol, propanol, tetrahydrofuran (THF) and acetonitrile are the organic modifiers most commonly added to MEKC buffers[13]. The addition of organic solvents to running buffers, however, also tends to increase separation time, generates migration time reproducibility problems as organic additives have a higher vapor pressure and tend to evaporate faster, and makes the buffer less environmentally friendly.

In our search for a more environmentally friendly MEKC buffer with modified and improved resolving power, speed, and selectivity, we came across the family of Seventh Generation™ Inc. products. Seventh Generation™ Inc. produces household products that are environmentally friendly and non-toxic. One of the products manufactured by Seventh Generation™ Inc., Free & Clear™ Dishwashing Liquid, contains three micelle forming agents sodium lauryl ether sulfate (SLES) (anionic), cocamidopropyl betaine (zwitterionic), and cocamide monoethanolamine (MEA) (nonionic) as shown in Figure 2.1 which are not readily commercially available in combination or separately. All three of these surfactants are more environmentally friendly than SDS according to the Danish EPA[26]. To the best of our knowledge none of these surfactants have been used previously as micelle forming agents for MEKC. The only reagent that closely resembles any of these that has been reported as a micelle forming reagent is SLES. Ding et al. has previously reported the use of SLES as a

surfactant for MEKC[27]. In this report, the surfactant was synthesized through the sulfoxidation of Brij-30, referred to as Brij-S. Ding et al. reported that the Brij-S molecule contained between 1 and 11 ethoxy groups and their buffer contained high

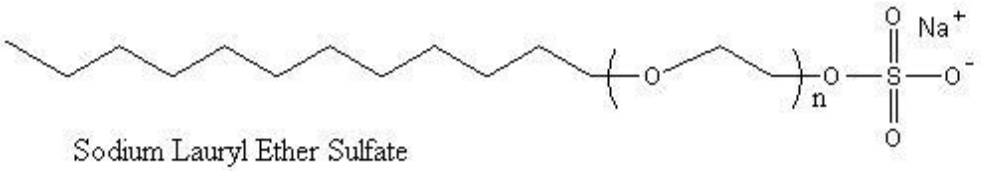

Sodium Lauryl Ether Sulfate

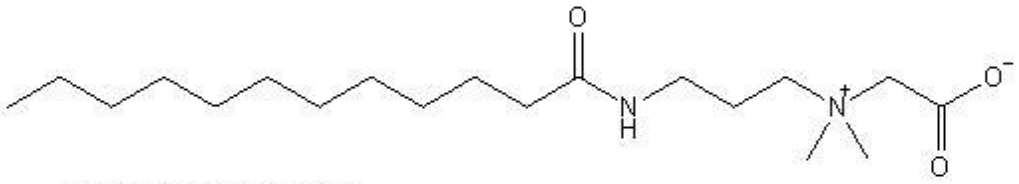

Cocamidopropyl Betaine

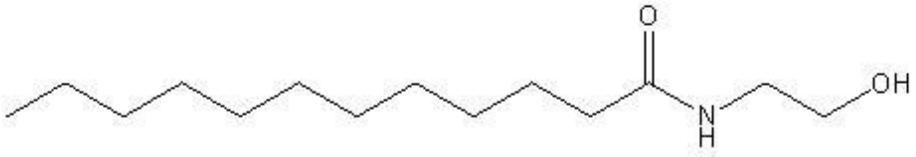

Cocamide MEA

Figure 2.1 - Chemical structures of the micelle forming agents in the Seventh Generation™ Free & Clear™ Dishwashing Liquid

concentrations of organic additives[27]. Conversely, the SLES in the Seventh Generation™ detergent has only 3 ethoxy groups. The addition of two other types of micelle forming agents, the lack of organic additives, and the use of more environmentally friendly reagents should create an alternative to SDS containing buffers. Along with the need for using only small volumes of buffers on microfluidic devices, this buffer helps to provide a truly "green" microfluidic-MEKC separation technique, which will be attractive for future use.

This chapter reports a MEKC buffer containing three environmentally friendly micelle forming agents, two of which, to our knowledge, have not been previously used for MEKC separations. This buffer provides faster separations than previously optimized MEKC buffers for amino acid separations, exhibits a different selectivity than SDS, generates equal or better efficiencies, and is completely void of organic solvent additives.

2.2 Materials and Methods

2.2.1 Reagents and Fluorescent Labeling

Sodium dodecyl sulfate, sodium borate, DMSO, sodium bicarbonate, and acetonitrile were purchased from Fisher Scientific. The amino acids alanine (A), arginine (R), asparagine (N), aspartic acid (D), glutamic acid (E), isoleucine (I), leucine (L), lysine (K), methionine (M), phenylalanine (F), proline (P), serine (S), threonine (T), tryptophan (W), and valine (V) were obtained from MP Biomedicals (Solon, OH) and were labeled with BODIPY FL STP ester sodium salt from Invitrogen (Eugene, OR). The amino acids were prepared by making 5 mM solutions of each amino acid in 0.15 M sodium bicarbonate pH = 9.1. A 5 mg vial of BODIPY FL was diluted with 1.0 mL of DMSO, and then 450 µl of the amino acid cocktails along with 50 µl of the labeling cocktail were combined in micro-centrifuge tubes at a molar ratio of 5.3:1, amino acid to BODIPY respectively. The samples were then placed on a shaker in the dark for ~4 h. Assuming complete reaction with the labeling compound the concentration of labeled amino acids was 0.92 mM. The samples were then stored in a freezer until use. For separations each amino acid cocktail was diluted 1:500 into the MEKC buffer. The new MEKC buffer was

prepared by combining varying percent concentrations (w/w) of Free & Clear™ Dishwashing Liquid from Seventh Generation™ Inc. (Burlington, VT) and 0.01 M sodium borate.

2.2.2 Microchip Design and Fabrication

2.2.2.1 Glass Microchip Fabrication

Photomasks fabricated using AutoCAD 2006 software (Autodesk, Inc.; San Rafael, CA), were submitted to Fineline Imaging (Colorado Springs, CO). The photomasks for this application had channels 25.4 μm wide which increased to 200 μm wide as the channels approached the solution reservoirs. The narrow sections of the channels where the injections and separations took place had the following dimensions: the sample, buffer, buffer waste and separation channels were 0.73, 1.20, 1.20, and 3.75 cm long, respectively. Microchips were fabricated with borosilicate glass (10.16 cm x 10.16 cm x .08 cm) (Telic; Valencia, CA), which had a chrome layer followed by a layer of AZ1500 positive tone photoresist. The glass plates from Telic were exposed through a photomask with the channel design on it using a UV exposure system (ThermoOriel, Stratford, CT). The plate was then placed in a photoresist developing solution (Microposit Developer, Shipley Co.; Marlborough, MA) for 90 s, and then rinsed with H_2O. Next, the plate was placed in chrome etchant (Transene, Co., Danvers, MA), and again rinsed with H_2O followed with drying under a stream of nitrogen. Finally, it was placed into a glass etching solution until the desired channel depth was reached. The buffered oxide glass etchant was comprised of (NH_4/HF, 10:1) which was combined with

H_2O and HCl at a final ratio of 1:4:2, respectively. The channel depth was measured using a profilometer (Ambios Technology; Santa Cruz, CA); the final channel dimensions were 50.1 μm wide and 10.1 μm deep. The glass plates were then cut into single microchips, 2.54 cm x 5.08 cm, using a glass dicing saw (MTI Crystal; Richmond CA). Access holes were drilled into the etched and diced plate at the terminal ends of the channels using 1.5 mm diamond tipped drill bits (Rio Grande; Albuquerque NM). An additional glass plate from Telic, without chrome and photoresist was diced into identical pieces to act as the cover plate for the device. The glass sections were then submerged in 5 M sulfuric acid for 10 min., followed by rinsing with H_2O. Each piece of glass was then swabbed with acetone, ethanol and H_2O using clean room swabs (Great Barrington, MA), and dried under nitrogen. A set of five cover plates and 5 etched pieces were placed in a glass slide holder and submersed in solution of 1000 mL H_2O and 25 mL Versa-Clean liquid soap (Fisher Scientific; Pittsburgh, PA) and placed in a sonicator for 12 minutes. After rinsing with copious H_2O and dried they were placed in acetone and sonicated for 12 minutes. Without drying they were placed in the etchant solution for 10 s, and then rinsed and placed in a hydrolysis solution (1:1:2, NH_4OH: 30% H_2O_2: H_2O) for 12 minutes. Finally they were rinsed and placed in flowing 18.1 MΩ H_2O and sonicated for 12 minutes. One of each of the cover plates were placed in contact with the etched side of the channel piece and clipped together with binder clips. The reservoirs were dried out and vacuum was applied to the reservoirs to pull the channels dry from the excess H_2O. The microchips were then placed in a 100 ^oC oven for 2 hours. Finally the two sides were irreversibly thermally bonded together in a kiln (Evenheat; Caseville, MI).

Solution reservoirs, 8 mm special wall glass tubing cut into 0.25 inch sections, were then attached above drilled access holes using epoxy (Epoxy Technology; Billerica, MA).

2.2.2.2 Poly(dimethysiloxane) Microchip Fabrication

A clean silicon wafer (Silicon Inc.; Boise, ID) was used as the substrate for the fabrication of the mold. An aliquot of negative tone photoresist SU-8 2010 (MicroChem Corp.; Newton, MA) was deposited on the wafer which was adhered to the chuck of a spin coater. A spin program was used to create a ~20 μm film on the surface. After a baking protocol to remove solvent from the photoresist, the photomask, designed in a similar fashion as before, was placed on top of the photoresist and illuminated with the UV exposure system. The wafer was place on hot plates for a post-bake procedure as suggested by the manufacturer and then developed in a SU-8 developing solution. This resulted in the mold for the fabrication of the microfluidic device.

To fabricate the poly(dimethylsiloxane) (PDMS) chip, the prepolymer and curing agent were mixed in a 10:1 ratio and degassed. The PDMS, 13 g, was poured on top of the silicon wafer mold, and 9 g was poured onto a cleaned 75 mm x 50 mm glass slide, which will act as the other side of the device. They were baked in an 80 ^{o}C oven for 15 minutes. The two pieces were then pulled off their substrates and placed in conformal contact with one another so the previous sides which were in contact with the substrates are now in contact. The resulting device was placed back in the oven for an additional 1 hour. Access holes were "punched" into the PDMS at the ends of the channels and with 3 mm biopsy punches. Solution reservoirs, ¼" sections of 8 mm special wall glass tubing, were attached using uncured PDMS as the adhesive, which required an additional baking time of 20 minutes to cure.

2.2.3 Separations

To prepare the chips for separations the channels were flushed with 1.0 M sodium hydroxide, followed by water, and then the MEKC buffer. All solutions were made using 18.0 MΩ ultra pure water (Barnstead; Dubuque, IA) and filtered through 0.45 μm syringe tip filters (Millipore; Bedford, MA). The separation voltages were applied using an in-house built power supply controlled with LabVIEW (National Instruments; Austin, TX). After injection of the sample, the separated fluorescently labeled amino acids were detected using laser induced fluorescence (LIF). The excitation source for the LIF detection system was a diode pumped Nd:YAG laser at 473 nm (CrystaLaser; Reno, NV). The laser beam was reflected off a 500 nm long pass dichroic mirror (Omega Optical Inc.; Brattleboro, VT) into a 40 x objective which focused the light into a section of the channel. The analyte emission was collected using the same objective and passed through a dichroic mirror, a 500 μm pinhole, and a 500-580 nm band pass filter (Omega Optical). The filtered signal was detected using a photomultiplier tube (Hamamatsu; Bridgewater, NJ). The signal was amplified with a low-noise current pre-amplifier (Stanford Research Systems; Sunnyvale, CA) which employed a 30 Hz low pass filter. This signal was collected at 100 HZ with a National Instruments 6036E data acquisition card in a PC.

2.3 Results and Discussion

2.3.1 MEKC Buffer Optimization

To initially study the MEKC buffer we chose to separate four BODIPY FL STP ester labeled amino acids, aspartic acid, phenylalanine, threonine, and proline with

widely varying hydrophobicities. The concentration of the Seventh Generation™ dishwashing liquid was varied between 0% and 10% (w/w) and combined with 10 mM sodium borate solutions to make a series of running buffers. The amino acids used in these separations were labeled with BODIPY FL STP ester and were diluted into the separation buffer at a concentration of 2 μM. Separations of the four amino acids were performed in all of the different running buffers, varying concentration (%, w/w) of Seventh Generation™ dish washing liquid and 10 mM sodium borate, with the same field strength, 900 V/cm, as shown in Figure 2.2.

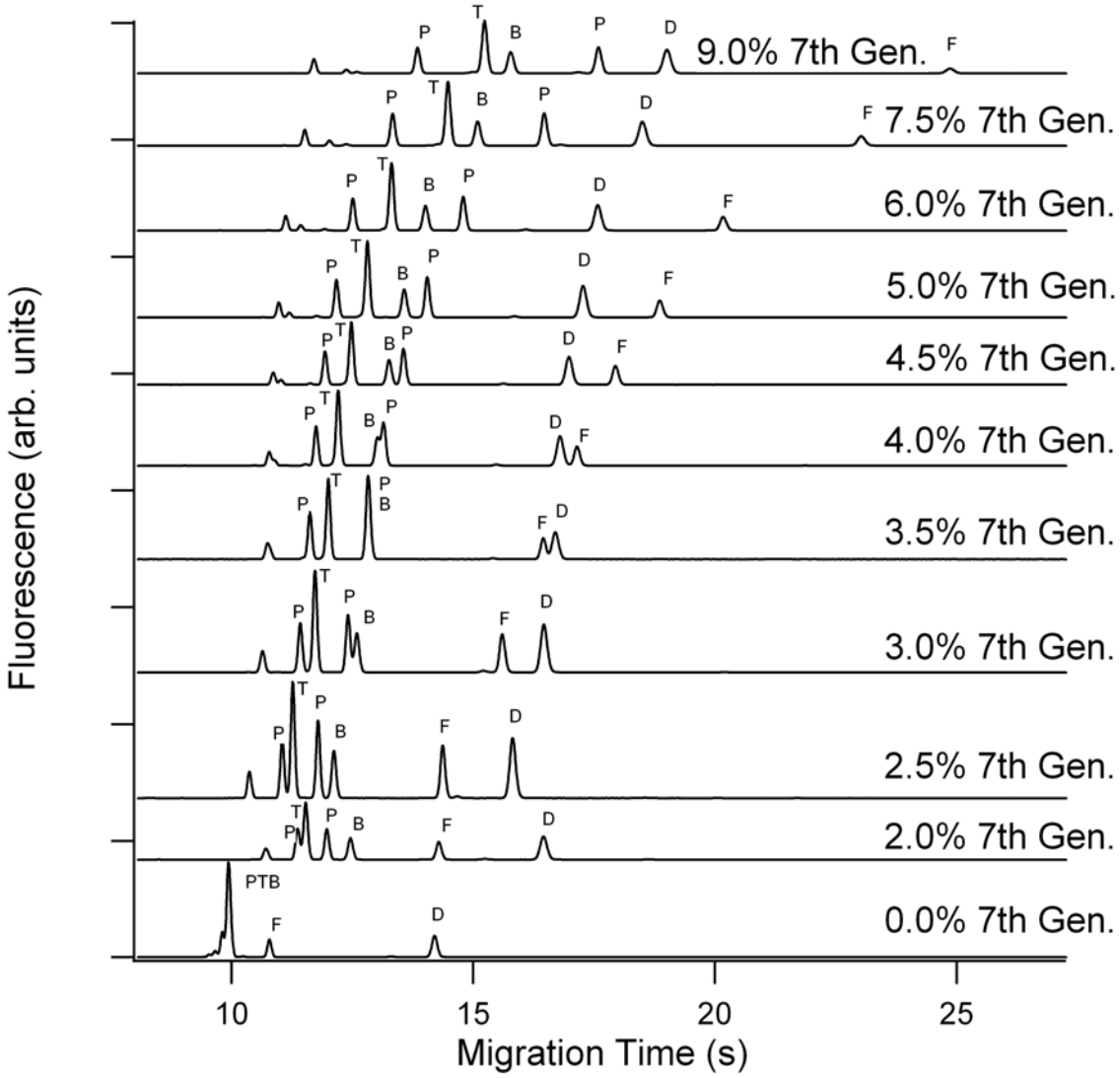

Figure 2.2 - Electropherogram of 4 BODIPY FL STP ester labeled amino acids. The amino acids are represented with their one letter abbreviations, and B represents the BODIPY FL blank.

using the 5.0% Seventh Generation™ dishwashing liquid yielded the fastest separations where all peaks were sufficiently resolved, with resolution of at least 1.5. The Seventh Generation™ buffer successfully separated the amino acids with nice Gaussian shaped peaks faster than previously optimized buffers developed in our group using SDS[28, 29] and with equal or higher separation efficiencies. For example the final peak, i.e.

phenylalanine, in the 5.0% Seventh Generation™ and SDS buffers in Figure 2.3 was detected 69% (9 s) faster and with 19% higher efficiency (~94 k) using the Seventh Generation™ buffer. The higher separation efficiencies for the Seventh Generation™ buffer compared to the SDS may be due to the fact that the Seventh Generation™ buffer is a mixed micelle system. Mixed micelle systems have been shown previously to generate higher separation efficiencies due to their decreased structural order and a lower surface charge density. This is believed to improve the mass transfer kinetics for the partitioning of the analyte between the buffer and the micelle.[30]

One interesting aspect of this buffer is that the selectivity changed with increasing surfactant concentration, e.g. the phenylalanine traded places with aspartic acid and proline traded places with the excess BODIPY peak with increasing surfactant concentration. This is a phenomenon that is not commonly seen in MEKC separations. Most previous reports which have examined the effect of surfactant concentration on

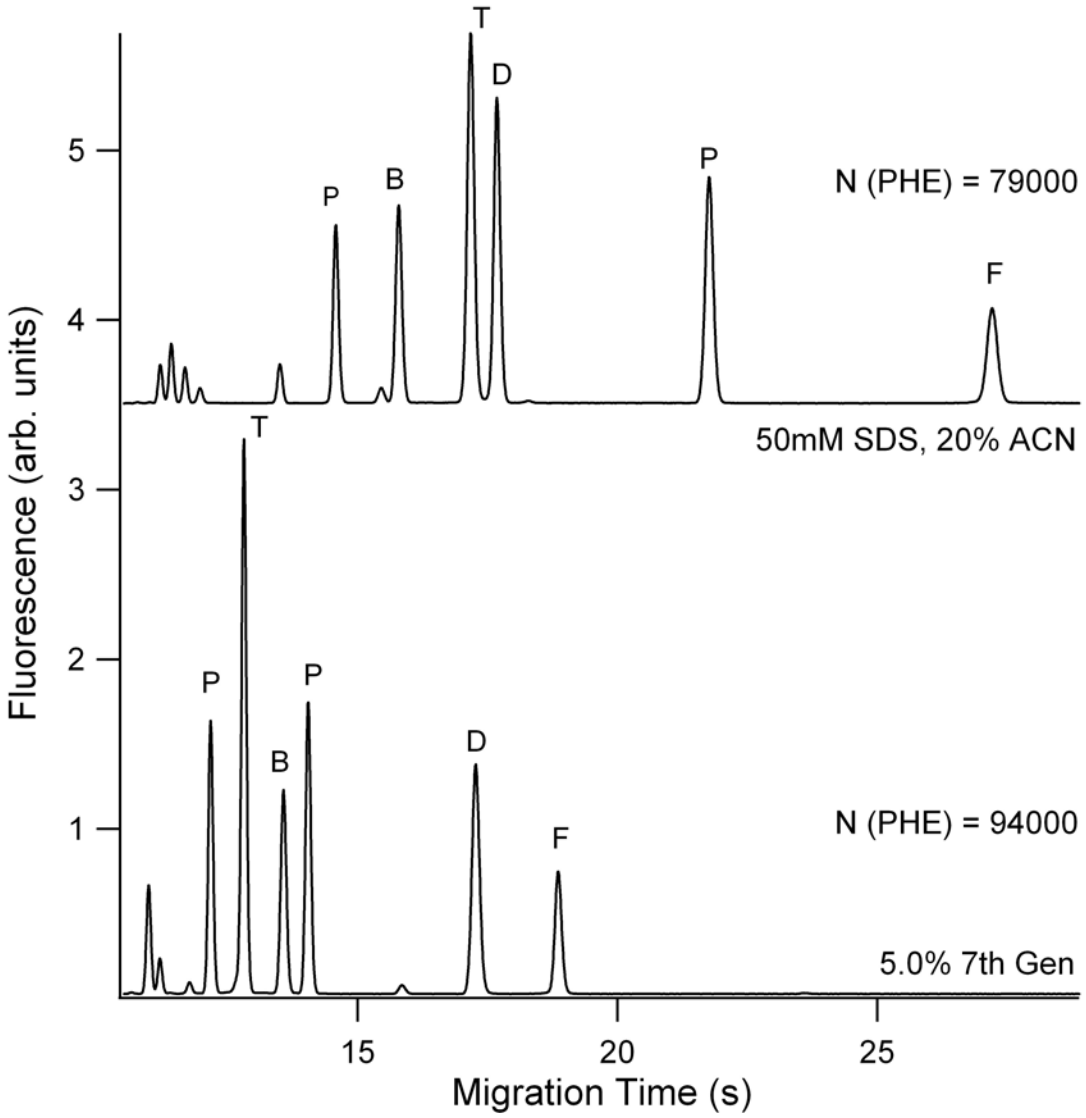

Figure 2.3 - Electropherogram of 4 amino acids in 5.0% Seventh Generation™ Dishwashing Liquid and 10 mM sodium borate, and in 50 mM SDS, 10 mM sodium borate, and 20% acetonitrile.

selectivity have shown that changing the surfactant concentration (i.e. phase ratio) does not modify the separation selectivity ($\alpha = k_y/k_x$).[31, 32] Selectivity, rather, is typically altered by changing the surfactant, using mixed micelles, or by the addition of organic modifiers.[31-34] There is, however, one recent report by Wang et. al. where increasing the SDS concentration altered the selectivity of 2-chlorophenol and 4-nitrophenol. The

authors in this report attributed the change in migration order to the amplified contribution of hydrogen bonding at high surfactant concentration levels.[35] The micelle forming agents in the buffer that we are using are capable of forming hydrogen bonds with the analytes used in this analysis and this may be the reason for the change in selectivity seen with the change in surfactant concentration.

While the actual concentrations of the surfactant used in the optimized separation buffer is not known, the MSDS for the solution allowed us to calculate a concentration range for each of the surfactants used. SLES, cocamidopropyl betaine, and cocamide MEA had concentration ranges in the 5% buffer of 3.5 mM to 35 mM, 1.4 mM to 14 mM, and 2.0 mM to 20 mM, respectively. In the longer term we would like to be able to obtain each surfactant in reasonably small quantities from the manufacturers to better examine the usefulness of each surfactant in different combinations and concentrations. One potential issue in using a commercial off-the-shelf product such as this is the batch-to-batch reproducibility. While this has not been specifically tested yet, the one 500 mL bottle that we have, at present, would be sufficient to last more than 20 years under daily use (50 μL/day) thus reducing the importance of such issues.

2.3.2 Separation of Hydrophobic Amino Acids

To examine the potential of the buffer to separate more hydrophobic analytes, we moved to a set of the most hydrophobic amino acids - phenylalanine, isoleucine, leucine, tryptophan, valine, and methionine. These amino acids were again labeled with BODIPY FL, and were separated on the same style glass microchip using the same injection and separation voltages. At 5.0% Seventh Generation™ buffer the peaks were not all

resolved. To increase the interaction of the hydrophobic analytes with the micelles, a higher concentration of Seventh Generation™ was used. The 10.0 % Seventh Generation™ buffer separated the amino acids to the point where the majority of the peaks were baseline resolved (Figure 2.4).

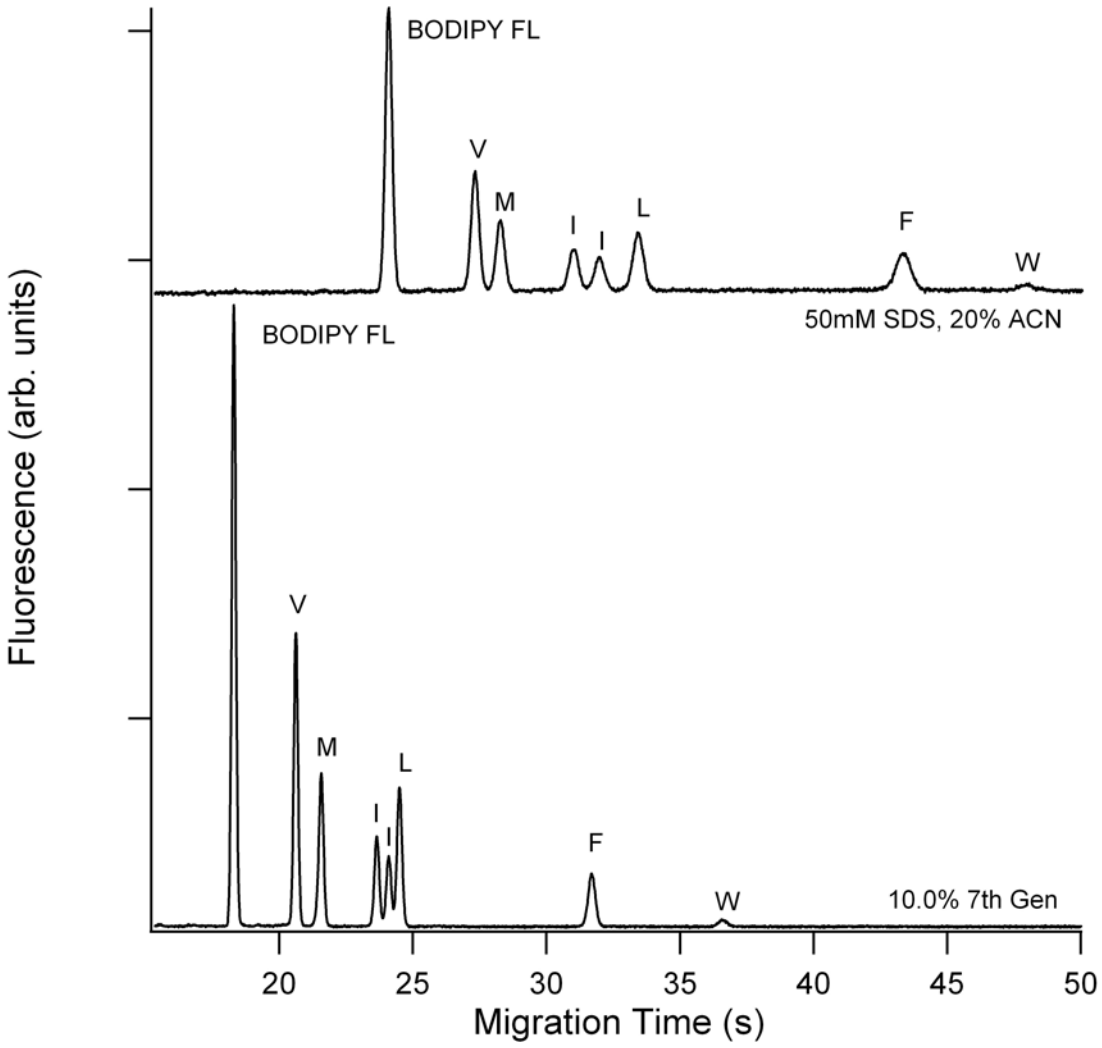

Figure 2.4 - Electropherogram of 6 hydrophobic amino acids in optimized MEKC buffer: 10.0% Seventh Generation™ Dishwashing Liquid, and 10 mM sodium borate, and in 50 mM SDS, 10 mM sodium borate, and 20% acetonitrile.

We also attempted to separate these six amino acids using a previously optimized 50 mM SDS, 10 mM sodium borate and 20% acetonitrile buffer for comparison. The 10.0%

Seventh Generation™ buffer overall gave higher efficiencies (211%) and shorter migration times (75%) compared to the SDS buffer with field strength of 900 V cm^{-1} (Table 2.1).

10% Seventh Generation™, 10 mM Sodium Borate							
	V	M	I	I	L	F	W
N	74000	66000	72000	77000	71000	61000	52000
t_r (s)	20.6	21.6	23.6	24.1	24.5	31.7	36.6

50 mM SDS, 20% Acetonitrile, 10 mM Sodium Borate							
	V	M	I	I	L	F	W
N	35000	33000	31000	33000	30000	25000	41000
t_r (s)	27.3	28.3	31.0	32.0	33.4	43.3	48.0

Table 2.1 - Theoretical plates and retention times for the separation of hydrophobic amino acids

2.3.3 Separation of Hydrophilic Amino Acids

To examine the potential for separating more hydrophilic compounds, we attempted the separation of six of the most hydrophilic amino acids proline, glutamic acid, aspartic acid, lysine, asparagine, and arginine were examined in this new buffer. The 5.0% Seventh Generation™ buffer completely separated the six amino acids (Figure 2.5). It provided substantially faster separations than the SDS containing buffer. The set of analytes was also separated with the same 50 mM SDS, 10 mM Borate buffer previously used but without the acetonitrile. The removal of the acetonitrile significantly increased the EOF; however, the separation was still slower than the separation performed in the Seventh Generation™ buffer as seen in Figure 2.5. Both buffers yielded high efficiency separations, where plate numbers obtained were above 100,000 plates and some peaks with ~200,000 plates. The second lysine peak in the Seventh

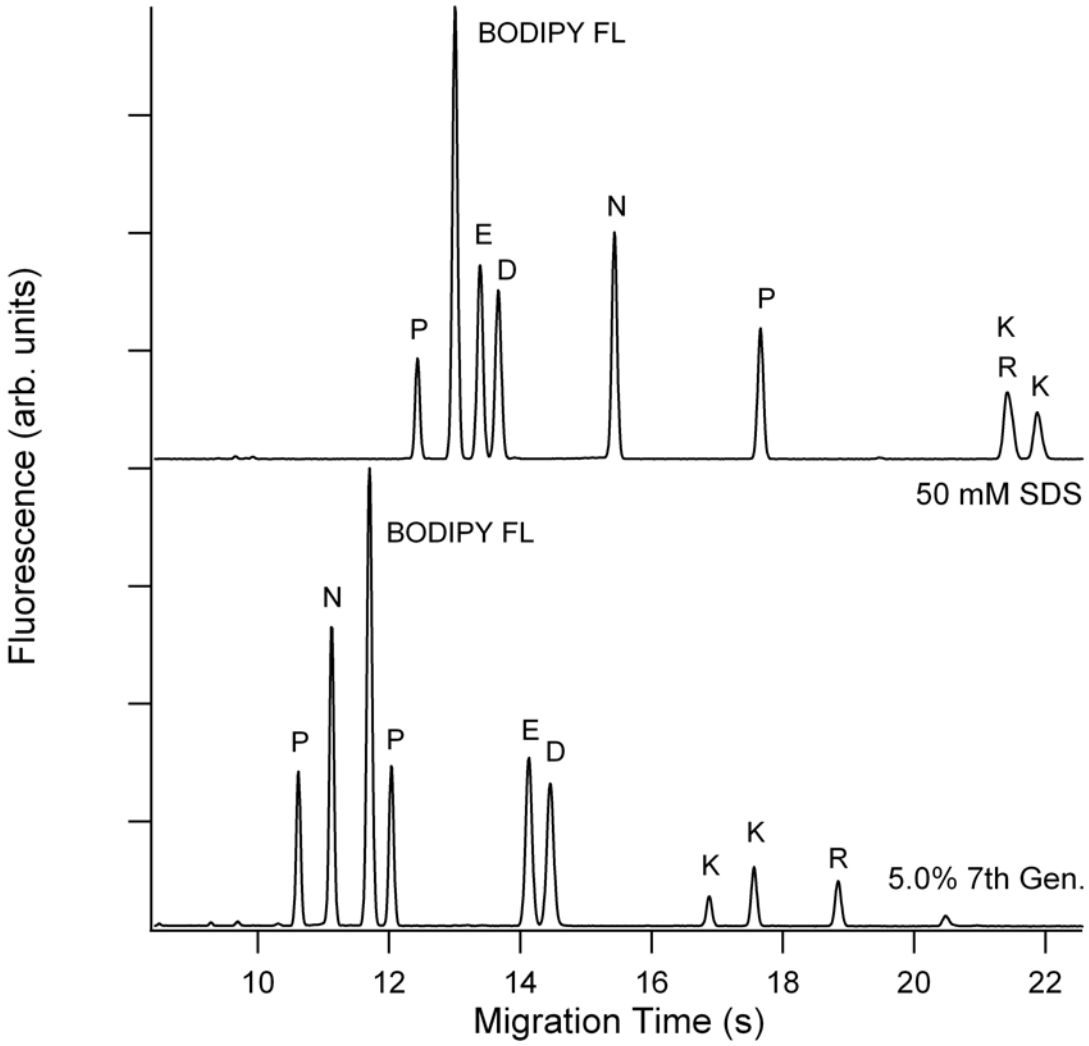

Figure 2.5 - Electropherogram of 6 hydrophilic amino acids in optimized MEKC buffer: 5.0% Seventh Generation™ Dishwashing Liquid, and 10 mM sodium borate, and in 50 mM SDS, and 10 mM sodium borate.

Generation™ buffer generated 180,000 plates, 10,200 N/s, and a plate height of 0.19 μm. Whereas for the 50 mM SDS and 10 mM sodium borate buffer generated 147,000 plates, 6700 N/s, and a plate height of 0.23 μm. With both buffers lysine gave two peaks. This was because lysine has two amine functional groups that can be labeled using with the derivatization agent. The multiple labeling was problematic with the 50 mM SDS and 10 mM sodium borate running buffer because the first lysine peak overlapped the arginine

peak, effectively making it impossible to separate Arg and Lys in the same separation. This was not a problem with the Seventh Generation™ buffer, as we were able to completely resolve the two amino acids. The second Lys peak in the Seventh Generation™ buffer generated 36% more theoretical plates and was 20% faster than the corresponding Lys peak in the best SDS buffer.

2.3.4 Serpentine Chip Separations

Finally a set of fifteen amino acids were separated using a serpentine style PDMS microfluidic device. This fluidic pattern has been previously reported and used to separate amino acids with a SDS, sodium borate and acetonitrile buffer.[29] Briefly the fluidic channels were 75 μm wide and had tapered turns where the channels were 25 μm wide, and all channels were 13 μm deep Figure 2.6. The separation channel was 32.3 cm long with LIF detection at 25.3 cm.

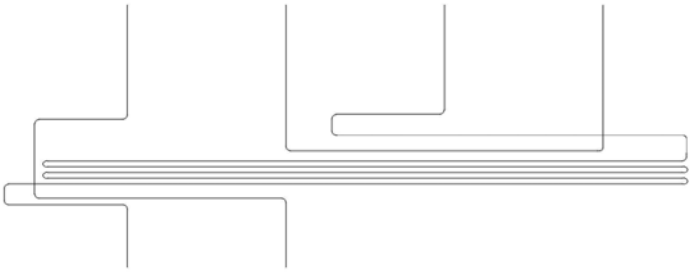

Figure 2.6 - Channel layout for serpentine chip separations

A MEKC buffer containing 6% Seventh Generation was used to separate the amino acids. For comparison the same analytes were separated using a 50 mM SDS and 10 mM sodium borate buffer. Both buffers generated high efficiency separations with field strengths of 415 V/cm, and yielding 375,000 plates, 3150 N/s and 1.5 x 10^6 N/m for Phe

in the seventh generation buffer, and 190,000 plates, 1660 N/s and 751,000 N/m for Phe in the SDS buffer as seen in Figure 2.7. In the previous separations on glass microfluidic devices the SDS based buffers had slower separation times, whereas in this case the Seventh Generation buffer was slower. Studies have shown that surfactants molecules can partition into PDMS,[29] the surfactants in the seventh generation buffer might have different interactions with the PDMS compared to the SDS which is a possible explanation for the increased separation times.

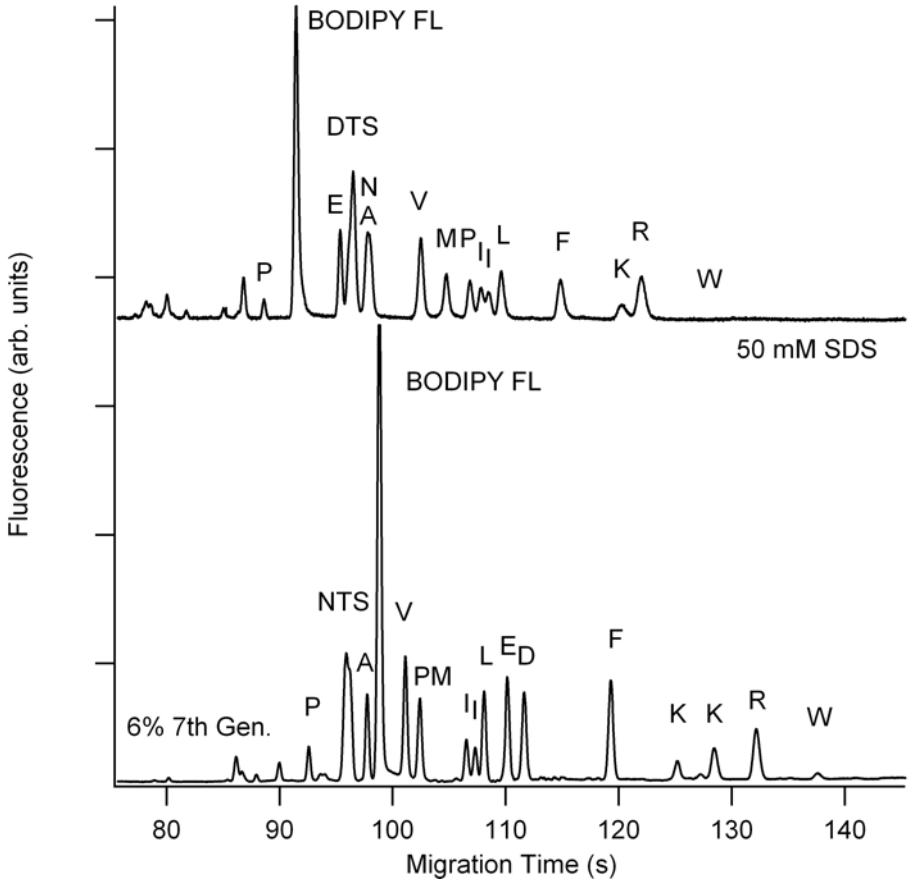

Figure 2.7 - Electropherogram of 15 amino acids in a MEKC buffer on a PDMS serpentine chip: 6.0% Seventh Generation Dishwashing Liquid, and 10 mM sodium borate, and in 50 mM SDS, and 10 mM sodium borate.

A change in selectivity of the buffer was again noticed here with major changes with respect to Asp and Glu. Fluorescently labeled amino acid separations have previously been performed on similarly fabricated devices and the authors reported much longer separation times at higher field strengths; however, the fluorescent tag previously used was much larger, 150 u, and was negatively charged. Both of which would increase the migration time of the analytes.

2.4 Concluding Remarks

The most attractive feature of this buffer is the decreased effect it has on the environment. Chemicals are assigned hazard ratings for their effect on humans and the environment, where the ratings for humans contain an alphabetic and numeric rating; only a numeric rating is used for the environment. For human hazard ratings the number relates to acute exposure, while the letter coding relates to chronic exposure. The numeric rating class 1, for example, refers to acute exposure with irreversible effects after exposure to low doses, and with class 5 there is no reason for concern regarding adverse effects to heath. The chronic classes are similar where class A is equivalent to class 1 as class E is to class 5. According to the 2001 Danish EPA report SDS, SLES, and cocamidopropyl betaine have environmental hazard class ratings of 3, 4, and 4, and human health hazards of 2D, 3E, and 4E, respectively. Therefore, the micelle forming agents in the Seventh Generation™ dishwashing liquid pose less of an environmental and human hazard than the most commonly used surfactant in MEKC, (i.e. SDS). This buffer also has the additional advantage of obviating the need for organic additives when optimizing partition coefficients. Also the evaporation of organic additives over the

course of a series of runs will generate changes in both the partition coefficient and the electroosmotic flow, thus affecting the migration time reproducibility. The absence of organic solvents in the Seventh Generation™, therefore, should produce more robust and reproducible separations. Finally, buffers without organic solvents also have a higher EOF, which allows for the successful injection of slower more negatively charged analytes. The change in the selectivity of the buffer, the decreased separation time, and the ability to tailor the surfactant concentration to resolve peaks of interest is a powerful characteristic of this buffer. These attributes along with the lack of organic solvents makes this new buffer a "green" option for MEKC analysis.

CHAPTER 3 - **Electrokinetic Trapping Using Titania Membranes Fabricated Using Sol-Gel Chemistry on Microfluidic Devices**

The majority of this chapter is to be published as: Hoeman, Kurt W., Lange, Jeffrey J., Roman, Gregory T., Higgins, Daniel A., Culbertson, Christopher T., *Electrophoresis,* **2009**, accepted.

3.1 Introduction

Microfluidic devices have many potential advantages over commercial scale chemical analysis instrumentation in that they can integrate multiple chemical processing steps with rapid and high efficiency separations onto a single monolithic device. Several different types of chemical processing and handling steps have been demonstrated on these devices including mixing, reactions, filtering, preconcentration and separations.[36, 37] These processing and handling steps have also been integrated with on-chip waveguides,[38, 39] lasers,[40, 41] and photodiodes[42] to generate devices capable of performing biochemical analyses with laser induced fluorescence (LIF) detection.[43, 44] Although LIF is an extremely sensitive detection method, its limit of quantitation generally lies within the nM to pM range of concentrations. In many cases, there exist samples in which the analyte of interest is too dilute to be detected even by LIF. To further improve LIF detection on microfluidic devices, especially for low concentration analytes, preconcentration methods need to be integrated with separation and detection.

Numerous examples of analyte concentration enrichment on microfluidic devices have been reported. These include field amplified sample stacking (FAS),[45, 46] electrokinetic trapping, isotachophoresis (ITP),[47-49] chromatographic preconcentration,[50, 51] micellar sweeping,[52, 53] and membrane preconcentration[54, 55] among others. In most previous microfluidic membrane preconcentration studies, the microfluidic devices have been fabricated using multilayer lithography and fabrication techniques that incorporate commercially available track etched membranes.[56-59] The track-etched membranes are sandwiched between two poly(dimethylsiloxane) (PDMS) layers in which channels have been molded. While the precise mechanism of concentration is not completely clear it is generally thought that it is related to the double layer overlap that occurs in the nanochannels. This double layer overlap results in a decrease in electroosmotic flow and also limits the ability of ions of the same charge as that on the pore walls from entering (i.e. Donnan exclusion). For slightly larger pores where double layer overlap is not expected, surface vs. bulk conductivity mismatches have been postulated as the concentration mechanism.[58-60] Sandwiching of nanoporous membranes into microfluidic devices does have some limitations including inefficient bonding between lithographic layers that can result in leaks and chemical compatibility issues with polymer microfluidics. In addition to these sandwiched type microfluidic configurations, on-chip analyte preconcentration has recently been achieved using hydrogel microplugs that are formed *in situ*.[61] These microstructures are limited, however, in that they are currently capable of generating relatively low enrichment factors (500x) and analyte leakage into the hydrogel plug has been observed. Similarly, Song et al. have demonstrated laser patterned membranes in microfluidic channels which can be used for concentration

enrichment.[54, 62] Finally, the use of microfluidic channels connected via nanofluidic channels (nanofluidic filters), have been used for preconcentration.[63-66] Electrokinetic transport in these nanochannels has been studied in depth, especially in relation to how double layer overlap in the nanochannels generates an asymmetric flow of cations and anions through these channels that results in the trapping of ions of the same charge as found on the channel walls in front of the nanochannels.[67-70] Wang et al. used this electrokinetic trapping mechanism to demonstrate million-fold preconcentration of GFP.[71] Electrokinetic trapping at nano/microchannel interfaces has also recently been shown to trap not just small analytes but larger particles as well.[60] Two potential limitations of these nano/micro interface devices are 1) the multiple step lithography processes required to fabricate them and 2) the small interfacial cross-sectional area between the channels that limit the speed at which analyte concentration can be performed.[72]

Fluid flow in microfluidic channel manifolds is generally laminar in nature due to the large surface area to volume ratio in the channels. The Reynolds numbers in such devices is often << 1. A variety of groups have taken advantage of such flow characteristics in order to form structures or create specific surface patterns in microchannels.[73-75] In relation to concentrating analytes, the most notable of these structures are membranes.[76] Zhao et al., for example, have demonstrated the synthesis of nylon membranes using laminar flow within microfluidic devices.[77] To date, however, there have been no reports that demonstrate the fabrication of nanoporous membranes on microfluidic devices using sol-gel chemistry. Sol-gel chemistry has proven to be extremely versatile in a number of fields including optics, electronics, catalysis, chemical

sensing, and chemical separation.[78, 79] Sol-gel chemistry is very versatile and encompasses a wide variety of functional materials that can be synthesized using different metal alkoxide precursors. Nanoporous and mesoporous materials with high porosities and low densities that are transparent can be easily fabricated.[80] There is no intrinsic reason that such materials cannot be synthesized in situ in microfluidic channels in order to create nanoporous membranes with specific surface functionalities. The chemical flexibility of sol-gel processing has the potential to generate a vast number of different membranes for specific physical processes.

In this chapter, the fabrication of titania nanoporous membranes using sol-gel chemistry where the membrane is fabricated at an intersection of channels on a microfluidic device is reported. The membranes were fabricated using laminar flow to bring a sol-gel precursor/alcohol and a water/alcohol solution into contact at an intersection. The size of the membranes could be controlled by varying the concentrations of the precursor and the water in the alcohol solutions. After formation of these membranes, electrokinetic trapping of 2,7-Dichlorofluorescein was performed. Concentration enrichment factors of over 4000x were obtained in about 400 seconds.

3.2 Materials and Methods

3.2.1 Reagents and Materials

Titanium isopropoxide ($Ti(OPr^i)_4$) (Gelest, Morrisville, PA) and anhydrous 2-propanol (IPA) (Sigma Chemical Co., St. Louis, MO) were used for membrane fabrication. The buffer for these studies contained sodium phosphate (Fisher Scientific,

Pittsburgh, PA). The analytes, 2,7-Dichlorofluorescein (DCF), Rhodamine B, and Rhodamine 6G (Acros, Geel Belgium) were used for the preconcentration studies. All solutions were made using 18.0 MΩ • cm ultra pure water (Barnstead; Dubuque, IA) and filtered through 0.45 μm syringe tip filters (Millipore; Bedford, MA).

Microchips were fabricated with white crown (B270) glass (Telic; Valencia, CA) photomask blanks. The chip design and fabrication process have been reported previously.[81] Briefly, the channel network included a 0.7 cm long sample channel (S),1.1 cm long waste (W) and running buffer (B) channels, and a 3.7 cm long separation channel (SP) (Figure 3.1 A). All channels were 50.1 μm wide and 10.2 μm deep. The glass plates, precoated with chrome and photoresist, were exposed through a photomask with the channel design using a UV exposure system. The channel depth was measured using a profilometer (Ambios Technology; Santa Cruz, CA). The remaining photoresist and chrome was removed and the glass plates were then cut into single microchips using a glass dicing saw (MTI Crystal; Richmond CA). Cover plates of the same type of glass were also cut to the appropriate dimensions. Four access holes were drilled above the channels with diamond tipped drill bit (Rio Grande, Albuquerque, NM). After extensive cleaning, the two glass pieces of glass were placed into contact with each other and then were thermally bonded in a kiln (Evenheat; Caseville, MI). Solution reservoirs, ¼" sections of 8 mm special wall glass tubing, were attached above two of the drilled access holes, W and SP, using epoxy (Epoxy Technology; Billerica, MA). Nanoport® assemblies (Upchurch Scientific; Oak Harbor, WA) were attached above the remaining two channels, S and B, with J-B weld. Figure 3.1 shows the orientation of channels and reservoirs with respect the titania membrane.

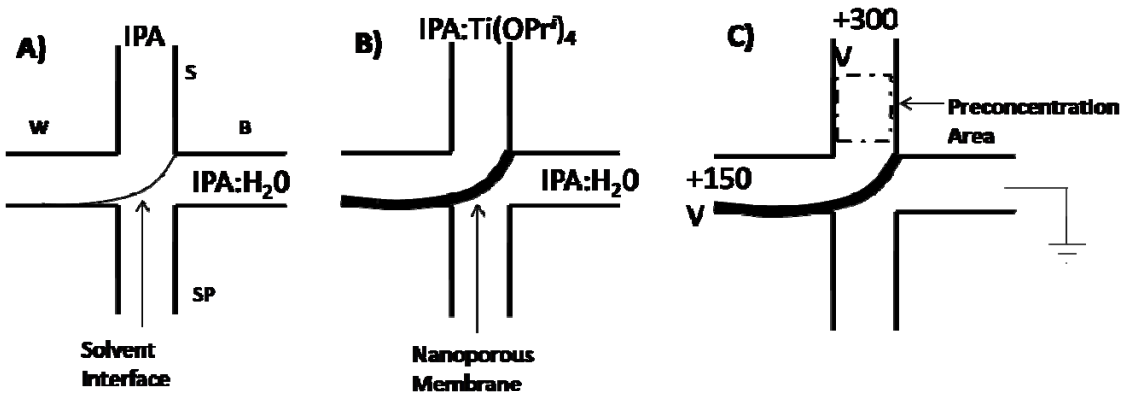

Figure 3.1 - Schematic illustration of the membrane fabrication shows A) the desired liquid-liquid interface position B) the membrane formation and C) the preconcentration voltage scheme. Key: sample channel (S), buffer channel (B), waste channel (W), and separation channel (SP)

3.2.2 Membrane Fabrication

The microfluidic devices were prepared for membrane formation by first rinsing with 1.0 M sodium hydroxide and methanol, followed by drying in a 100 ^{o}C oven for 2 hours. Syringe pumps, equipped with 500 μL Hamilton syringes (model 81220), were connected to fused silica capillary (150 μm i.d. with a total volume of 5 μL; Polymicro Technologies, Phoenix, AZ) and used to deliver fluids to the microfluidic device to fabricate the membranes. Syringe A was filled with anhydrous 2-propanol, and syringe B was filled with a mixture of water and 2-propanol. The ratio of water and 2-propanol varied depending on desired thickness of the membrane. Syringe A was loaded onto an infusion and withdrawal syringe pump (NE-1000; New Era Pump Systems, Wantagh, NY). Syringe B was loaded onto an infusion only syringe pump (11 Plus; Harvard Apparatus, Holliston, MA). Using lure lock and Nanoport® fittings, the syringes were connected to the ports on the microfluidic device. Syringe A was fitted to the sample reservoir and Syringe B to the buffer reservoir. Both pumps were then used in infusion

mode at varying rates so that a liquid-liquid interface was visible at the intersection of the channels. The interface between the fluids was stable due to the laminar flow within the channels. The flow rates were ~3.00 μL/min and ~1.00 μL/min for A and B, respectively. Flow rates were then adjusted so the interface exited the intersection into the waste channel and not into the separation channel, i.e. similar to how the sample/buffer interface would look for a standard gated injection on a microfluidic device. Once the interface was stabilized, the pumps were stopped and the capillary attached to syringe A was disconnected from the microchip so the reactive species could be loaded into it. This capillary was placed into a microcentrifuge tube containing anhydrous 2-propanol. The pump was switched to withdrawal mode, and allowed to pull for 10 min at 3.0 μL/min, and then for 2 min at 1.0 μL/min, to allow the flow to stabilize in the reverse direction. A 35% (v/v) sol-gel precursor solution was made with $Ti(OPr^i)_4$ in anhydrous 2-propanol, immediately prior to its use. With syringe pump A still in withdrawal mode, a ~233 nL plug of the precursor solution was drawn into the capillary by pulling for 14 s at 1 μL/min. The end of the capillary was then rinsed off in anhydrous 2-propanol, to prevent any precursor from the exterior of the capillary from entering the stock 2-propanol. The capillary was then placed back in the microcentrifuge tube containing the anhydrous 2-propanol. The pump was then run for 3.75 min at 1 μL/min to pull the precursor plug further into the capillary. This generated an anhydrous 2-propanol plug in front of the precursor plug and served to delay the entrance of the precursor plug into the intersection until the liquid-liquid interface could be reestablished when the capillary was re-attached to the microfluidic device prior to membrane fabrication. The capillary was then reconnected to the chip and the pumps were changed

back to the settings used to optimize the interface. The two syringe pumps were then turned back on and when the precursor passed through the intersection it reacted with the water in the solution on the other side of the interface and created a nanoporous membrane. After the membrane was formed, the 2-propanol solutions were pumped for an additional 10 min to ensure the entire precursor solution was out of the channels. The channels were then flushed with water followed by 80 mM sodium phosphate, pH 11.50; i.e. the sample buffer for analyte concentration studies. A pH of 11.5 was chosen after a qualitative study was performed using different pH buffers. The results of this study showed faster and higher levels of concentration enrichment at higher pH's. The devices were allowed to sit for 24 hours before any preconcentration studies, providing sufficient time for the buffer to penetrate the nanoporous membrane. There was no investigation into membrane performance as a function of time after formation. So this time was set somewhat arbitrarily.

3.2.3 Analyte Preconcentration

To determine the ability of the membrane to concentrate analytes, a 16 bit CCD camera (Roper Scientific) attached to a Nikon TE2000U epi-illuminescent inverted microscope with an Hg-Arc lamp and a FITC filter cube was used to image a section of the channels and membrane. Voltages were applied to the channels via platinum electrodes using a custom designed Bertan high voltage power supply. The magnitudes of the applied voltages were controlled using an in-house written LabView program.

After letting a chip with a titania membrane sit for at least 24 hours, the channels were flushed with new buffer by replacing the buffer in the reservoirs and applying

negative pressure to the reservoirs. The analyte to be concentrated was then placed in the sample reservoir and pulled through the chip with negative pressure applied at the waste reservoir. The chip was then affixed to the stage of the inverted microscope and platinum electrodes placed in the reservoirs to apply the necessary electric fields to the device. To monitor the preconcentration, the CCD camera was set to collect 100 ms images every 15 s. To prevent photobleaching of the analyte between images, the manual shutter for the epi-illuminescence system was opened and closed every 15 s to coincide with the CCD camera. Depending on the level of preconcentration, neutral density filters were used to prevent oversaturation of the pixels on the CCD camera. Two different filters were used ND4 and ND8 which decreased the initial light intensity to 25% and 12.5%, respectively. The fluorescence intensity of analyte standards were measured using the same camera conditions in a chip of the same channel dimensions while the analyte was electroosmotically moved through the device. All images were captured using WinView32 software (Roper Scientific, Trenton, NJ) and analyzed using ImageJ software (NIH).

3.3 Results and Discussion

3.3.1 Membrane Fabrication

Titania nanoporous membranes were fabricated by hydrodynamically bringing together an anhydrous 2-propanol solution containing 35% (v/v) titanium isopropoxide with a 2-propanol solution containing varying amounts of water as described in the experimental section above. The thicknesses of the sol-gel membranes generated were both a function of 1) the interaction time between the sol-gel precursor and the water and

2) the % water in the 2-propanol solution. In general, the thickness of each membrane formed increased along the length of the membrane from the corner of the channel intersection where the S and B channels met to the other end of the membrane where the SW and S channel met (See Figure 3.1 A). The widths of the channels reported below were made at the center point of the membrane in the intersection. Membranes fabricated using either 50:50 or 60:40 solutions of H_2O in IPA resulted in membranes with thicknesses that averaged 4.7 μm or 39.5 μm. The 5 μm thick membrane will be referred to as the thin membrane and the 40 μm thick membrane will be referred to as the thick membrane. Although it was apparent from simple optical microscopy that the membranes spanned the width of the channel intersection, the vertical characteristics of the membrane could not be determined through simple bright field microscopy. Previous work in our group was performed in order to better understand the morphology of the membrane. Especially in regards to the shape of the sides of the membrane and whether the membrane spanned the entire depth of the channel intersection. One of the thin membranes was imaged using multiphoton microscopy. After the membrane was fabricated in the microfluidic manifold, the manifold was filled with 1 mM fluorescein and allowed to sit for ~ 2 hrs prior to imaging. Cross sections of the membrane over the depth of the channel demonstrated an intact vertical sidewall with constant width.[82, 83]

3.3.2 Preconcentration

Concentration enrichment was performed by applying 300 V to the sample reservoir 150 V to the waste reservoir, while the channels on the other side of the membrane were grounded. The voltage at the waste reservoir was applied to induce a small electroosmotic flow away from the membrane and into the waste channel.[8, 84]

Previous papers have shown that this helps to improve the preconcentration at nano/micro interfaces. This smaller voltage in the adjacent channel aids in continual buffer replenishment. This prevents large electric field gradients from forming at the concentration enrichment zone that can de-stack the analytes, that could effectively decrease the level of enrichment.[8, 84] Initially, one of the thin membranes fabricated with 35% titanium isopropoxide and 50:50; H_2O:IPA was studied by concentrating 31 nM DCF in 80 mM sodium phosphate, pH = 11.50. After 145 s of analyte concentration, the intensities measured by the CCD camera were near the limit of linearity for the response of the pixels, so the ND4 filter was inserted. After 325 s the ND4 was removed and the ND8 filter was inserted for the same reason. Figure 3.2 shows fluorescence micrograph images captured with the CCD camera of preconcentration near the nanoporous membrane at four different times, and the colors are added for enhanced contrast.

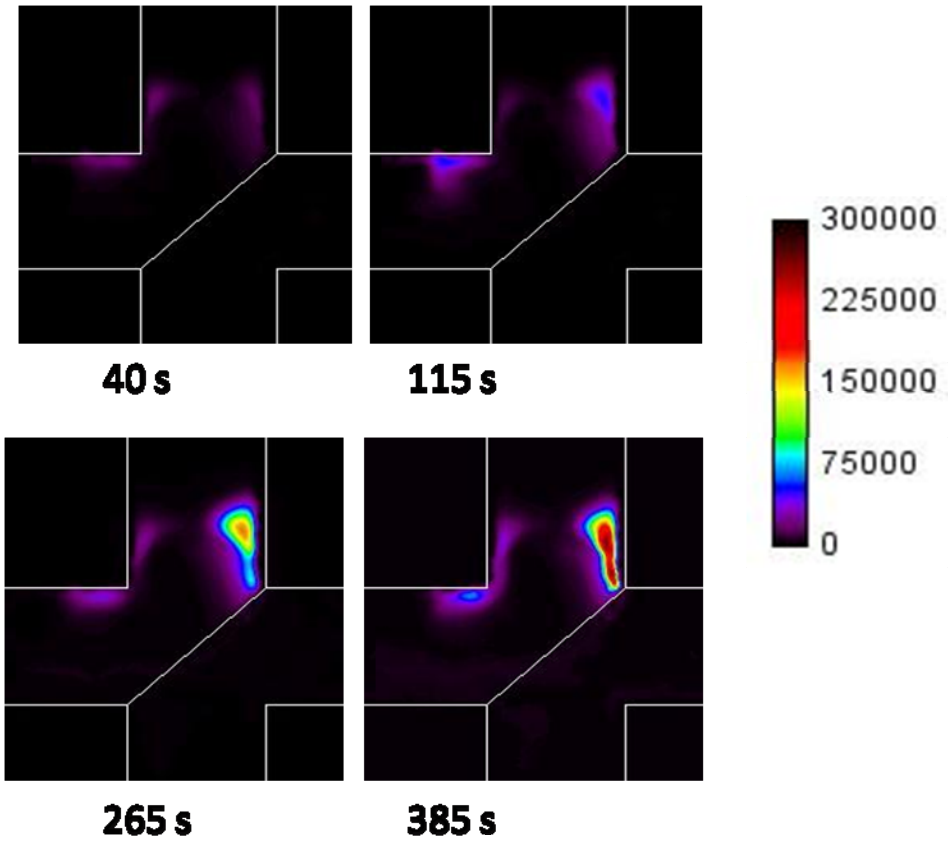

Figure 3.2 - Fluorescence micrographs taken at 40, 115, 265, and 385 s after preconcentration voltages were applied.

In these devices the preconcentration plug did not span the width of the channels. The majority of the preconcentration occurred on the left side of the channel near the membrane in the area where the electric field lines were of the greatest magnitude. Therefore, the manner in which the concentration enrichment levels and factors were calculated must be defined. For the data shown in Figure 3.3, both the maximum intensity at a single pixel (0.57 μm^2) and the average pixel count over 266 pixels (151 μm^2) are reported. Pixel sizes were calculated by measuring the number of pixels across a channel of known width. All of the data were background subtracted. The data for the images taken with the ND filters in the light path were multiplied by factors of 3.76 and

7.34 for the ND4 and ND8 filters, respectively. These values were determined from the actual change in intensity measured with the same standards at each light intensity level. The light intensity level correction factors were close to the values given on the filters themselves of 4 and 8, respectively. The maximum pixel count indicates that the sample was concentrated to above 130 μM. This was a concentration enrichment factor of over 4000X.

In previous reports of preconcentration over nanoporous membranes or at microfluidic-nanofluidic junctions, the manner in which the concentration factor was calculated has been discussed by some groups;[54, 61, 64] however, it is not always explained. The concentration factor reported is greatly dependent upon this calculation. For example, for the data shown in Figure 3.3 there was a 38% difference in the measured maximum count at a single pixel (288,000) and the mean intensity for 266 pixels (179,000 counts). Also, if the averaged area was decreased from 266 pixels to only 9 pixels (5.1 μm^2) the average count increased to 279,000. This value is 148% greater than the 266 pixel area that encompassed the majority of the concentration region. The number of pixels used for averaging, therefore, changes the mean intensity significantly as shown in Figure 3.4. For the purposes of this chapter, we report both maximum intensity values as well as mean values with the area/number of pixels used. The maximum values are reported because they give an idea of the greatest amount of concentration enrichment; however, it is not an extremely accurate representation of the system, as line scans from the CCD camera show pseudo-Gaussian shaped enrichment profiles as seen in Figure 3.5.

In addition, the maximum pixel location moved between each acquired image (i.e. 15 seconds) by as much as 10 pixel lengths due to flow instabilities. Kim et. al. have reported the creation of fluid vortices under similar conditions due to the nonequilibrium electroosmotic flow,[85] as discussed in Chapter 1. Some form of averaging over a defined area, therefore, was necessary in order to better understand the actual levels of analyte enrichment. The images in Figure 3.2 correspond with the data in Figure 3.3.

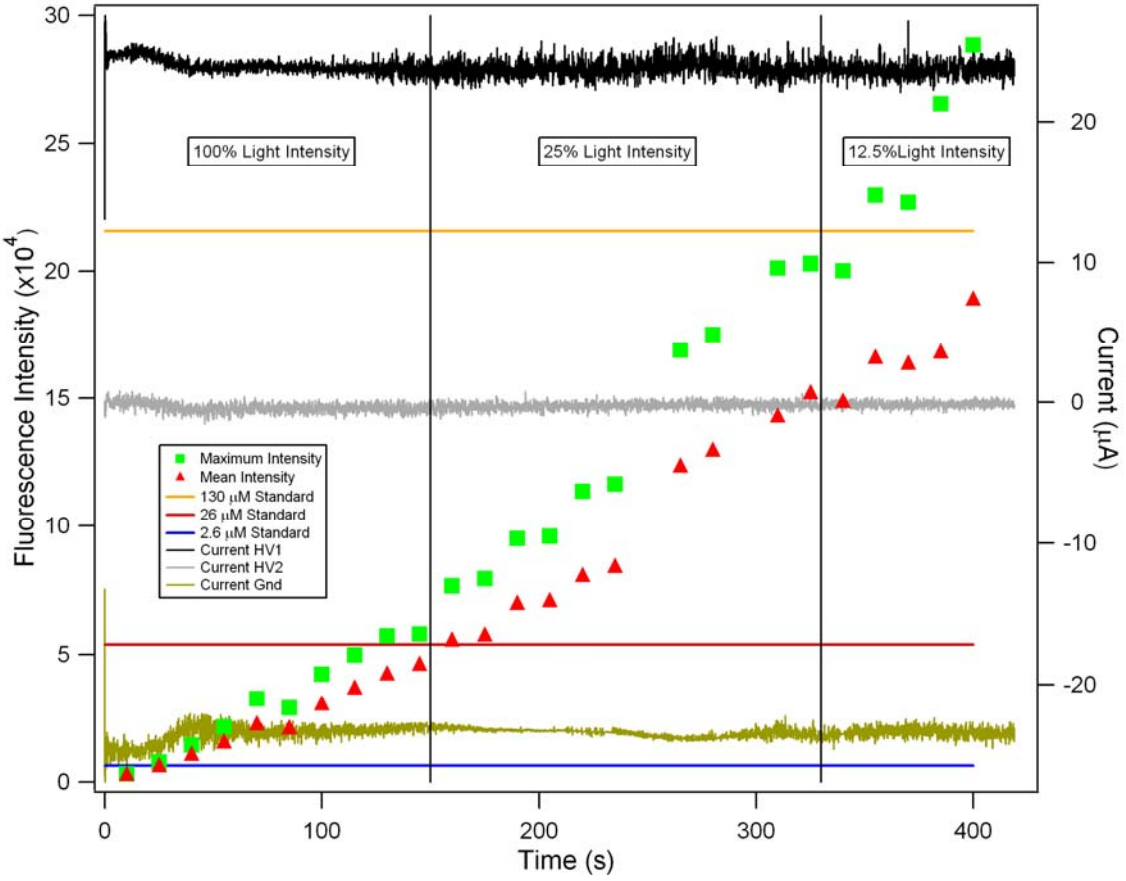

Figure 3.3 - Data showing the preconcentration of DCF in 80 mM Sodium Phosphate (pH = 11.5). Concentration standard values for 2.6, 26, and 130 μM are shown. The light intensity was decreased with a ND4 filter and ND8 filter after 145 s and 325 s, respectively. Current Traces are also shown for the three electrodes used for preconcentration.

The current from the high voltage power supply was monitored and recorded during the concentration enrichment. Figure 3.3 shows that there was virtually no change in the current during the period of concentration enrichment. The current through the membrane during the enrichment period averaged ~23 μA. The slight increase in current at the start of the preconcentration, we believe, can be attributed to the establishment of a small charge depletion zone near the membrane, as previously reported.[59] After the formation of the charge depletion zone, the remaining constant current flow indicated constant flow of the cations, which were carrying the current through the membrane. Further identification of a charge depletion zone was verified by applying a voltage between the two channels on the anodic side of the membrane after a concentration enrichment study. The current measured at the grounded terminal was lower than expected initially and slowly grew to the expected current between the two unobstructed reservoirs. This initial decrease in current was due to the charge depletion zone. Previous reports of microchip preconcentration report mechanisms for preconcentration such as double layer overlap and electroosmosis of the second kind. The preconcentration device used in this report contained a negatively charged membrane. The concentration enrichment that we saw with our membranes was most likely due to Donnan exclusion, which is closely related to double layer overlap. For this mechanism, when the electric field is initiated, solvated counter ions (i.e. cations in this case) freely pass through the membrane. The negatively charged membrane, on the other hand would repel co-ions (i.e. anions in this case), accounting for the concentration enrichment of the negatively charged DCF.

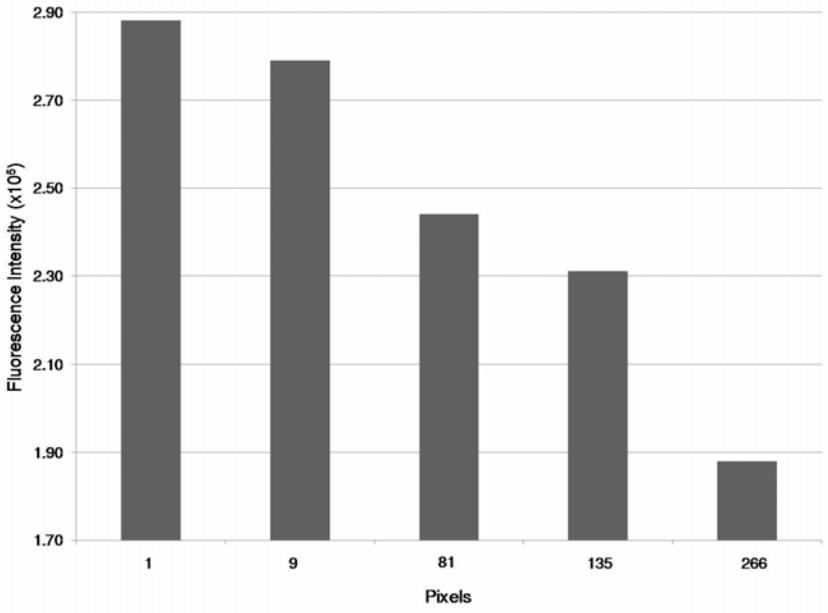

Figure 3.4 - Effect of changing the number of pixels used to measure the concentration enrichment levels.

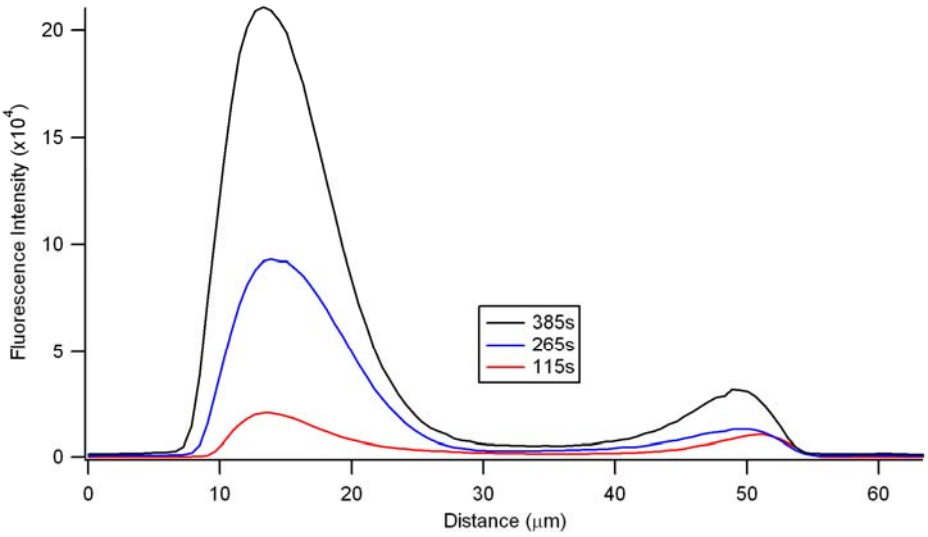

Figure 3.5 - Line scans showing the Gaussian shaped profiles of the enriched DCF

Thicker membranes were fabricated using the same microchip channel pattern. These membranes were fabricated in the same way as the thin membranes but using a 60:40 H_20:IPA instead of a 50:50 solution. Concentration enrichment was performed on

this device in a similar manner as above but with a few differences. For this study, the concentration of DCF was decreased to 10 nM and the ND8 filter was used for the entire length of the preconcentration. The voltages were applied until the intensity reached a plateau. Voltage was then applied to the sample reservoir and the ground electrode was moved to the waste channel (W) to electrokinetically pump the enriched analyte out of the analysis region and to replenish the channels with fresh buffer and analyte for additional analyte concentration studies. This analysis was run in triplicate, and the maximum intensity values are shown in Figure 3.6. The data collected for the thick membrane was acquired with the ND8 filter in the path of the excitation source, so the data was multiplied by 7.34 to correct for the filter. The thicker membrane did not preconcentrate to the same level as the thin membrane. This device concentrated to ~20 μM or by a factor of 2000 in 900 s. This concentration was calculated from a graph of concentration standards that displayed a linear relationship between the analyte concentration and pixel intensity (Figure 3.7). The thick membrane reached a limit to its ability to concentrate analyte as the concentration enrichment reached a plateau after 900 seconds. The data collection was terminated at 1005 s because the rollover in intensity was a common feature in multiple data sets and the error between multiple runs had also decreased which led the authors to believe concentration enrichment had ceased. This limitation was not seen with the thin membranes where the concentration increased until the pixels in the CCD camera were saturated even with the ND8 filter in place. The thinner membrane also preconcentrated approximately 10 times faster than the thick membrane. The preconcentration rate was determined by fitting linear least squared lines to the data in Figure 3.3 and Figure 3.6 and comparing the slopes of the lines.

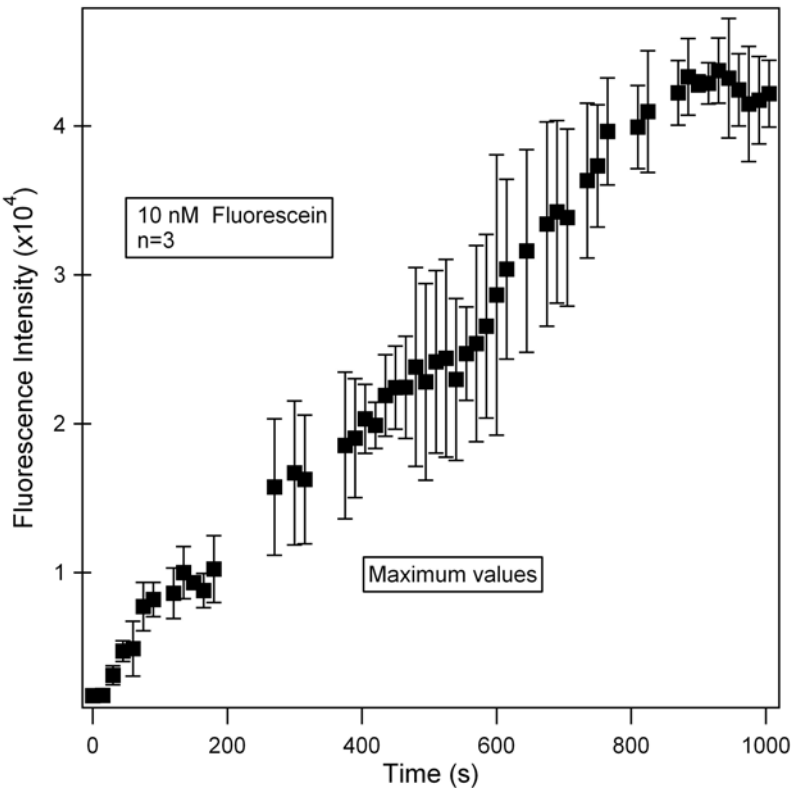

Figure 3.6 - Concentration enrichment profile of 10 nM DCF.

The difference in analyte concentration rates is probably at least partially dependent upon the membrane thickness. Thicker membranes should be more resistant to mass transport of ions through the membrane. If the resistance of the membrane increases the current should decrease in accordance with Ohm's law. The current through the membrane was monitored during the preconcentration with the same voltages applied identically as with the thinner membrane. The current measure through the thick membrane was ~10 μA compared to 23 μA for the thin membrane, a decrease of 57%. The decrease in current through the membrane may account for some or all of the differences seen in the enrichment rates between the thin and thick membranes. Further studies, however, on multiple membranes could be performed to determine the exact relationship.

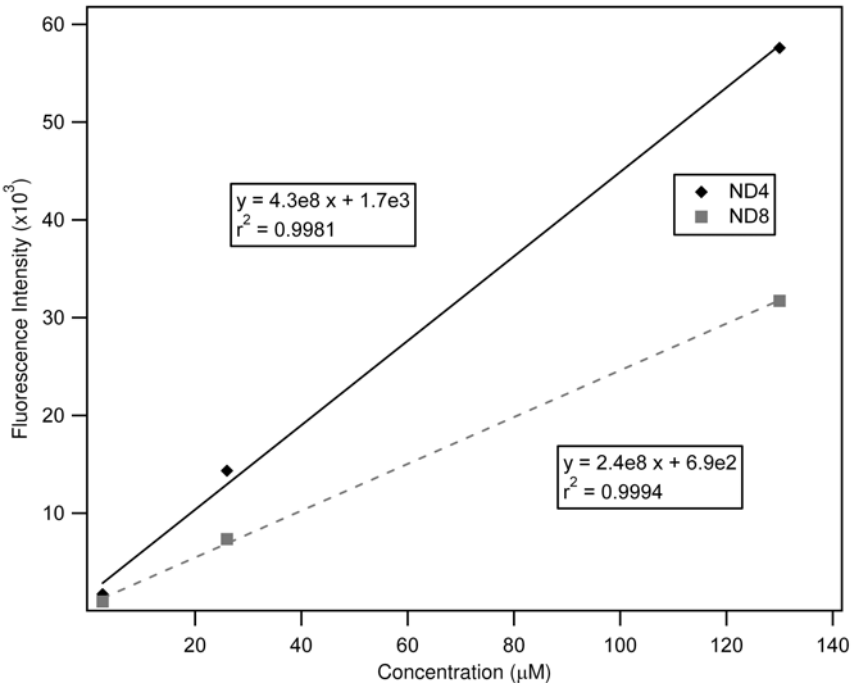

Figure 3.7 - Fluorescence intensity standards for DCF measured with the CCD camera for concentrations of 2.6, 26 and 130 µM.

Finally, it should be noted that the plug of enriched analyte might also be concentrated along z-axis in the channel as well as the x- and y-axis. Because of this possibility, all of the data collected in this study was taken with the z focus at the same location in the channel. Changing the focus point in the channel was seen to affect the intensity as much as 25%.

3.3.3 Ion Selectivity

Other researchers have reported microfluidic preconcentration devices which show cation/anion selectivity. Kim et. al. reported a device which concentrates anionic compounds but does not concentrate cationic compounds.[63] The devices reported above produce interesting results depending upon the charge of the analytes. The titanium oxide based membrane should have a negative charge at pH 11.50.[86] Preconcentration

studies were performed as above, however, using Rhodamine B and Rhodamine 6G (R6G) on the thick membrane. R6G, a cation, did concentrate; however, the enrichment occurred in the membrane and not in a region separated from the titania membrane.

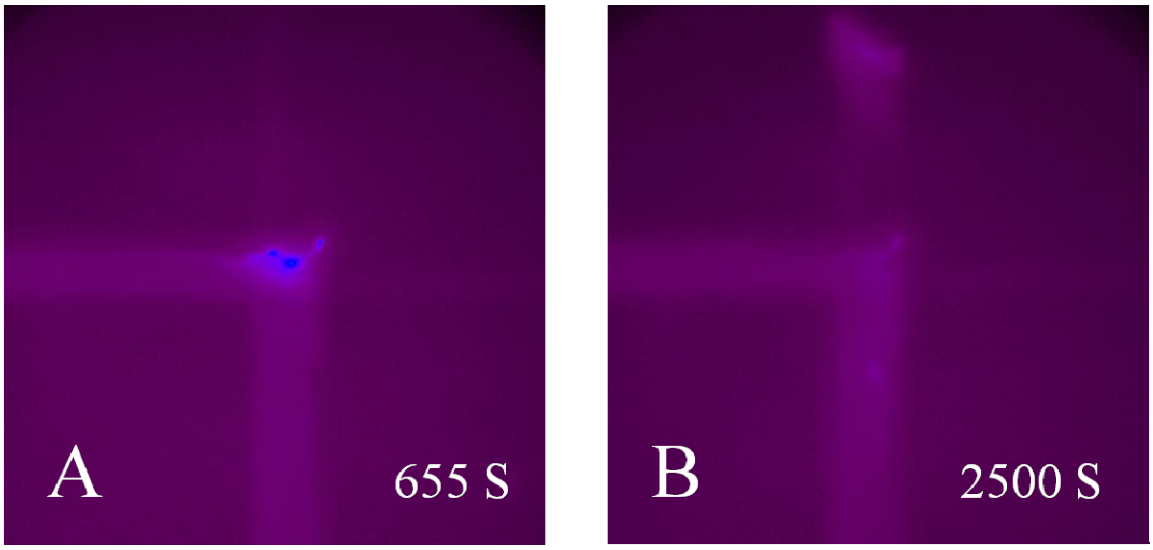

Figure 3.8 - CCD images of the concentration enrichment of Rhodamine 6G (A) and Rhodamine B (B), color artificially added for enhancement.

We believe this was due to the interaction between the positively charged R6G and negatively charged titania surface. This further supports the hypothesis that it was Donnan exclusion that was responsible for the preconcentration. Rhodamine B, a zwitterion, concentrated in a manner similar to DCF. Interestingly, however, the rate of concentration was much slower than that of DCF on the thick membrane. The Rhodamine B preconcentrated to only approximately 15% the level of the DCF in 2500 s i.e. two and a half times longer than for DCF. CCD images of the Rhodamine concentration enrichment is show in Figure 3.8.

3.3.4 Membrane Reproducibility

While the sol-gel based nanoporous membranes reported above were easy to fabricate it was difficult to generate reproducible membrane thicknesses for a given water:IPA ratio. Novel methods to fabricate more reproducible membrane thicknesses are still being investigated. The hydrolysis reaction of $Ti(OPr^i)_4$ and water has many aspects that can affect the resulting membrane quality. Both the $[Ti(OPr^i)_4]$ and $[H_2O]$ affect the membrane. The width of the membrane was easily altered via changing the $[H_2O]$. However, membranes fabricated by the same method often varied in their thickness, their attachment to both the top and bottom of the channel, and even their color/opaqueness. To further optimize the membrane formation it would be helpful to perform further analysis such as to gather SEM images to determine the pore diameter and membrane structure. The membranes, however, are too fragile, and the membrane cannot be accessed in a manner that does not result in its total destruction. With the current configuration therefore, performing such imaging was not possible. Additional chip designs might allow for membrane fabrication where further analysis steps could be achieved. Possible designs might include fabricating a membrane on a glass/PDMS device where the channel and cover plate could be separated. However, $Ti(OPr^i)_4$ readily absorbs into PDMS,[87] and this makes quantifying the amount of precursor that reaches the intersection very difficult.

3.4 Concluding remarks

Analyte concentration enrichment is necessary for many analytical problems. Here we have developed a method to fabricate titania membranes using sol-

gel chemistry in a microfluidic chip. These devices have an increased area at the microfluidic/nanofluidic interface of the preconcentrator, allowing fast preconcentration of analytes via Donnan exclusion. Analyte enrichments of greater than 4000 in 400 seconds were generated.

CHAPTER 4 - **Fabrication and Characterization of Paper Based Microfluidic Devices Used for the Detection of Acetoacetate in Artificial Urine**

4.1 Introduction

Traditionally microfluidic devices are fabricated out of glass or polymer based substrates. Into these substrates micrometer sized channels are etched or molded. These devices have been shown to be very useful for many different applications. Typically, microfluidics device are much less expensive than bench top analytical devices, however, they still require expensive substrates, equipment for fabrication, and detection hardware, limiting their usefulness. A commonly stated goal of microfluidics is to make small devices useful for field analysis. While research using glass and polymer based microfluidics remains very popular, a few groups have begun to examine other materials and approaches to the fabrication of microfluidic devices for field based analysis. One of the most interesting recent approaches is the use of paper as a substrate material. Whitesides and coworkers originally reported the fabrication of paper based microfluidic devices.[88-91] These innovative devices were fabricated by soaking a piece of paper substrate in a photoresist, followed by exposure through a photomask and a developing step to remove uncross-linked polymer. Channels in these devices were defined using the negative tone photoresist SU-8. Several biological assays were demonstrated on these devices. Abe et.al. developed similar paper microfluidic devices, and have fully automated the process by using a inkjet printer to dispense small amounts of toluene onto

polystyrene infused paper. The dispensed toluene selectively dissolves the hydrophobic polymer leaving behind a channel network.

These devices have exciting possible applications in the field of colorimetric biological assays. Glucose, protein, and pH assays have recently been demonstrated on paper microfluidic devices.[88, 89, 92] There are many additional biologically relevant assays that could be performed using this technology.

Assays in which fluid is drawn across a solid porous substrate through the use of capillary pressure are called lateral flow assays (LFA). Most platforms encompass multiple analyte regions for complexation or reaction of analytes with the sample. The resulting product is typically a compound that can be easily detected by the eyes as the result of a visible color change. LFAs that utilize antibody-antigen interactions have multiple names, immunoaffinity chromatography and immunochromatographic chromatography. A common example of one of these devices is the home pregnancy test. Human chorionic gonadotropin (hCG) is a hormone that is secreted by the placenta into the bodily fluids shortly after pregnancy begins. In LFA home pregnancy tests, the hCG is bound to antibodies and indicators to give the user a color change or a small electronic display can indicate a positive test via electrochemical detection.[93, 94] Many LFAs use colloidal gold, detectable by the human eye at high concentrations, modified with surface antibodies which will bind at detection regions to the target molecule for the assay.

At the present, the devices being fabricated have multiple limitations associated with the polymer used for defining the channels on the paper substrate. Some of the limitations include extensive fabrication times, channels too hydrophobic for immediate use, and solvent compatibility. The motivation of this research was to improve the ease

of fabrication and use through the development of a novel polymer for defining the channels. The devices discussed in this chapter have overcome the limitations of the previously reported devices, and have been used to perform novel paper microfluidic assays.

Paper microfluidics devices show great promise in the field of LFA. They can be fabricated very inexpensively and are capable of performing very rapid analysis. The ketone assay devices discussed later in this chapter can be fabricated at a cost of $0.26 per device. The paper devices can be patterned with the necessary channels to carry out multiple assays from a single sample introduction region. This rapidly evolving field has the potential to change the way disease diagnosis and monitoring is performed in developing regions around the world and here at home.

Untreated diabetics often suffer from a condition called Diabetic Ketoacidosis (DKA), where the levels of ketones in the blood and urine are elevated. Low insulin levels decrease the uptake of glucose into cells causing cells to search for alternate energy sources. When the decreased insulin level is detected, the body begins several processes that mimic fasting. Since cell uptake of glucose is prevented, glycolysis also ceases. Now the process gluconeogenesis, the formation of glucose from pyruvate, is accelerated to provide energy to the body. The cells cannot uptake the glucose due to low insulin levels, which is also the reason for increased glucose levels in the body when insulin levels are very low. Pyruvate is a major component of the Krebs cycle and the Krebs cycle is disrupted when pyruvate concentrations are very low. Elsewhere, free fatty acids are converted into acetyl coenzyme A (acetyl-CoA), another reactant in the Krebs cycle. Acetyl-CoA is no longer integrated into the Krebs cycle and instead diverted to

mitochondrial ketone body formation.[95, 96] The ketone bodies produced are acetoacetate and *beta*-hydroxybutyrate. These compounds are used primarily by the brain and heart as an alternate energy sources. If these compounds are created in large quantities the pH of blood is lowered. Blood pH is generally stable, 7.35 - 7.45, and slight changes can cause proteins in the blood to denature resulting in tissue damage. DKA is prominent in type 1 diabetes and can be fatal if untreated. With the increased ketone levels in the blood, ketone levels are also heightened in the urine. Testing urine is less invasive than testing blood and is typically how ketone levels are monitored. For similar reasons increased levels of ketone bodies in the urine are also indications of starvation and low carbohydrate diets. Recently, elevated levels of ketones in the body at the onset of type 1 (insulin-dependent) diabetes have been linked to potential future instabilities in glycemic index.[97] Careful monitoring of DKA can greatly affect future treatments and prevent unnecessary complications.

Other changes in urine may also be monitored for clinical reasons. The pH of urine varies between 8 and 4.5, although it is typically between pH 6 and 7. Changes in urine pH can be indicative of certain health related issues. Changes in the pH can be a sign of different types of kidney stones.[98-101] Decreased urine pH can be an indicator of the most common type of kidney stones, uric acid, while increased pH can be a symptom of calcium phosphate stones.

In this chapter, the fabrication of paper based microfluidic devices is reported. The channels in these devices are defined using a novel photocurable polymer mixture possessing enhanced properties and capable of performing clinically relevant biological assays related to diabetes.

4.2 Materials and Methods

4.2.1 Reagents and Substrates

Two types of paper substrates were used to fabricate the devices reported below, qualitative grade cellulose fiber filter paper (Fisherbrand P8; Fisher Scientific), and Durx® 670 cleanroom wipes (Berkshire; Great Barrington, MA). The cleanroom wipes were composed of 55% cellulose and 45% polyester, and the filter paper was 100% cellulose. The paper products were patterned with different combinations of the following chemicals SU-8 2010 and 2002 (MicroChem Corp; Newton, MA), Zipcone UA, Zipcone UE, methacryloxypropyl PDMS (RMS-033) (Gelest; Morrisville, PA), NOA 74 optical adhesive (Norland Products; Cranbury, NJ), and 2,2-dimethoxy-2-phenylacetophenone (DMAP) (Acros; Geel, Belgium). The ketone assay used the following reagents, ethyl acetoacetate (Aldrich; St. Louis, MO), sodium nitroprusside (Fisher Scientific; Pittsburgh, PA), and glycine (Acros). The target for this assay was acetoacetate, which was synthesized from the ethyl acetoacetate via the saponification of the ethyl acetoacetate with sodium hydroxide. [102] Specifically, 0.45 mL of the ethyl acetoacetate was diluted to a volume of 15.0 mL with 0.2 M sodium hydroxide and placed in the refrigerator for 48 hours prior to use. This assay was to mimic ketone detection in urine, the artificial urine contained 1.1 mM lactic acid, 2.0 mM citric acid, 25 mM sodium bicarbonate, 170 mM urea, 2.5 mM calcium chloride, 90 mM sodium chloride, 2.0 mM magnesium sulfate, 10 mM sodium sulfate, 7.0 mM potassium dihydrogen phosphate, 7.0 mM dipotassium hydrogen phosphate, and 25 mM ammonium chloride dissolved in 18.0 MΩ water adjusted to pH 6.0 with 1.0 M hydrochloric acid.[88] Yamada's universal indicator, 25 mg thymol blue, 60 mg methyl red, 300 mg

bromothymol blue, and 500 mg phenolphthalein dissolved in 500 mL of ethanol and neutralized to a green color with 50 mM NaOH and diluted to 1.0 L with H_2O, was used for pH studies on these devices.[103]

The photomasks used for these devices were low-resolution masks printed on ink-jet transparencies using a Hewlett-Packard printer (HP 1160cp; Palo Alto, CA). The designs were created using either Microsoft PowerPoint (Redmond, WA) or AutoCAD 2006 software (Autodesk, Inc.; San Rafael, CA).

4.2.2 Fabrication of Paper Devices

These devices were initially fabricated on the cleanroom wipes using the SU-8 photoresist to confirm the previous results.[88-91] The method involved cutting 1" by 2" section of the substrate and placing a small amount (~ 0.5 mL) of SU-8 2010 on the paper and rolling out the excess photoresist with a glass stirring rod. This was placed on a hotplate and baked at 130 °C for 10 min to remove the organic solvents and then allowed to cool for 2 minutes. Next the device was exposed to UV light through the photomask using a flood exposure system (ThermoOriel, Stratford, CT), the device received 900 mJ/cm^2. The device was post baked on the hotplate for an additional 10 min at 130 °C followed by cooling at room temperature for 2 min. Finally the device was developed in an acetone bath for 2 min and allowed to air dry. The resulting device exhibited very hydrophobic channels which would not readily wick aqueous solutions. Treating the devices with an oxygen plasma cleaner for 1 minute increases the hydrophillicity of the channels. The same fabrication method was used on other substrates and the results will be discussed later in this chapter.

Paper devices were also fabricated using novel polymeric materials. Initially, devices were fabricated with commercially available UV curable acrylate functionalized silicone using a similar fabrication process. The baking steps were unnecessary as the polymer is not solvated in organics. The mask was placed directly on the liquid polymer and UV exposure induced polymerization. Exposure was followed by development in acetone. Different polymer compositions were tested and the results will be discussed later in this chapter.

4.2.3 Flow Directionality

The cleanroom wipes are composed of cellulose fibers hydroentangled with polyester fibers. The manufacturer's fabrication of these devices imparts a machining directionality onto the product. Striations are created on the cellulose side of the cleanroom wipe, exhibiting increased fiber density. In order to study the fluid flow characteristics multiple devices were fabricated from different designs where there was a main flow channel that branched into multiple channels at different angles. An example of photomask used to fabricate these devices is shown in Figure 4.1. The main channel was always aligned with the paper striations and the flow into the side channels was measured as a ratio compared to the area filled in the coaxial channel.

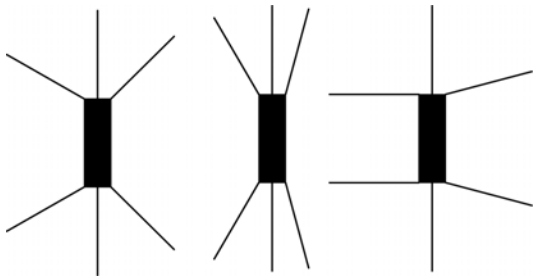

Figure 4.1 - Photomask used for flow directionality studies on cleanroom wipes

4.2.4 Ketone Assay

The presence of acetoacetate in artificial urine can be detected from the complexation of the analyte with sodium nitroprusside. To enhance the assay the analyte first reacts with glycine to form an imine, which causes a more intense color change when it reacts with the nitroprusside.[102] The reaction scheme is shown in Figure 4.2.

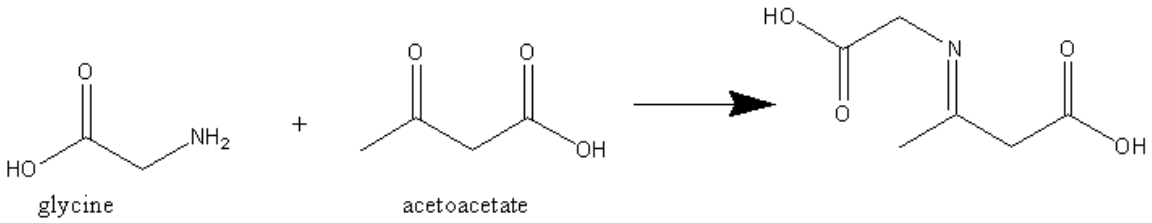

Figure 4.2 - Reaction of acetoacetate with glycine

Previous reports state that the glycine and nitroprusside will react without the presence of acetoacetate, causing the premature decomposition of the nitroprusside salt.[104] This two step scheme created the necessity for a derivatization zone on the device where the acetoacetate could react with the glycine prior to complexation with the nitroprusside salt. Figure 4.3 shows the channel dimensions used for this device. First a 0.700 μL aliquot of 5.0% sodium nitroprusside (w/w) in 5.0% dimethylformamide (DMF) (v/v) in H_2O was deposited in the circular detection pad. Next, a 0.700 μL aliquot of 100 mM glycine in 100 mM phosphate buffer (pH 9.4) was dispensed into the middle derivatization zone. Both areas were allowed to dry for 5 minutes prior to sample spotting. The acetoacetate sample from the refrigerator was diluted into the artificial urine before use. Upon use, 10 μL of sample was placed into the sample region on the right and allowed to migrate towards the derivatization zone and finally to the detection pad. The device was allowed to dry in room temperature air before analysis.

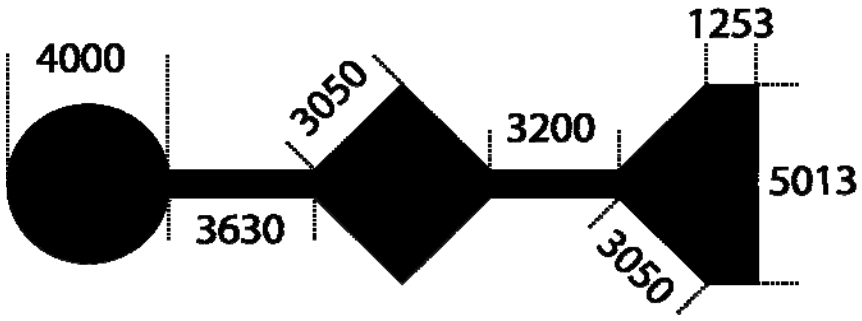

Figure 4.3 - Channel design used for the ketone assay, all measurements in microns and the channel width was 700 µm, created in AutoCAD

4.2.5 pH Assay

The device fabricated for this test consisted of single channels with triangle shaped detection regions. The Yamada universal indicator was spotted in this triangle region and allowed to dry twice. Aliquots of 0.3 µL were spotted each time. When ready for use 5 µL of sample was deposited onto the spotting region and allowed to migrate towards the detection pad. The color change is immediate and some of the colors decay with time. Slightly wet samples were scanned with the desktop scanner without damage.

4.2.6 Multilayer Devices

Devices were also fabricated similarly to previously reported multilayer paper devices.[90] These devices were made from two separate pieces of patterned paper. The top layer was patterned with two unconnected channels separated by ~7.0 mm and the bottom later with a connecting channel. The ends of the connecting channels had small circular regions, ~4 mm diameter, to increase the overlap of the channels. The bottom layer was adhered to a glass slide with double stick tape. Another section of tape, of similar length, had access holes created with a biopsy punch above the ends of the single channel and was placed above the bottom layer. Small amounts of cellulose fibers were

compressed into circles approximately 4 mm in diameter and less than 1 mm thick. These were placed above the terminal ends of the single channel where the double stick tape had been removed. Finally, the top layer was properly aligned and adhered to the bottom layer. An aliquot of dyed H_2O was added to one end of the multilayer device and the fluid migrated, was transported to the bottom channel, and back to the other end of the top layer, with no noticeable leaking.

4.2.7 Measurements and Data Processing

Optical micrographs for the flow directionality studies were captured using a digital camera (DS-5M; Nikon; Japan) attached to a camera port on a stereomicroscope (SMZ-1500; Nikon). Area calculations were made using Image J (NIH). The images for the ketone assay were captured on a color flat bed scanner (ScanMaker 4900; Microtek International; Hsinchu, Taiwan). The images were processed using Photoshop CS4 (Adobe Systems Inc.; San Jose, CA). The images were converted to CMYK color profile and the integrated color density was measured over the area of the detection region. The resulting integrated densities were subtracted from the blank and multiplied by negative one to achieve positive values; these values are the adjusted integrated densities (AID). These values were plotted against the concentration of the analyte and fitted to a quadratic fitting function using Igor Pro (WaveMetrics Inc.; Lake Oswego, OR).

4.3 Results and Discussion

4.3.1 Optimization of Paper Devices

Initial reports describing the fabrication of paper microfluidic devices used the negative tone SU-8 photoresist to pattern the channels in the paper. Fabricating devices

using this method heeds some limitations including long fabrication times and the additional step of oxygen plasma treatment to create hydrophilic channels. The goal of this research was to find a new more promising polymer that no longer had the limitations associated with the SU-8 patterned paper. SU-8 photoresist contains a photo initiator that catalyzes a polymerization reaction upon exposure to UV light. In our search for a more suitable polymer we looked at other chemicals that can undergo photo initiated polymerization. Gelest, a common manufacturer of silicon based polymers and monomers, produces multiple acrylate and methacrylate modified silicones that undergo photo initiated polymerization.

Initially, these devices were fabricated with the protocol explained in this chapter using the Zipcone UA. To examine the integrity of the channels H_2O, dyed with food coloring, was added to the channels. Extensive leaking outside the channel boundaries was noticed. Inspection with a microscope showed non-uniform polymer coating of the substrate attributed to small pores in the cross linked polymer. However, one immediate advantage was noticed, there was no need for oxygen plasma treatment, i.e. aqueous solutions wicked immediately into the substrate. In an attempt to increase the homogeneity of the polymer coating, excess polymer was no longer removed with a glass rod prior to exposure and the exposure energy was decreased from 900 to 225 mJ/cm^2. The result was a uniform polymer covering, still on the order of the paper thickness. Care was taken to remove any air bubbles between paper substrate and the bottom glass slide or the photomask. Addition of fluid now showed complete retention in the patterned channel. These devices were fabricated with large channel widths, ~1.5 mm, in optimized devices smaller channels are desirable as they decrease the necessary sample

size. Smaller channels (50-200 μm) were patterned from a high resolution photomask, and the features were not resolved after developing. This was attributed to over exposure, and the exposure energy was decreased to 135, 90 and 45 mJ/cm^2. At 45 and 90 mJ/cm^2 the excess polymer was not sufficiently cross linked. Exposure energies of 135 mJ/cm^2 resulted in devices where small 200 μm features could be patterned, however we noticed that after just a few hours of sitting at room temperature the polymer began cracking extensively. This was also associated with a curling of the device, attributed to the polymer shrinking. Additionally, the devices were not flexible, as any torque applied, caused severe cracking of the polymer. These attributes were unforeseen and made the devices not applicable for paper microfluidic devices.

In a second attempt to produce an acceptable photocurable polymer, a different formulation for a photocurable PDMS was found on an internet blog.[105] This polymer comprised 10 g of methacryloxypropyl functionalized PDMS (RMS-033, Gelest; Morrisville, PA) mixed with 200 mg of 2,2-dimethoxy-2-phenylacetophenone (DMAP, Acros; Geel, Belgium) dissolved in 400 mg xylenes. Devices were fabricated with this polymer using the same method as the Zipcone UA. Different energies were used for the crosslinking of the polymer (225 – 450 mJ/cm^2), but all of the resulting devices exhibited very hydrophobic channels which would not wick fluid, and decreased channel definition compared to the Zipcone UA devices. The crosslinked polymer had a very tacky surface. It was, however, much more flexible and did not crack or curl after curing and sitting at room temperature. These properties and the fact that it was a methacrylate functionalized silicone lead to a third polymer formulation attempt, a mixture of the Zipcone UA and this RMS-033/DMAP mixture. These two polymers were mixed at different weight

percents and patterned on the cleanroom wipes. The resulting polymers took on the properties of the major component in the mixture, i.e. the mixtures high in zipcones had too much cracking and mixtures higher in photocurable PDMS resulted in hydrophobic channels.

A fourth polymer formulation was then attempted using photocurable adhesives manufactured by Norland Optical Adhesives (Cranbury, NJ). One product NOA 74 contained a mixture of isodecyl acrylate (15-35%), trimethylpropane polyoxypropylene (4-15%) and a mercapto-ester (43-65%). The exact mercapto-ester is unknown as it is a trade secret. Devices were fabricated with the same protocol as above, however, the optical adhesive adhered the photomask to the paper device. Separation of the mask from the paper device resulted in damage to the substrate, but selective polymerization was demonstrated.

As in previous attempts, the NOA 74 adhesive was mixed at specific weight percents with the Zipcone UA. Devices fabricated with this mixture exhibited promising properties. The resulting polymer did not adhere to the photomask, so the already inexpensive ink-jet printed transparencies could be cleaned and reused. They must be cleaned because the area below the opaque regions of the mask has uncured polymer but it can easily be removed by swabbing with acetone. Only small amounts of polymer were needed for the fabrication of these devices, but the amount is dependent on the paper substrate used. The polymer amounts were optimized and the devices required 25 and 30 $\mu L/cm^2$ for the filter paper and cleanroom wipes, respectively. These devices exhibited very hydrophilic channels, well defined channel dimensions, fabrication times

from start to finish of less than 3 minutes, and required only 53 mJ/cm^2 of energy for crosslinking. These devices looked very promising.

4.3.2 Characterization of Paper Microfluidic Devices

Fluid flow on these devices was dependant on the paper substrate, and for the cleanroom wipes the directionality of the paper striations. The cleanroom wipes, made of polyester and cellulose, have a directionality associated with the wipe. These devices are hydroentangled 55% cellulose and 45% polyester. The hydroentangling process creates "striations" in the paper substrate. The striations are high density areas of fibers. The striations play an important role in the flow characteristics on the paper fluidic devices. According to Giddings,[1] fluid flow in paper and thin layer chromatography is driven by the capillary pressure;

$$\Delta p = \frac{2\gamma}{r} \tag{4.1}$$

where γ is the surface tension and r is the radius of curvature of the advancing fluidic meniscus. An assumption can be made that the paper products can be modeled as a simple bed of capillaries with similar capillary radii, r_c. For this application r_c would be half the distance between adjacent fibers. If the advancing meniscus had zero contact angle then $r = r_c$, and if there was a contact angle, θ, then $r = r_c \cos\theta$. Giving the capillary pressure;

$$\Delta p = \frac{2\gamma\cos\theta}{r_c} \tag{4.2}$$

Average flow velocity, $\langle v \rangle$, through a capillary is defined as:

$$\langle v \rangle = \frac{\Delta p r_c^2}{8L\eta} \tag{4.3}$$

where $\Delta p/L$ is a constant pressure gradient in the capillary and η is the solution viscosity. Combining equations 4.2 and 4.3 and replacing L with the distance the fluid has traveled, X_f, the following equation is obtained for fluid velocity in a paper device;

$$\langle v \rangle = \frac{r_c \gamma \cos\theta}{4 X_f \eta} \tag{4.4}$$

Therefore velocity is directly proportional to the distance between fibers in a paper microfluidic device, and decreases as the fluid travels further into the channel. Velocity can be defined as distance traveled per unit time, so equation 4.4 can be rearranged to;

$$X_f \frac{dX_f}{dt} = \frac{r_c \gamma \cos\theta}{4\eta} \tag{4.5}$$

If equation 4.4 is integrated with the assumption that the distance traveled is zero at time zero, then distance traveled in a device is given as;

$$X_f = \sqrt{t\left(\frac{r_c \gamma \cos\theta}{2\eta}\right)} \tag{4.6}$$

Some terms in equation 4.6 will be the same for devices fabricated on different substrates, i.e. all devices are used with aqueous solutions and both materials are made of hydrophilic materials, so the surface tension, meniscus angle and viscosity should be similar for all devices. Therefore the only aspect that should affect fluid velocity and distance of travel is the effective distance between the fibers.

The difference in fluid flow was initially noticed with devices fabricated with channels in the form of a cross with equal lengths extending from a central pad, as shown in Figure 4.4 A. When fluid was added to the central reservoir the channels parallel to the striations filled approximately 3 times faster.

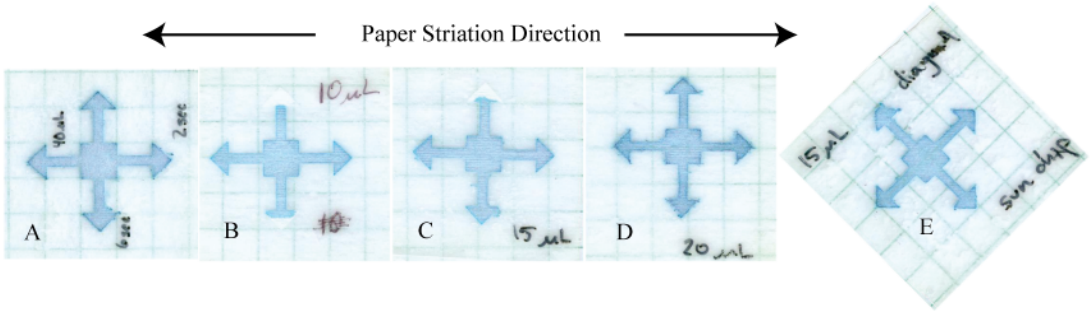

Figure 4.4 - Demonstration of fluid flow distance and speed vs. cleanroom wipe striation direction.

On the same devices, 10 µL of fluid would completely fill the parallel channels whereas 20 µL was required to fill all of the channels. When all the channels were oriented at 45° from the fibers, the channels all filled at the same rate and only 15 µL was required to fill all the channels.

In order to further examine this fluid flow behavior, devices were fabricated with the dimensions shown in Figure 4.1. The ratio of fluid flow into a perpendicular channel compared to parallel channel for widths of 500, 700 and 1000 µm was approximately 50%. As the fluidic interface meets the striations in the cleanroom wipe the distances between fibers decrease which also decreases the velocity. This, in turn, decreases the distance traveled. Generally, as the angle between the fiber and channel decreased, the flow ratio increased.

Fluid velocity was also measured as a function of spotting volume on devices with a long (17 cm) serpentine channel. This channel design was fabricated on both paper substrates. For the case of the cleanroom wipes, the paper striations were oriented at 45° from the long channel portions to minimize the time fluid would flow across the striations. Different fluid amounts () were added to the reservoirs and the flow distance was measured as a function of time on both paper substrates. The final flow distances

were 4.46, 4.44, 4.22, 7.94, 9.90, and 10.81 cm for 20, 30 and 40 µL depositions on the FP and CRW, respectively. Figure 4.5 represents the distances measured with Image J software for the different fluid volumes and paper substrates. These flow characteristics confirm the theory outline above. As the fiber density increased the flow velocity and distance the fluid traveled decreased. The flow velocity and distance were initially defined as a function of the pressure on the capillary. This pressure was the external atmospheric pressure forcing the fluid into the paper channel. In these devices the channels were defined on both sides of the paper affecting the applied pressure.

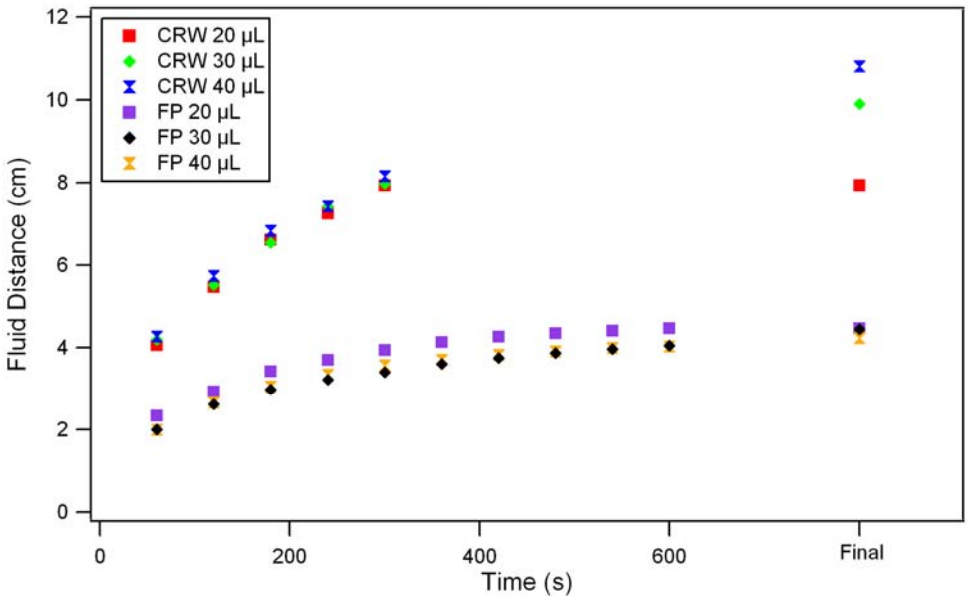

Figure 4.5 - Fluid distance traveled as a function of spot volume vs. time for 17 cm serpentine channels fabricated on cleanroom wipes (CRW) and filter paper (FP).

When a fluid is dispensed onto the spotting region of the device, not all of the fluid immediately flows down the channel. Especially for large volumes there is a bead of fluid formed at the reservoir, and this bead forms on top and bottom of the device. Due to gravity there is an increased bead of fluid on the underside of the horizontally

positioned device. This effectively reduced the capillary pressure. For the cleanroom wipe the flow velocity was much higher, which decreased the effect this lowered capillary pressure has on the flow characteristics. Conversely, the filter paper with its decreased velocity was affected by this to a much larger extent. The volume spotted was proportional to the size of the bead formed on the bottom of the device; therefore the larger volumes had an increased negative pressure gradient at the channel head. This was one reason the larger volumes exhibited decreased flow distances. Evaporation is another factor that affects the flow distance, and increasing flow times are increasingly affected by evaporation. However, increased flow distances also increase the surface area which also increases the speed of evaporation. So evaporation affected the flow distances on both substrates, but in different ways.

After polymer optimization and flow characterization, the limiting channel features and densities were measured. A photomask was created in AutoCAD to mimic a previously used design to define the limiting channel dimensions and densities.[91] The photomask used is shown in Figure 4.6.

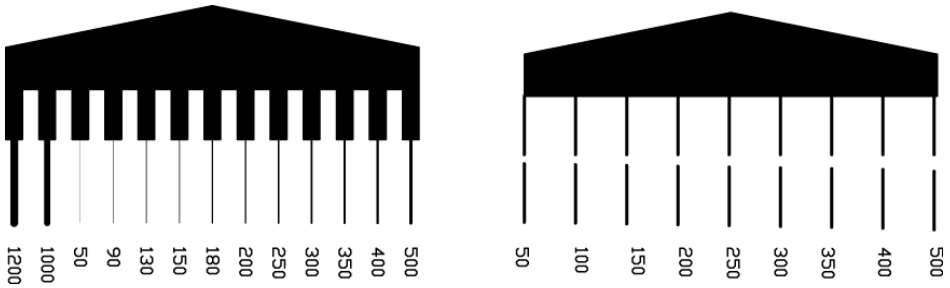

Figure 4.6 - Photomask design used to measure channel and barrier feature dimensions, the units are in microns

The channel dimensions were verified using a microscope and computer software. This pattern was fabricated on filter paper and cleanroom wipes where the striation

directionality was both parallel and perpendicular to the fluidic channels. To test for fluidic patterning 35 mL aliquots of dyed H_2O were added to these devices and allowed to sit for 15 minutes. Upon inspection the minimum channel features that filled with fluid were 90 µm, 130 µm, and 90 µm and the minimum barrier width was 500 µm, 300 µm, and 150 µm for the cleanroom wipe parallel to striation orientation, cleanroom wipe perpendicular to striation, and the filter paper, respectively. The major difference in these characteristics was the barrier width. This difference was attributed to the striation. There were instances where fluid flow along fibers in a striation was noticed transporting the fluid to the other side of the barrier. The ability to fabricate devices with higher channel densities is advantageous as it decreases the overall size of the necessary device. The filter paper also had a higher degree of definition in the channel walls.

4.3.3 Ketone Assay Results

This assay was designed to measure acetoacetate, a chemical commonly found in the urine of a diabetic. The acetoacetate was synthesized as discussed earlier and diluted into the artificial urine at 16 mM, and serial diluted to 8, 4, 1.5 and 0.5 mM. These assays were carried out on devices fabricated from the design in Figure 4.3, on the filter paper. Filter paper was chosen because of the decreased flow velocity, giving added time for the complexation of acetoacetate with glycine. The paper absorbed the sample fluid almost immediately, however, the channels required 15 minutes to dry, and additional time for the colors to develop. Figure 4.7 represents the same assay chip at different times. The reaction kinetics have previously been studied in great detail,[102] but the studies were carried out in solution and since these devices were allowed to dry the kinetics were affected.

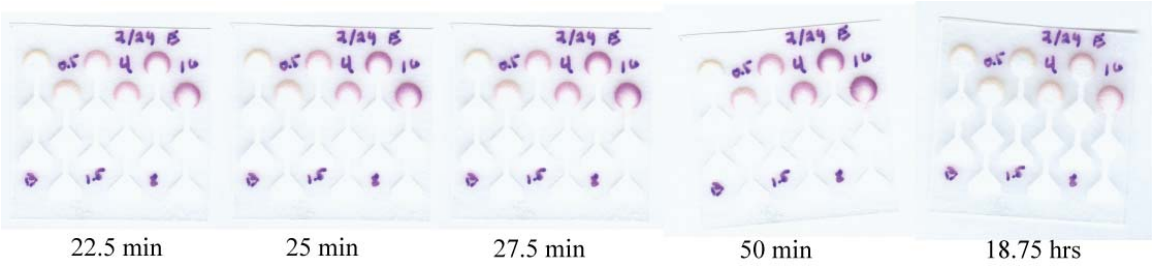

Figure 4.7 - Scanned images of the ketone assay devices at varying times

The areas of the detection pads were measured using Adobe Photoshop and the adjusted integrated densities (AID) were plotted against sample concentrations. Triplicate measurements were performed and are shown in Figure 4.8. The data was fitted to a quadratic fit, the equations and correlation coefficients are shown in Table 4.1.

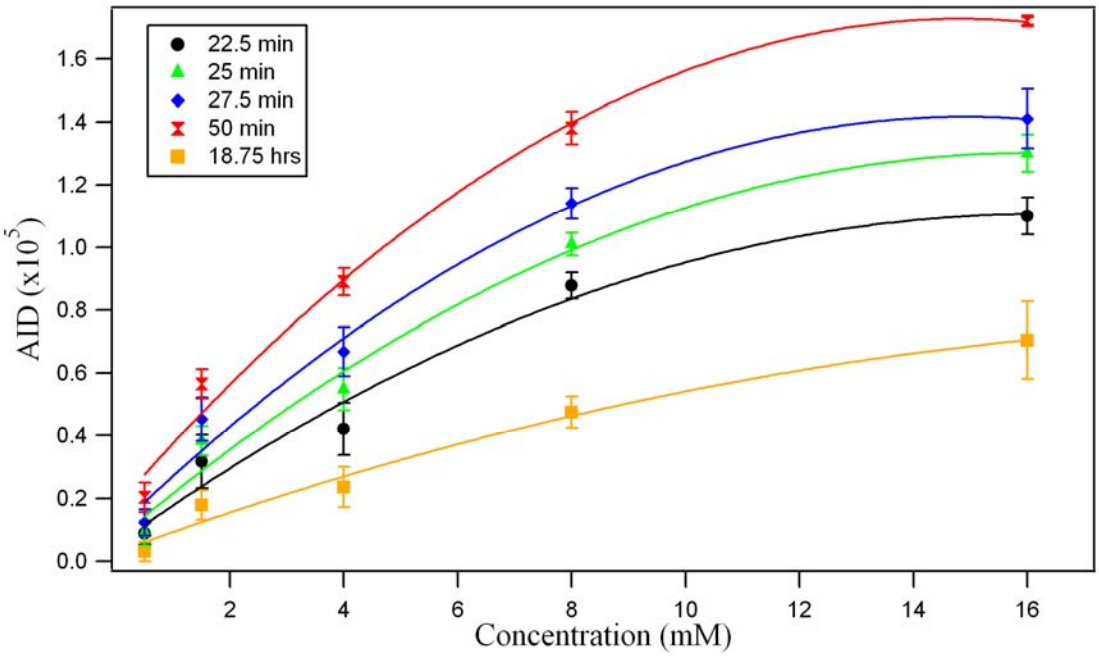

Figure 4.8 - Ketone Assay, measured AID for known acetoacetate concentrations as a function of time, n = 3.

Time	*Quadratic*	*Linear*	*Constant*	r^2
22.5 min	-4.04E+08	1.30E+07	5.12E+03	0.976
25.0 min	-4.81E+08	1.54E+07	6.67E+03	0.983
27.5 min	-5.92E+08	1.77E+07	1.00E+04	0.984
50.0 min	-7.08E+08	2.10E+07	1.73E+04	0.990
18.75 hrs	-1.51E+08	6.66E+06	2.77E+03	0.981

Table 4.1 - Quadratic fitting information for the ketone assay results in Figure 4.8

The measured values changed with time as expected from previous reports. The results from a kinetic study of the measured AID versus time for a 16 mM acetoacetate sample are shown in Figure 4.9. There was a definite change in measured AID, as a function of time for this assay; however, after approximately 40 minutes the change in signal was minimal.

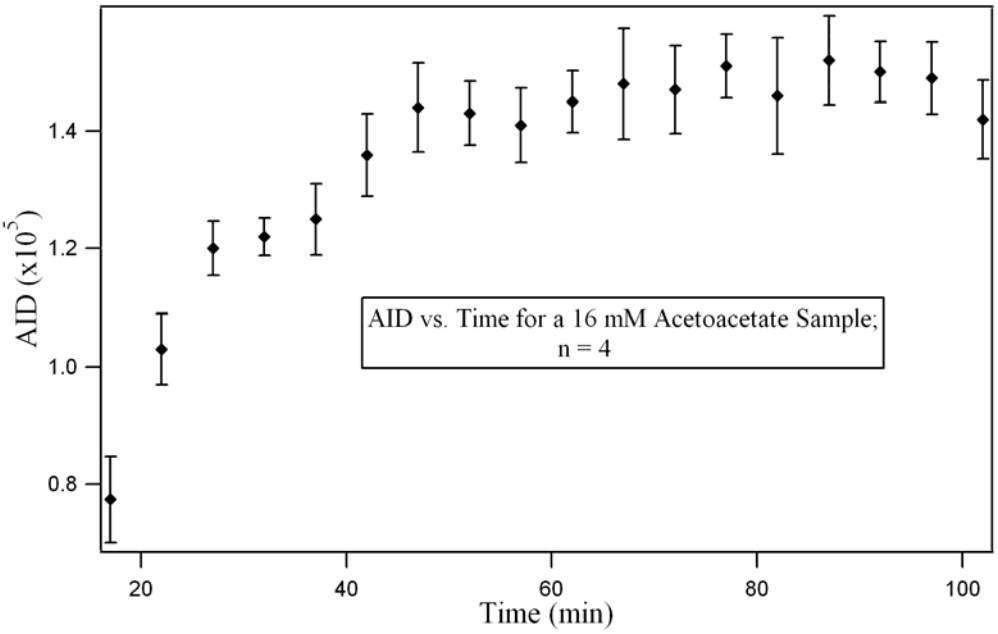

Figure 4.9 - Kinetic study for ketone assay

We have demonstrated the ability to semi-quantitatively measure the acetoacetate levels in artificial urine using paper microfluidic devices. The time between sample

introduction and measurement play an important role in the assessment of ketone levels. From the kinetic study it appears that after approximately 40 minutes major changes in the color have ceased and appropriate measurements can be made.

4.3.4 pH Assay Results

One of the additional goals of paper microfluidic devices is to increase the number of different assays performed on a single device. The ability to perform the multiple assays from a single sample could greatly decrease disease diagnosis time for health care professionals. Another assay that could be easily performed on urine sample is pH. Devices were fabricated as described earlier in this chapter. An example of the assay detection region is shown in Figure 4.10. The color changes for the pH assay were immediate, making the measurement difficult due the wet substrate. In Figure 4.10 the top portion is a scanned image acquired only 2 min after spotting of the sample, while the channels are not completely dry. The color differences are most noticeable at this point. When the channels are allowed to dry completely, the color changes are no longer distinguishable. This coincides with the definition of pH; a measurement of the concentration of hydrogen ions in solution. There was no attempt to quantify this assay, as this is only a qualitative technique. The pH device demonstrated similar capabilities compared to traditional pH paper, in distinguishing the difference of solutions in this pH range.

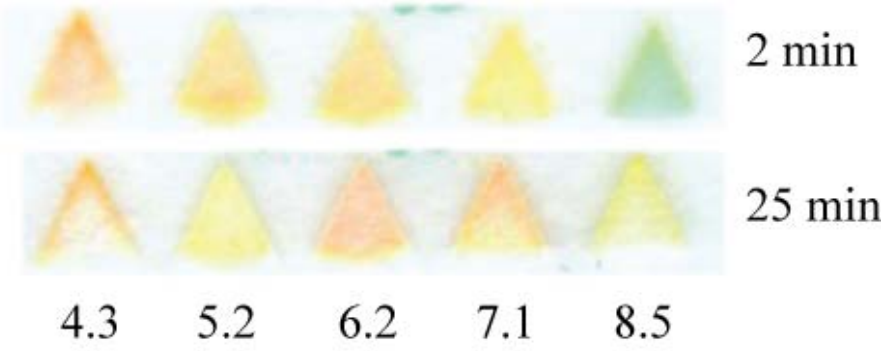

Figure 4.10 - Results from the pH assay on a paper microfluidic device with the corresponding pH's

4.3.5 Advantages of New Devices

This new blend (50:50; Zipcone UA: NOA 74) of commercially available polymers that has been used to fabricate paper microfluidic devices has a few major advantages over the previously reported devices. The first advantage is the speed of fabrication. Compared to the SU-8 paper devices fabricated by Whitesides and coworkers, these devices can be fabricated in approximately 3 minutes, almost ten times faster.[88-91] Abe et. al. reported devices requiring even more time, over 2 hours, from start to finish.[92] The speed is an important advantage, but probably not the most important. These new devices obviate the need to treat the channels with an oxygen plasma cleaner to create hydrophilic channels. This requirement makes field analysis unrealistic. Infrastructure needed to operate such instrumentation is not common in remote locations. The decreased energy required for polymerization is also a potential advantage. From the standpoint of green living lower power consumption is inherently better for the environment. Again, considering usage and fabrication in remote locations, high intensity UV light sources require considerable power and cost, which could be

problematic. One previous report does include using natural sunlight, 6 min at 12 p.m. on June 25, 2008, as the polymerization source.[91] The device shown in Figure 4.4 E was polymerized in natural sunlight for 100 s at 4 p.m. on January 30, 2009. The decreased light intensity, from the sun, does increase the polymerization time compared to in-lab fabricated devices, but our devices are again fabricated much faster. The future applications for these devices are still being examined. Although the currently reported uses all relate to biological samples this will most likely change with extension to other scientific fields. The devices fabricated with the polystyrene infused paper would have limited application to aqueous based uses, whereas these new devices have shown compatibility with common organic solvents.

4.4 Concluding Remarks

The development of new paper based microfluidic devices with improved characteristics has a promising future in the field of clinical analysis of common biological relevant samples. Understanding the fluidic flow parameters, dependent on the paper substrate chosen, allow for the correct design of future applications and assays. For example, a future application may require rapid fluidic transport and a substrate with large pore/fiber distances would be required.

CHAPTER 5 - **Surface Plasmon Resonance Detection of Proteins Using a Titanium Dioxide Modified Surface**

5.1 Introduction

5.1.1 SPR Background and Significance

Proteomics, the study of global protein expression in cells, is of great interest to a variety of researchers studying the etiology of diseases. Many diseases result (or manifest themselves) due to changes in protein expression. A better understanding of how protein expression changes during the development of a disease would allow both earlier diagnoses and identify potential target molecules for treatment. There is considerable interest in understanding how protein expression changes. Proteins can be detected by a variety of methods and techniques. In proteomics, some methods for studying proteins are 2-D gel electrophoresis and Mass Spectrometry, these techniques, however, are time consuming and very expensive.[106] Other techniques such as refractive index detection or UV/Vis are less expensive but have limitations. Typical refractive index (RI) detectors tend to have the poorest sensitivity with detection limits in the high μM range, and UV/Vis absorbance detection at 200 nm in the low μM range. There is at present no sensitive, universal method for detecting proteins which are separated via CE or high-performance liquid chromatography (HPLC). In this chapter we report our attempts at a method for the sensitive detection of proteins using surface plasmon resonance (SPR), where the SPR will be used as a RI detector. Refractive index (η) is

the relationship of how fast light travels in different mediums (υ) when compared to its speed in a vacuum (c) :

$$\eta = c/\upsilon \tag{5.1}$$

Any change in the properties of a medium will change its optical properties and give a refractive index change. While SPR has been traditionally used to monitor specific ligand-analyte and antibody-antigen interactions[107-109] it can be modified for use as a bulk refractive index detector. This method would obviate the need to label analytes and worry about multiple labeling issues. This could potentially allow for lower limits of detection (LOD), which is necessary in the fields of disease research, where protein expression is altered and researchers desire the ability to detect low concentrations and small concentration changes of these proteins over time. There are problems involved in detecting proteins at these at low concentrations such as the inherent nature of proteins to adsorb to surfaces. Although universal detectors exist in the form of RI and UV/Vis absorbance, they tend to lack the sensitivity necessary to detect low abundance regulatory proteins.

The goal of this research was to create a novel protein resistant surface on a gold substrate to use as a sensitive label free SPR detector of proteins at the end of a microfluidic channel. In order to realize a sensitive, robust, universal SPR detector for proteins we needed to minimize the protein adsorption. Many different researchers have shown the ability to prevent protein adsorption onto surfaces. When dealing with gold as the surface, Whitesides and his group found that the use of ethylene glycol terminated thiol molecules work the best. It is known that thiol compounds tend to form Self Assembled Monolayers (SAM) when placed in the presence of a gold surface. The use of ethylene glycol SAM's will lead to a moderately hydrophilic surface as well as a surface

that has been shown to be biocompatible, which would complement its use for protein detection.[110-115] The synthesis of SAM's is a simple process, and allows for tailoring of the SAM along the way so their properties can be changed for different chemical applications. The basic formula of the thiol compound that we were interested in is: $HS(CH_2)_m(OCH_2CH_2)_nOH$. Changing the number of CH_2 groups in the alkane chain can drastically change the physical properties of the SAM.[110] When $m \geq 10$ the region of the alkane chain tends to be completely trans-extended, this is an attractive property so the formed layer will have a uniform thickness.[110] Pale-Grosdemange et. al. have shown that changing the number of ethylene glycol units that terminate the alkane chain changes the properties of the SAM as well, and their experiments have shown that $n = 3$ is the optimal number of units to prevent protein adsorption and for ease of synthesis.[110]

The novel surface that will be discussed in this chapter is a TiO_2 thin layer terminated with the similar ethylene glycol groups to prevent protein adsorption. An additional goal of this project was to increase the sensitivity of the detector. Sensitivity could be increased by terminating the protein resistant surface with a stationary phase, to transiently preconcentrate the analytes near the surface to increase the LOD, creating a more sensitive detector.

5.1.2 SPR Theory

SPR is a very sensitive detection method for many substances, including proteins. SPR works by monitoring the refractive index within ~200 nm of a gold-dielectric interface. The detection volume can be a continuously flowing solution above the surface or a patterned surface that allows ligand-analyte interactions. The detection takes place

by focusing a laser line onto a gold surface, an IR laser in this case. The light is focused in such a way that it impinges upon the surface at many different angles of incidence, and the reflection of the light is monitored by an array detector. There are two instrumental setups for SPR. One method uses a laser which is scanned through different angles and the resulting reflection is collected with the detector. The second method employs optics which allows the laser light to interact with the surface at many angles simultaneously, and the array detector monitors the reflectance at each angle. The second method was used for this research. When the light interacts with the surface it is possible for the light to cause the free electrons on the gold surface to oscillate in resonance with the incident light. These oscillating electrons are called surface plasmons (SP). SP's can have different energies that are dependent upon the dielectric function of the metal (ε_m) and the adjacent medium (ε_d), as shown by this equation:

$$k_{sp} = \frac{\omega}{c}\sqrt{\frac{\varepsilon_m \varepsilon_d}{\varepsilon_m + \varepsilon_d}} \qquad (5.2)$$

In the equation, k_{sp} is the wave vector of the SP, ω/c is the wave vector in a vacuum, and the dielectric constant is the square of the index of refraction.[109, 116-118] One common way to excite surface plasmons occurs when the dielectric functions of adjacent mediums are of different signs. For example gold has a negative dielectric function, and water has a positive dielectric function. This is why these two substances are most commonly used for SPR. The laser light used to excite the SP must be p-polarized light, and must be coupled to the surface via a prism. This is because light must impinge on the surface at an angle that is beyond the critical angle (θ_c) for a glass/air interface, defined from Snell's law as:

(5.3) $$\theta_c = \sin^{-1}\left(\frac{n_2}{n_1}\right)$$

where n_1 is the RI of the denser medium and n_2 is the RI of the less dense medium. The electric component of the p-polarized light must be in the same plane of incidence with the gold surface to initiate SPs on the surface. Laser light is usually coupled to the surface using a prism in what is known as the Kretschmann configuration which can be seen in Figure 5.1, this causes the oscillation of SPs on the surface.[109, 116, 117]

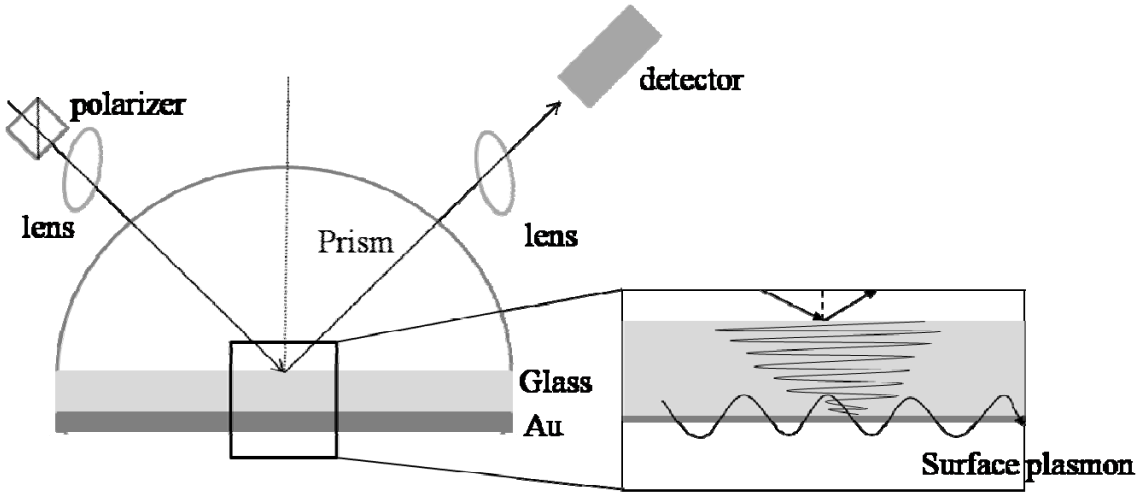

Figure 5.1 - Kretschmann Configuration and the creation of surface plasmons (inset)

This oscillation at the surface will cause the reflected light at a specific angle of incidence to decrease. This decrease in intensity can be measured by the array detector. The electric field generated by the plasmons extends out between 200 and 300 nm from the surface.[108, 109] This means that the gold on the surface must be very thin, usually around 50 nm in order to sense RI changes at the surface or in bulk solution. The thin gold surface decreases the active volume to between 150 to 250 nm from the surface. It is also

important to note that the oscillating plasmons are dependent upon the RI of the surroundings at the surface, so an environmental change will cause a shift in the SPR angle which can be monitored. That is, if a material with a different refractive index is within the necessary distance from the surface then a change in the SPR angle will be seen. RI and SPR are both very sensitive to changes in temperature. So maintaining a constant temperature is very important when reproducible analytical measurements are desired. Therefore, these devices can be used as a refractive index detector, and moreover as a universal detector since no functionalization of the analyte is necessary.

5.2 Materials and Methods

5.2.1 Synthesis of SAM

The synthetic route for these SAM's is relatively simple and consisted of 3 steps. In the first step 3.05 mL of triethylene glycol was refluxed with 0.34 mL of 50% aqueous NaOH (w/w) under nitrogen. After 1 hr, 0.932 mL of 11-bromo-1-undecene was added and the two compounds were stirred at ~100 ^{o}C for 24 hours in a nitrogen atmosphere. The resulting compound was then extracted four times with hexanes, rotary evaporated, and then purified by column chromatography. This resulted in the following compound $HO(CH_2CH_2O)_3(CH_2)_{10}CH_2$, the ^{1}H NMR's for this product and the starting materials are in Appendix A. NMR's were acquired only in $CDCl_3$ with one exception. The first product had an unexpected triplet at 2.5 ppm, this was expected to be the terminal OH. The addition of D_2O caused this peak to be eliminated and a new peak at ~4.8 ppm to show up in the spectrum. The next step in the synthesis was to add a thiol acetate group to the terminal double bond. This was accomplished by adding the olefin 300 mM in

methanol, 3 equivalents of thiolacetic acid, 10 mg AIBN, and irradiating with 365 nm light (UV exposure system, ThermoOriel, Stratford, CT) for 5 hours. The resulting compound then had the acetate group removed, accomplished by refluxing with 0.1 M HCL in an alcohol solution for 5 hours. The reactants were then rotary evaporated and then purified by column chromatography. The final compound collected was $HS(CH_2)_{11}(OCH_2CH_2)_3OH$. The NMR showed the multiple peaks that confirmed the product. The peaks at 5.0 and 5.7 ppm that were previously seen, corresponding to the terminal vinyl group, are eliminated and the new peak at 2.5 ppm was due do the hydrogen's on the carbon bonded to the sulfur atom. All NMR data corresponded to previous reports on synthesis of this compound.[110]

The next step was to create the SAM on the gold surface. This was accomplished by cleaning the gold surface by oxygen plasma for 5 minutes, to remove any contaminates from the surface. The thiol compound was then dissolved in absolute ethanol at 1.0 mM and put in contact with the surface where it remained for 24 hours.[110, 113]

5.2.2 Titanium Dioxide Surface Fabrication

Titanium isopropoxide (Gelest) dissolved in anhydrous 2-propanol solutions were used to create thin titanium dioxide surface on gold coated coverslips. These films were created by two different methods, dip and spin coating. The substrates were dip coated using an in house built dip coater in the Higgins Group. The devices were attached to the dipping arm and lowered into a 9.0 mM titanium isopropoxide solution, held fully submerged for 5 seconds and then removed. This dipping cycle was performed twice on each substrate. Although the devices appear dry after dipping they were allowed to sit at

room temperature for 2 hours prior to further use in a covered petri dish. These films were expected to be on the order of 2 nm.[119] Titania films were also created via a spin coating process. The substrate was attached to a Teflon base with double sided tape and attached to the spin chuck. An aliquot, 65 μL, of 9.0 mM titanium isopropoxide was deposited on the surface and spun at 2000 rpm for 35 seconds. The substrates were removed and allowed to dry for 2 hours prior to further use at room temperature in a covered petri dish.

5.2.3 Titania Modification

The surfaces were modified with different functional groups in order to alter the surface properties of the films. Previous alteration of the surface chemistry of titania has been demonstrated.[87] Functionalization of the surface was carried out in aqueous solution in a glass beaker. Prior to functionalization, the glass beaker was filled with the modification solution to modify the silanol groups on the beaker surface. This was necessary to ensure modification of the substrate surface and not the glassware. The modification solution was replaced prior to substrate functionalization. The solutions used were 20 mM aqueous solutions of 2-[methoxy(polyethylenoxy)propyl]trimethoxysilane and aminopropyltriethoxysilane yielding ethylene oxide and amine functionalized surfaces, respectively. Prior to functionalization the surfaces were dipped in a 30% ethylamine solution for a few seconds, and then rinsed in water. The titania on gold surfaces were then placed in the appropriate functionalization solution at 60 °C for 4 hours. After heating the surfaces were rinsed with water and dried in a stream of nitrogen and allowed to dry in a covered petri dish for 1 hr prior to further use.

5.2.4 Surface Characterization

Change in the surface chemistry was monitored with water contact angle measurements and x-ray photoelectron spectroscopy (XPS). Contact angle measurements were collected with an in house built apparatus previously described.[120] Briefly, a machined mirror/substrate holder was placed on the stage of a Nikon SMZ-1500 stereomicroscope. The holder had a ledge horizontal to the stage to hold the substrate and a ledge machined at 45° to the stage to hold a mirror. The microscope was focused onto the mirror to image the substrate from a perpendicular viewpoint. A 5 μL droplet of water was placed on the substrate surface, after 1 min an image was captured with a digital camera attached to the camera port. The image was processed with Nikon ACT-2U software to measure the angle between the surface and the droplet.

XPS data was collected by Chundi Cao in Dr. Keith L. Hohn's research group in the Department of Chemical Engineering here at Kansas State University. Data was collected for the following surfaces, bare gold, Au-TiO_2, and Au-TiO_2-PEG.

5.2.5 SPR Instrumentation

There were two different SPR measurement devices used in this research. Both SPREETA devices were manufactured by Texas Instruments in collaboration with Nomadics. Initially the TSPR1A1700100 sensor was used with a SPREETA evaluation module kit, consisting of a docking station for the sensor, a plastic flow cell, and computer integration cables. Upon discontinuation of this sensor the TSPR2K11 sensor was used with the SensiQ Discovery instrumentation. The discovery and new sensor had dual stainless steel flow channels for real-time background subtraction and an additional integrated valve for sample injection. The sensor schematic is shown in Figure 5.2.

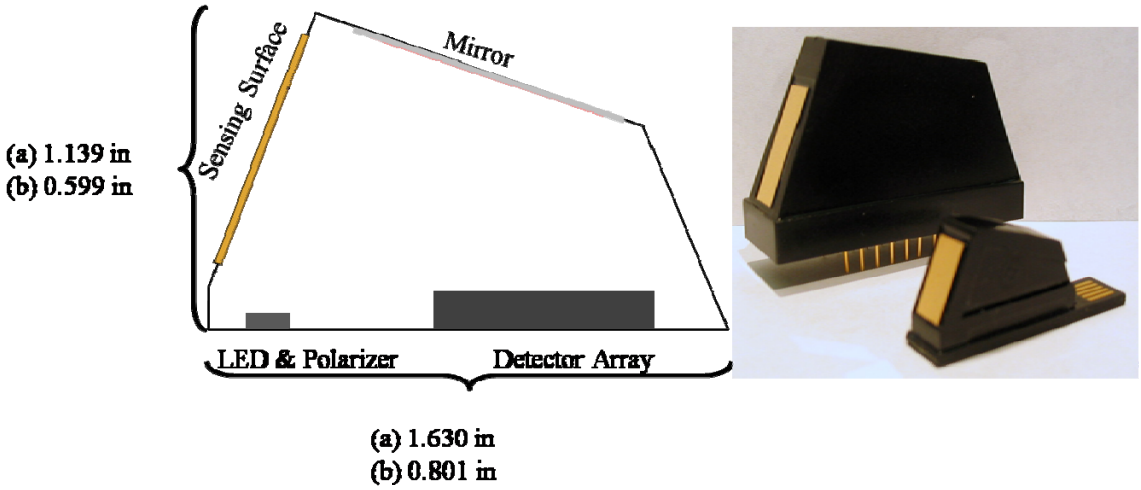

Figure 5.2 - Sensor schematic and sizes of the TSPR1A1700100 (a) and TSPR2K11 (b) sensors and image of both sensors

The sensors both contained totally enclosed optics. A small LED mounted with a polarizer that shines onto the back of the gold coated section of glass. The light that reflects off the surface is directed towards a mirror that reflects the light to a detector array. The sensors were shipped with gold coated surfaces on the device, which had to be removed to attach the fabricated titania and SAM surfaces. The gold was removed by swabbing the surface with aqua-regia using cleanroom swabs. Beneath the gold was an additional titanium adhesion layer, removed by swabbing with the same solution used to etch glass, previously described in chapter 2. New surfaces were attached to the clean SPREETA surface using index matching oil to ensure no loss of signal intensity. Flow cells were attached to the new surfaces, and a seal preventing fluid leakage was created by pressure from tightening screws. Fluidic connections were made with PEEK tubing. Various buffers and sample solutions were used to test the surfaces for their abilities to prevent protein adsorption.

5.3 Results and Discussion

5.3.1 Surface Characterization

5.3.1.1 Contact Angle Measurements

Initially the surfaces were characterized via water contact angle measurements, as outlined above. Measurements were taken on the following surfaces; Gold/Gold Oxide, TiO_2 coated gold, aminopropyl modified TiO_2 coated gold, and polyethylene glycol modified TiO_2 coated gold, Figure 5.3. The contact angle measurements were 78.5 ± 2.2, 63.2 ± 3.6, 40.8 ± 3.9 for the Au, Au-TiO_2, and Au-TiO_2-PEG, respectively (n = 4). The aminopropyl surface was not used for SPR analysis but, to monitor the modification via silane chemistry its contact angle was 65° (n = 1).

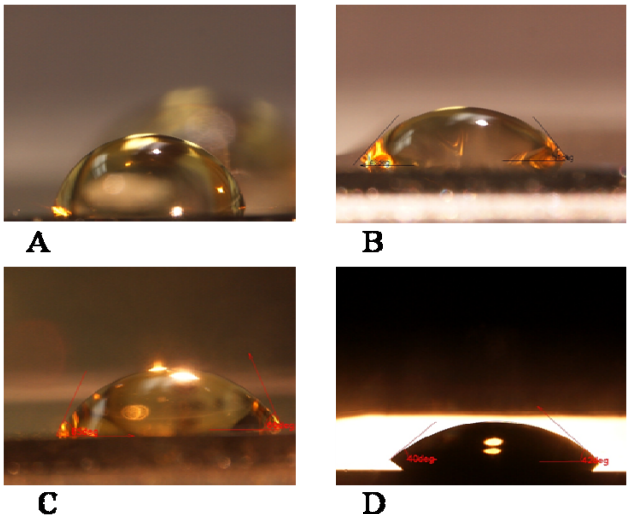

Figure 5.3 - Contact angle measurements on Au (A), Au-TiO_2 (B), Au-TiO_2-aminopropyl (C), and Au-TiO_2-PEG (D).

These measurements demonstrated the expected results. The surface with the terminal ethylene oxide groups should be the most hydrophilic and exhibit the lowest contact

angle. In general, as the expected hydrophillicity of the surface increase the surface contact angle decreased.

5.3.1.2 XPS

The XPS survey scans were collected on the Au, Au-TiO_2, and Au-TiO_2-PEG surfaces. The data shown in Figure 5.4 was the collected XPS spectra for the Ti 2p region, showing the presence of titanium after surface formation via the dip coating process. Figure 5.5 shows the O 1s region, which demonstrates the increase in oxygen on the surface, the shift in binding energy between the Au-TiO_2, and Au-TiO_2-PEG was expected due to the PEG modification.

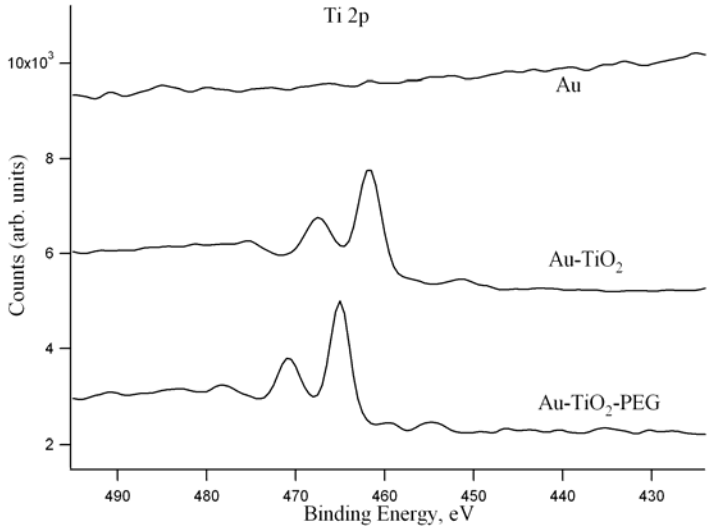

Figure 5.4 - XPS survey spectra for Ti 2p region for Au, Au-TiO_2, and Au-TiO_2-PEG surfaces.

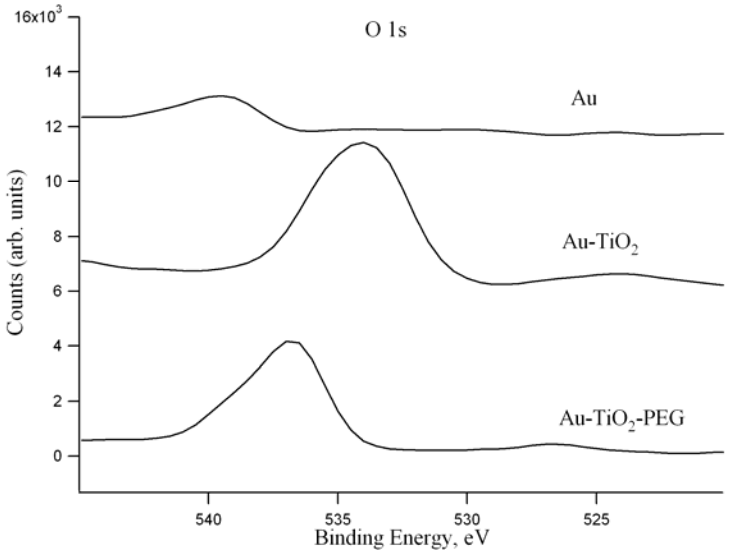

Figure 5.5 - XPS survey spectra for O 1s region for Au, Au-TiO2, and Au-TiO2-PEG surfaces.

5.3.2 SPR Measurements

The initial data was collected with the TSPR1A1700100 sensor and the SPREETA evaluation module kit. The channel input was connected to a 4-way valve (Upchurch Scientific; Oak Harbor, WA) and the 3 other valve ports were connected to; a syringe mounted on a syringe pump containing buffer, a syringe with 347 mM Lysozyme in buffer, and a waste line. The buffer used for this initial study was 50 mM SDS, 10 mM sodium borate in a 20 % acetonitrile (v/v) solution. Both syringe pumps were set at 30 μL/min and the valve was positioned to pump the buffer over the SPR surface. After signal stabilization the valve was switched for 150 s and the response was monitored. Multiple 150 s injections were performed, the first and second injection are shown in Figure 5.6.

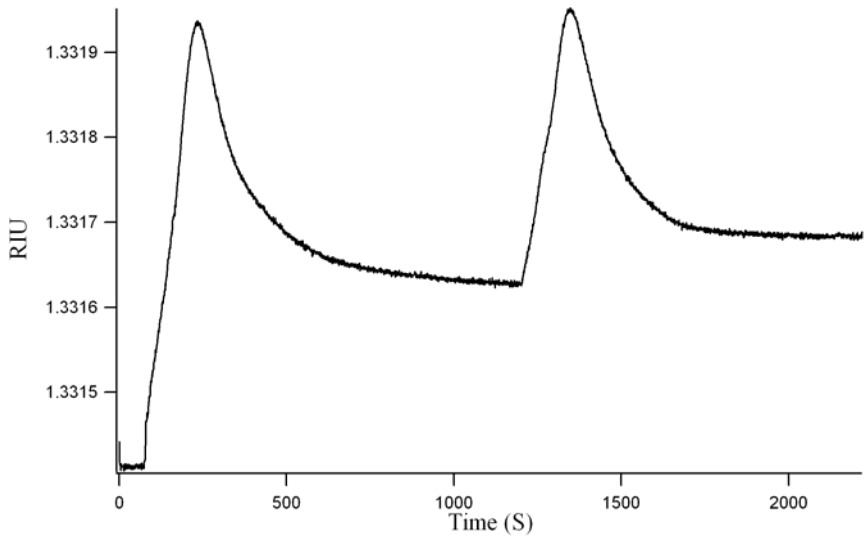

Figure 5.6 - SPR sensogram of 150 s injections of 347 mM Lysozyme over a bare Au surface; 30.0 µL/min flow rate.

The resulting sensogram showed the detection of Lysozyme. The response did not return to the baseline indicating protein adsorption on the gold surface. An advantage of using the SPREETA devices was the ease in switching between surfaces with different chemical modification. The same sensor can be used with a multiple surfaces. Next a SAM modified surface was attached to the sensor. An injection of 50 mM Lysozyme was monitored over the surface, the resulting sensogram is show in Figure 5.7.

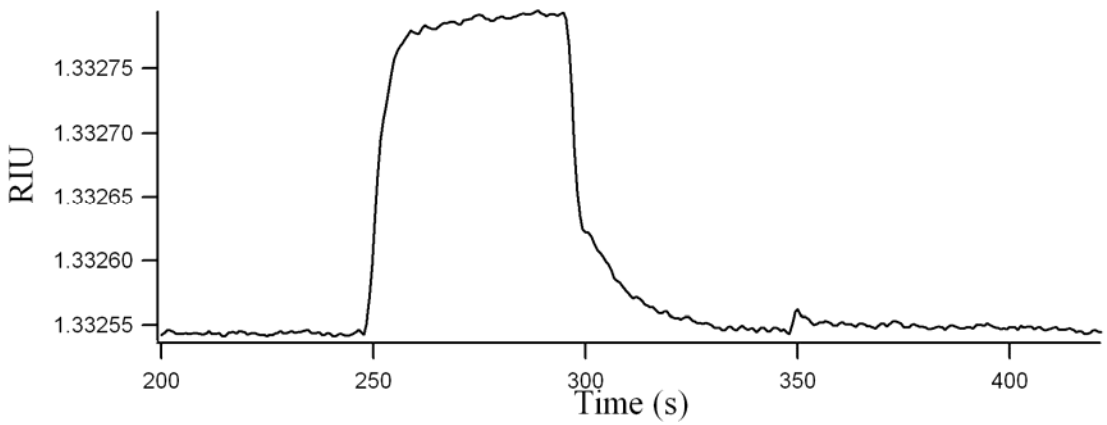

Figure 5.7 - SPR sensogram of 50 mM Lysozyme injections over a SAM modified gold surface

The SAM surface exhibited resistance to protein adsorption on the surface. This was noted because the sensor response returned to baseline after injection of sample. A 1 mg/mL sample of Lysozyme in the same buffer was injected over a Au-TiO2-PEG surface with the same buffer conditions, Figure 5.8.

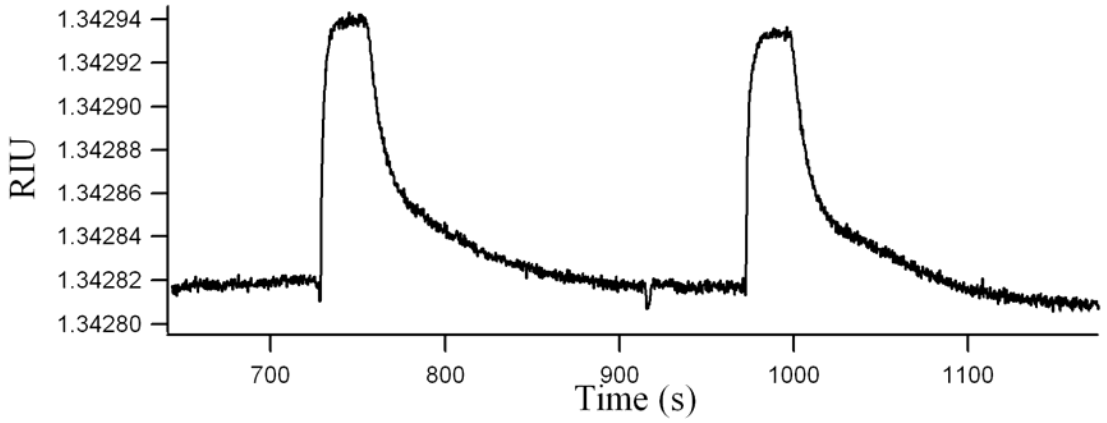

Figure 5.8 - SPR sensogram of 1 mg/mL Lysozyme injections over an Au-TiO2-PEG surface

This surface also demonstrated the ability to resist protein adsorption to the titania modified surface. In previous reports, the SAM surfaces was said to be unstable requiring new surfaces frequently.[110] SAM and TiO_2-PEG were tested over a period of a

few weeks to test their stability. The titania surface showed protein resistance for a period of 4 weeks and the SAM surface began to decay after 2 weeks. Figure 5.9 shows the results from the temporal study.

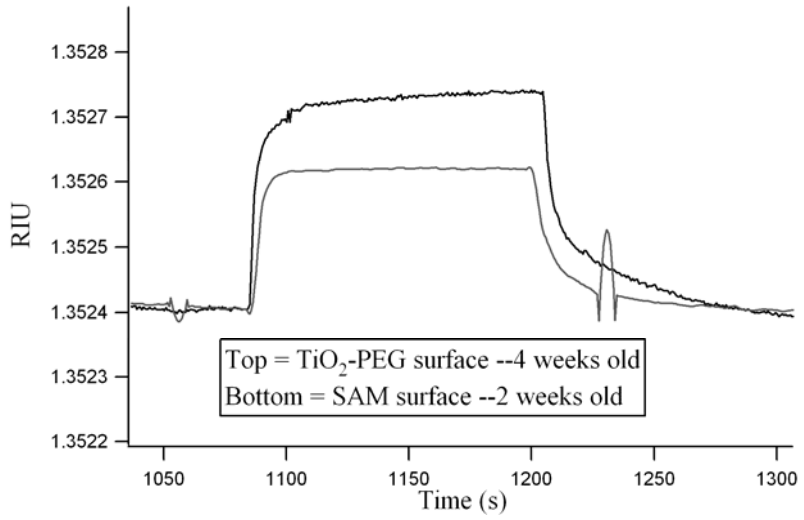

Figure 5.9 - Temporal study showing SPR sensograms of 1 mg/mL Lysozyme detection on SAM and TiO2-PEG surfaces.

Although both surfaces demonstrated protein resistance, the titania surface exhibited larger signal difference compared to the SAM which could increase the LOD for proteins when using this surface. This increase in signal response for the titania surface could possibly be due to titania surface roughness which would increase the surface area increasing the sites for protein interaction.

After this temporal study we switched to the new TSPR2K11 sensor in conjunction with the SensiQ Discovery instrumentation due to discontinuation of the TSPR1A1700100 sensor. The major advantage of the new sensor is real-time background subtraction. Temperature variations are a common problem with SPR measurements and this sensor helps to eliminate signal changes contributed to fluctuations in temperature. The new sensor also had increased resolution and an

increased refractive index range. All of the results for the first sensor were replicated with similar results.

SPR is commonly used to monitor interactions with a sample flowing past the sensor and a ligand bound to the surface, i.e. ligand-analyte binding and dissociation constants. Commonly, prior to sample analysis, the surface will be passivated to prevent non-specific adsorption.[121-123] This process had not been used with results previously reported in this chapter. However, this might be important as the PEG surface modification chemical is bulky and could prevent complete surface modification due to steric hindrance. Analyte interactions with the surface can also be altered dependent upon the buffer composition. Complications associated with these two ideas were examined by passing 0.1 mg/ml Lysozyme over previously unused Au-TiO_2-PEG surfaces with different buffers. Figure 5.10 shows that buffer composition does play a role in the signal measured as well as the prevention of protein adsorption to the surface. A more suitable buffer composition might prevent any and all surface adsorption.

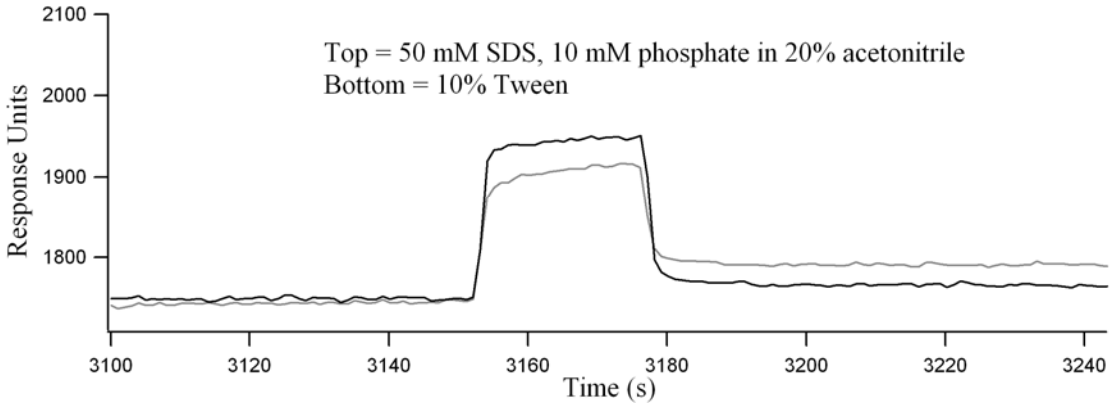

Figure 5.10 - SPR sensogram of 0.1 mg/mL Lysozyme on unused TiO2-PEG surfaces with different buffers

SPR has also been used as a post column detector for traditional separation techniques.[124-127] Some of the previous reports have used the TSPR1A1700100 SPREETA sensor.[124] Our initial attempts were to connect the sensor to a Waters HPLC and use it as a post column detector. After several attempts, with less than favorable results, we realized that this sensor would not be applicable for the research goal of this project. The initial goal of this project was to use SPR as a "universal" detector for microfluidic separation analysis. The new sensor had one major disadvantage, the sampling rate. In order to sufficiently record separations it is necessary to have 21 data points across a Gaussian peak.[128] This sensor has a sampling rate of 1 Hz, which is 50 times slower than the first sensor. Peaks in microfluidic analysis commonly have widths of less than 1 second. This was an over-looked implication when we switched to the second sensor.

5.4 Concluding Remarks

This chapter discusses the fabrication of a titania surface fabricated on a gold substrate which can be further modified with terminal ethylene oxide functional groups capable of preventing protein adsorption. Titania was studied because of the expected increase in temporal stability when compared to SAM's. There are many aspects of this project that were not completed, due to an abrupt end to the project. The ability to easily fabricate inexpensive protein resistant surface has a potential use in SPR analysis. Further optimization and characterization of the surface is necessary. The use of this device in conjunction with microfluidics is exciting, but with the limited sampling rate, is not feasible at this point in time. Potential future work includes: better characterization

of titania surface, end capping the surface in sterically hindered areas to prevent protein interactions, and appropriate buffer composition for the analyte of interest.

CHAPTER 6 - **Conclusions and Future Outlook**

The projects discussed in this dissertation encompass a wide variety of analytical problems associated with the separation sciences. An interesting previously unreported aspect of MEKC was presented in Chapter 2. Future experiments with this novel buffer would include using the micelle forming agents in their pure forms, without all the fillers associated with the dishwashing soap product.

Titanium dioxide was used in multiple forms in the research reported herein, and has potential use in projects where it was not used. First we used titania for the fabrication of sol-gel nanoporous membranes at the junction of microfluidic channels. This is a very interesting area of microfluidics and better characterization of the membrane could enhance its properties further. Different channel geometries that would allow access to the membrane could aid in this understanding. Titania was also used to create protein resistant surfaces for surface plasmon resonance analysis. This project was largely affected when the manufacturer decided to discontinue the sensor we were using and switch to a newer model. With the new model, the sampling rate was decreased 50 fold. The surface modifications show yet another function of the compound TiO_2 further analysis of these surfaces and a faster sampling rate could yield a very powerful microfluidic detection mechanism.

Finally, the paper based microfluidic devices, have a very exciting future in the field of portable analysis devices. There are many biological assays that can be performed using these devices. Titania was not used in this application, but why not? It

has the interesting property that it creates hydroxyl radicals in the presence of UV light. This property is utilized in many applications of our everyday lives already, and could be incorporated with these devices. Spotting titanium isopropoxide on the paper substrate should create TiO_2 on the substrate; this property could be used to catalyze detection mechanisms for assays.

In the literature there have been claims about the use of paper microfluidics in developing nations. This is important; however, I think there are plenty of applications here at home. They have the potential to help engage a future generation of scientists. With the cost effective aspect of this project and the ease of fabrication, there is no reason that "young" scientists could not make and use these devices in classrooms across the country. This would give them an exciting view of the potential chemistry has in the future.

CHAPTER 7 - **References**

(1) Giddings, J. C. *Unified Separation Science*; Wiley-Interscience, 1991.
(2) Poole, C. F. *The Essence of Chromatography*; Elsevier: Amsterdam, 2003.
(3) Karger, B. L.; Snyder, L. R.; Horvath, C. *An Introduction to Separation Science*; John Wiley & Sons: New York, 1973.
(4) Heiger, D., N. *High Performance Capillary Electrophoresis*, 2nd. ed.; Hewlett-Packard: France, 1992.
(5) Cunico, R. L.; Gooding, K. M.; Wehr, T. *Basic HPLC and CE of Biomolecules*; Bay Bioanalytical Laboratory: Richmond, CA, 1998.
(6) Jacobson, S. C.; Culbertson, C. T. In *Separation Methods in Microanalytical Systems*; Kutter, J. P., Fintschenko, Y., Eds.; CRC Press: Boca Raton, FL, 2006, pp 19-54.
(7) Schoch, R. B.; Han, J.; Renaud, P. *Rev. Mod. Phys* **2008**, *80*, 839.
(8) Höltzel, A.; Tallarek, U. *J. Sep. Sci.* **2007**, *30*, 1398-1419.
(9) Beebe, D. J.; Mensing, G. A.; Walker, G. M. *Annual Review of Biomedical Engineering* **2002**, *4*, 261-286.
(10) Terabe, S.; Otsuka, K.; Ichikawa, K.; Tsuchiya, A.; Ando, T. *Anal. Chem.* **1984**, *56*, 111-113.
(11) Makino, K.; Itoh, Y.; Teshima, D.; Oishi, R. *Electrophoresis* **2004**, *25*, 1488-1495.
(12) Silva, M. *Electrophoresis* **2007**, *28*, 174-192.
(13) Pappas, T. J.; Gayton-Ely, M.; Holland, L. A. *Electrophoresis* **2005**, *26*, 719-734.
(14) Chiu, T.-C.; Lin, Y.-W.; Huang, Y.-F.; Chang, H.-T. *Electrophoresis* **2006**, *27*, 4792-4807.
(15) Terabe, S. *Anal. Chem.* **2004**, *76*, 241A-246A.
(16) Issaq, H. J. *Electrophoresis* **1999**, *20*, 3190-3202.
(17) Iadarola, P.; Cetta, G.; Luisetti, M.; Annovazzi, L.; Casado, B.; Baraniuk, J.; Zanone, C.; Viglio, S. *Electrophoresis* **2005**, *26*, 752-766.
(18) Ho, Y.-H.; Wu, H.-L. *Electrophoresis* **2006**, *27*, 2300-2309.
(19) Cifuentes, A. *Electrophoresis* **2006**, *27*, 283-303.
(20) Pumera, M. *Electrophoresis* **2007**, *28*, 2113-2124.
(21) Cheung, R. H. F.; Marriott, P. J.; Small, D. M. *Electrophoresis* **2007**, *28*, 3390-3413.
(22) Nishi, H. *J. Chrom. A*. **1997**, *780*, 243-264.
(23) Zhu, X.; Shaw, P. N.; Pritchard, J.; Newbury, J.; Hunt, E. J.; Barrett, D. A. *Electrophoresis* **2005**, *26*, 911-919.
(24) Amini, A. *Electrophoresis* **2001**, *22*, 3107-3130.
(25) Shou, M.; Smith, A. D.; Shackman, J. G.; Peris, J.; Kennedy, R. T. *Journal of Neuroscience Methods* **2004**, *138*, 189-197.
(26) Torben Madsen, H. B. B., Dorthe Nylén, Anne Rathmann Pedersen, Gitte I. Petersen, and Flemmin Simonsen; Danish EPA, 2000.

(27) Ding, W.; Fritz, J. S. *Analytical Chemistry* **1997**, *69*, 1593-1597.
(28) Roman, G. T.; Carroll, S.; McDaniel, K.; Culbertson, C. T. *Electrophoresis* **2006**, *27*, 2933-2939.
(29) Roman, G. T.; McDaniel, K.; Culbertson, C. T. *Analyst* **2006**, *131*, 194-201.
(30) Little, E. L.; Foley, J. P. *J. Microcol. Sep.* **1992**, *4*, 145-154.
(31) Mazzeo, J. R. In *Handbook of Capillary Electrophoresis,* 2 ed.; Landers, J. P., Ed.; CRC, 1997, pp 49-73.
(32) Poole, S. K.; Poole, C. F. *Analyst* **1997**, *122*, 267-274.
(33) Poole, C. F.*,* 1 ed.; Elsevier, 2003, pp 644-659.
(34) Poole, S. K.; Poole, C. F. *Analytical Communications* **1997**, *34*, 57-62.
(35) Wang, M.; Wu, D.; Yao, Q.; Shen, X. *Analytica Chimica Acta* **2004**, *519*, 73-78.
(36) Broyles, B. S.; Jacobson, S. C.; Ramsey, J. M. *Anal. Chem.* **2003**, *75*, 2761-2767.
(37) Roper, M. G.; Shackman, J. G.; Dahlgren, G. M.; Kennedy, R. T. *Anal. Chem.* **2003**, *75*, 4711-4717.
(38) Mogensen, K. B.; Kwok, Y. C.; Eijkel, J. C. T.; Petersen, N. J.; Manz, A.; Kutter, J. P. *Anal. Chem.* **2003**, *75*, 4931-4936.
(39) Wang, Z.; El-Ali, J.; Engelund, M.; Gotsaed, T.; Perch-Nielsen, I. R.; Mogensen, K. B.; Snakenborg, D.; Kutter, J. P.; Wolff, A. *Lab Chip* **2004**, *4*, 372-377.
(40) Vezenov, D. V.; Mayers, B. T.; Conroy, R. S.; Whitesides, G. M.; Snee, P. T.; Chan, Y.; Nocera, D. G.; Bawendi, M. G. *J. Am. Chem. Soc* **2005**, *127*, 8952-8953.
(41) Vezenov, D. V.; Mayers, B. T.; Wolfe, D. B.; Whitesides, G. M. *Appl. Phys. Lett.* **2005**, *86*, 041104/041101-041104/041103.
(42) Kamei, T.; Paegel, B. M.; Scherer, J. R.; Skelley, A. M.; Street, R. A.; Mathies, R. A. *Anal. Chem.* **2003**, *75*, 5300-5305.
(43) Burns, M. A.; Johnson, B. N.; Brahmasandra, S. N.; Handique, K.; Webster, J. R.; Krishnan, M.; Sammarco, T. S.; Man, P. M.; Jones, D.; Heldsinger, D.; Mastrangelo, C. H.; Burke, D. T. *Science* **1998**, *282*, 484-487.
(44) Cellar, N. A.; Burns, S. T.; Meiners, J.-C.; Chen, H.; Kennedy, R. T. *Anal. Chem.* **2005**, *77*, 7067-7073.
(45) Yang, H.; Chien, R. L. *J. Chromatogr., A* **2001**, *924*, 155-163.
(46) Shiddiky, M. J. A.; Shim, Y.-B. *Anal. Chem.* **2007**, *79*, 3724-3733.
(47) Wainright, A.; Williams, S. J.; Ciambrone, G.; Xue, Q.; Wei, J.; Harris, D. *J. Chromatogr., A* **2002**, *979*, 69-80.
(48) Kaniansky, D.; Masar, M.; BielcÌŒikova, J.; Ivanyi, F.; Eisenbeiss, F.; Stanislawski, B.; Grass, B.; Neyer, A.; Johnck, M. *Anal. Chem.* **2000**, *72*, 3596-3604.
(49) Bodor, R.; Madajová, V.; Kaniansky, D.; Masár, M.; Jöhnck, M.; Stanislawski, B. *J. Chromatogr., A* **2001**, *916*, 155.
(50) Yang, W.; Sun, X.; Pan, T.; Woolley, A. T. *Electrophoresis* **2008**, *29*, 3429-3435.
(51) Yu, C.; Davey, M. H.; Svec, F.; Frechet, J. M. J. *Anal. Chem.* **2001**, *73*, 5088-5096.
(52) Sera, Y.; Matsubara, N.; Otsuka, K.; Terabe, S. *Electrophoresis* **2001**, *22*, 3509-3513.
(53) Liu, Y.; Foote, R. S.; Jacobson, S. C.; Ramsey, J. M. *Lab Chip* **2005**, *5*, 457-465.
(54) Song, S.; Singh, A. K.; Kirby, B. J. *Anal. Chem.* **2004**, *76*, 4589-4592.

(55) Long, Z.; Liu, D.; Ye, N.; Qin, J.; Lin, B. *Electrophoresis* **2006**, *27*, 4927-4934.
(56) Cannon, D. M., Jr.; Kuo, T.-C.; Bohn, P. W.; Sweedler, J. V. *Anal. Chem.* **2003**, *75*, 2224-2230.
(57) Dai, J.; Ito, T.; Sun, L.; Crooks, R. M. *J. Am. Chem. Soc* **2003**, *125*, 13026-13027.
(58) Zhang, Y.; Timperman, A. T. *Analyst* **2003**, *128*, 537-542.
(59) Zhou, K.; Kovarik, M. L.; Jacobson, S. C. *J. Am. Chem. Soc* **2008**, *130*, 8614-8616.
(60) Kovarik, M. L.; Jacobson, S. C. *Anal. Chem.* **2008**, *80*, 657-664.
(61) Dhopeshwarkar, R.; Sun, L.; Crooks, R. M. *Lab Chip* **2005**, *5*, 1148-1154.
(62) Song, S.; Singh, A. K.; Shepodd, T. J.; Kirby, B. J. *Anal. Chem.* **2004**, *76*, 2367-2373.
(63) Kim, S. M.; Burns, M. A.; Hasselbrink, E. F. *Anal. Chem.* **2006**, *78*, 4779-4785.
(64) Lee, J. H.; Chung, S.; Kim, S. J.; Han, J. *Anal. Chem.* **2007**, *79*, 6868-6873.
(65) Pu, Q.; Yun, J.; Temkin, H.; Liu, S. *Nano Lett.* **2004**, *4*, 1099-1103.
(66) Wang, Y.-C.; Han, J. *Lab Chip* **2008**, *8*, 392-394.
(67) Chatterjee, A. N.; Cannon, D. M.; Gatimu, E. N.; Sweedler, J. V.; Aluru, N. R.; Bohn, P. W. *J Nanopart Res* **2005**, *7*, 507-516.
(68) Jin, X.; Joseph, S.; Gatimu, E. N.; Bohn, P. W.; Aluru, N. R. *Langmuir* **2007**, *23*, 13209-13222.
(69) Kuo, T. C.; Sloan, L. A.; Sweedler, J. V.; Bohn, P. W. *Langmuir* **2001**, *17*, 6298-6303.
(70) Pennathur, S.; Santiago, J. G. *Anal. Chem.* **2005**, *77*, 6772-6781.
(71) Wang, Y. C.; Stevens, A. L.; Han, J. *Anal. Chem.* **2005**, *77*, 4293-4299.
(72) Mao, P.; Han, J. *Lab Chip* **2009**, *9*, 586-591.
(73) Dusseiller, M. R.; Niederberger, B.; Staedler, B.; Falconnet, D.; Textor, M.; Voeroes, J. *Lab Chip* **2005**, *5*, 1387-1392.
(74) Jahn, A.; Vreeland, W. N.; DeVoe, D. L.; Locascio, L. E.; Gaitan, M. *Langmuir* **2007**, *23*, 6289-6293.
(75) Kenis, P. J. A.; Ismagilov, R. F.; Whitesides, G. M. *Science* **1999**, *285*, 83-85.
(76) de Jong, J.; Lammertink, R. G. H.; Wessling, M. *Lab Chip* **2006**, *6*, 1125-1139.
(77) Zhao, B.; Viernes, N. O. L.; Moore, J. S.; Beebe, D. J. *J. Am. Chem. Soc* **2002**, *124*, 5284-5285.
(78) Wright, J. D.; Sommerdijk, N. A. J. M. *Sol-Gel Materials: Chemistry and Applications*; Gordon and Breach Science Publishers, 2001.
(79) Morishima, K.; Bennett, B. D.; Dulay, M. T.; Quirino, J. P.; Zare, R. N. *J. Sep. Sci.* **2002**, *25*, 1226-1230.
(80) Collinson, M. M. *Microchim Acta* **1998**, *129*, 149-165.
(81) Meyer, A. R.; Clark, A. M.; Culbertson, C. T. *Lab Chip* **2006**, *6*, 1355-1361.
(82) Roman, G. T., Kansas State University, Manhattan, KS, 2006.
(83) Hoeman, K. W.; Lange, J. J.; Roman, G. T.; Higgins, D. A.; Culbertson, C. T. *Electrophoresis* **2009**, accepted.
(84) Hatch, A. V.; Herr, A. E.; Throckmorton, D. J.; Brennan, J. S.; Singh, A. K. *Anal. Chem.* **2006**, *78*, 4976-4984.
(85) Kim, S. J.; Wang, Y.-C.; Lee, J. H.; Jang, H.; Han, J. *Phys. Rev. Lett.* **2007**, *99*, 044501.
(86) Parks, G. A. *Chem. Rev.* **1965**, *65*, 177-198.

(87) Roman, G. T.; Culbertson, C. T. *Langmuir* **2006**, *22*, 4445-4451.
(88) Martinez, A. W.; Phillips, S. T.; Butte, M. J.; Whitesides, G. M. *Angew. Chem., Int. Ed.* **2007**, *46*, 1318-1320.
(89) Martinez, A. W.; Phillips, S. T.; Carrilho, E.; Thomas, S. W.; Sindi, H.; Whitesides, G. M. *Anal. Chem.* **2008**, *80*, 3699-3707.
(90) Martinez, A. W.; Phillips, S. T.; Whitesides, G. M. *Proc. Natl. Acad. Sci.* **2008**, *105*, 19606-19611.
(91) Martinez, A. W.; Phillips, S. T.; Wiley, B. J.; Gupta, M.; Whitesides, G. M. *Lab Chip* **2008**, *8*, 2146-2150.
(92) Abe, K.; Suzuki, K.; Citterio, D. *Anal. Chem.* **2008**, *80*, 6928-6934.
(93) Chard, T. In *The Immunoassay Handbook,* 2nd. ed.; Wild, D., Ed.; Nature Publishing Group: London, 2001, pp 572-583.
(94) Hung, P. J.; Lee, P. J.; Sabounchi, P.; Aghdam, N.; Lin, R.; Lee, L. P. *Lab on a Chip* **2005**, *5*, 44-48.
(95) Fleckman, A. M. In *Principles of Diabetes Mellitus*; Poretsky, L., Ed.; Kluwer Academic Publishers: London, 2002, pp 273-292.
(96) Krentz, A. J.; Holt, H. B. In *Emergencies in Diabetes*; Krentz, A. J., Ed.; John Wiley & Sons, Ltd.: West Sussex, England, 2004, pp 1-32.
(97) Sassa, M.; Yamada, Y.; Hosokawa, M.; Fukuda, K.; Fujimoto, S.; Toyoda, K.; Tsukiyama, K.; Seino, Y.; Inagaki, N. *Diabetes Res. Clin. Pract.* **2008**, *81*, 190.
(98) Parks, J. H.; Coe, F. L.; Evan, A. P.; Worcester, E. M. *Nephrol., Dial., Transplant.* **2009**, *24*, 130-136.
(99) Daudon, M.; Traxer, O.; Conort, P.; Lacour, B.; Jungers, P. *J. Am. Soc. Nephrol.* **2006**, *17*, 2026-2033.
(100) Cameron, M. A.; Maalouf, N. M.; Adams-Huet, B.; Moe, O. W.; Sakhaee, K. *J. Am. Soc. Nephrol.* **2006**, *17*, 1422-1428.
(101) Maalouf, N. M.; Cameron, M. A.; Moe, O. W.; Adams-Huet, B.; Sakhaee, K. *Clin. J. Am. Soc. Nephrol.* **2007**, *2*, 883-888.
(102) Laios, I. D.; Pardue, H. L. *Anal. Chem.* **1993**, *65*, 1903-1909.
(103) Foster, L. S.; Gruntfest, I. J. *J. Chem. Ed.* **1937**, *14*, 274.
(104) Masami, K.; Yuzo, H., G01N33/64 ed.: Japan, 1989; Vol. JP1224667A.
(105) van der Linden, H. In *http://mail.mems-exchange.org/pipermail/mems-talk/2002-January/006029.html*, 2009.
(106) Chambers, G.; Lawrie, L.; Cash, P.; Murray, G. I. *Journal of Pathology* **2000**, *192*, 280-288.
(107) Nelson, B. P. F., A. G.; Brockman, J. M.; Corn, R. M. *Analytical Chemistry* **1999**, *71*, 3928-3934.
(108) Frutos, A. G.; Corn, R. M. *Analytical Chemistry* **1998**, *70*, 449 A - 455 A.
(109) Smith, E. A.; Corn, R. M. *Applied Spectroscopy* **2003**, *57*, 320A-332A.
(110) Pale-Grosdemange, C.; Simon, E. S.; Prime, K. L.; Whitesides, G. M. *J. Am. Chem. Soc.* **1991**, *113*, 12-20.
(111) Jiang, X. B., Dereck A. Thant, Mamie, M. Whitesides, George M. *Analytical Chemistry* **2004**, *76*, 6116-6121.
(112) Ostuni, E. Y., Lin. Whitesides, George M. *Colloids and Surfaces B: Biointerfaces* **1999**, *15*, 3-30.
(113) Prime, K. L. W., George M. *Science* **1991**, *252*, 1164-1167.

(114) Chapman, R. G. O., E.; Liang, M. N.; Meluleni, G.; Kim, E.; Yan, L.; Pier, G.; Warren, H. S.; Whitesides, G. M. *Langmuir* **2001**, 1225-1233.
(115) Ostuni, E. C., R. G.; Holmlin, R. E.; Takayama, S.; Whitesides, G. M. *Langmuir* **2001**, *17*, 5605-5620.
(116) Homola, J. *Surface Plasmon Resonance Based Sensors*; Springer, 2006.
(117) Maier, S. A. *Plasmonics: Fundamentals and Applications*; Springer, 2007.
(118) Shalaev, V. M.; Kawata, S. *Nanophotonics with Surface Plasmons*; Elsevier, 2007.
(119) Grunwaldt, J.-D. G., U. Baiker, A. *Fresenius Journal of Analytical Chemistry* **1997**, *358*.
(120) Roman, G. T.; Hlaus, T.; Bass, K. J.; Seelhammer, T. G.; Culbertson, C. T. *Analytical Chemistry* **2005**, *77*, 1414-1422.
(121) Baird, C. L.; Courtenay, E. S.; Myszka, D. G. *Analytical Biochemistry* **2002**, *310*, 93.
(122) Liu, X.; Song, D.; Zhang, Q.; Tian, Y.; Liu, Z.; Zhang, H. *Sensors and Actuators B: Chemical* **2006**, *117*, 188.
(123) Myszka, D. G. *Analytical Biochemistry* **2004**, *329*, 316.
(124) Whelan, R. J.; Zare, R. N. *Anal. Chem.* **2003**, *75*, 1542-1547.
(125) Castillo, J. R.; Cepria, G.; de Marcos, S.; Galbán, J.; Mateo, J.; Ruiz, E. G. *Sensors and Actuators A* **1993**, *37-38*, 582-586.
(126) Cepria, G.; Castillo, J. R. *Journal of Chromatography A* **1997**, *759*, 27-35.
(127) Jungar, C.; Strandh, M.; Ohlson, S.; Mandenius, C.-F. *Analytical Biochemistry* **2000**, *281*, 151-158.
(128) Felinger, A. *Data analysis and signal processing in chromatography*; Elsevier Science B.V., 1998.

APPENDIX A - ^{1}H NMR Data for Chapter 5

Figure A.1 - ^{1}H NMR of triethylene glycol starting material

Acquisition Time (sec)	3.7010	Comment	STANDARD 1H OBSERVE		
Date	Jan 12 2006	Date Stamp	Jan 12 2006		
File Name	C:\Documents and Settings\Leila Maurmann\Desktop\hoemanglycol				
Frequency (MHz)	399.78	Nucleus	1H	Number of Transients	16
Original Points Count	22208	Points Count	32768	Pulse Sequence	s2pul
Receiver Gain	44.00	Solvent	CHLOROFORM-d		
Spectrum Offset (Hz)	2007.3860	Sweep Width (Hz)	6000.60	Temperature (degree C)	29.000

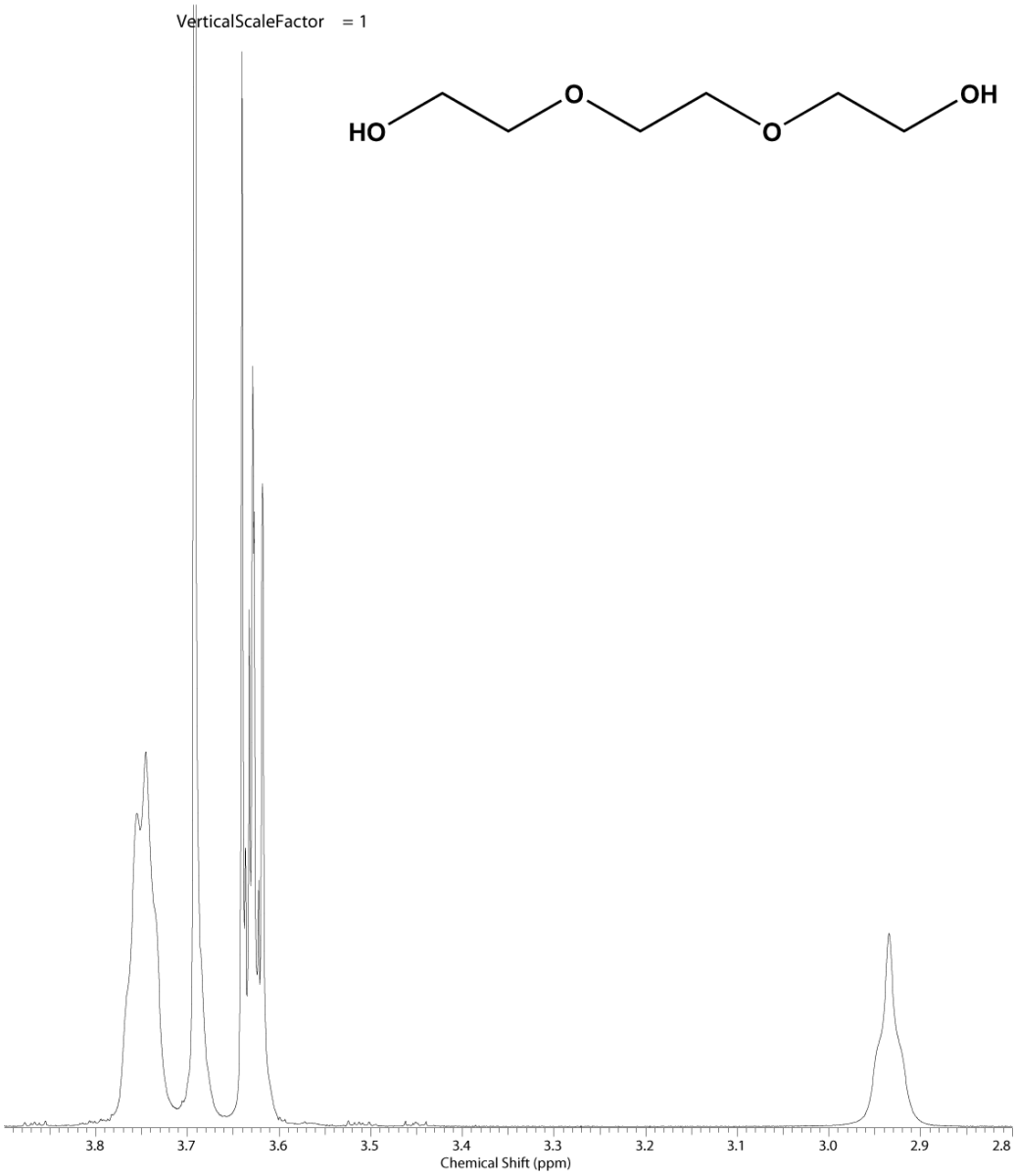

Figure A.2 - ^{1}H NMR of 1-bromo-11-undecene

Acquisition Time (sec)	3.7010	Comment	STANDARD 1H OBSERVE		
Date	Jan 12 2006	Date Stamp	Jan 12 2006		
File Name	C:\Documents and Settings\Leila Maurmann\Desktop\hoemanUndecBr				
Frequency (MHz)	399.78	Nucleus	1H	Number of Transients	16
Original Points Count	22208	Points Count	32768	Pulse Sequence	s2pul
Receiver Gain	44.00	Solvent	CHLOROFORM-d		
Spectrum Offset (Hz)	2007.3860	Sweep Width (Hz)	6000.60	Temperature (degree C)	29.000

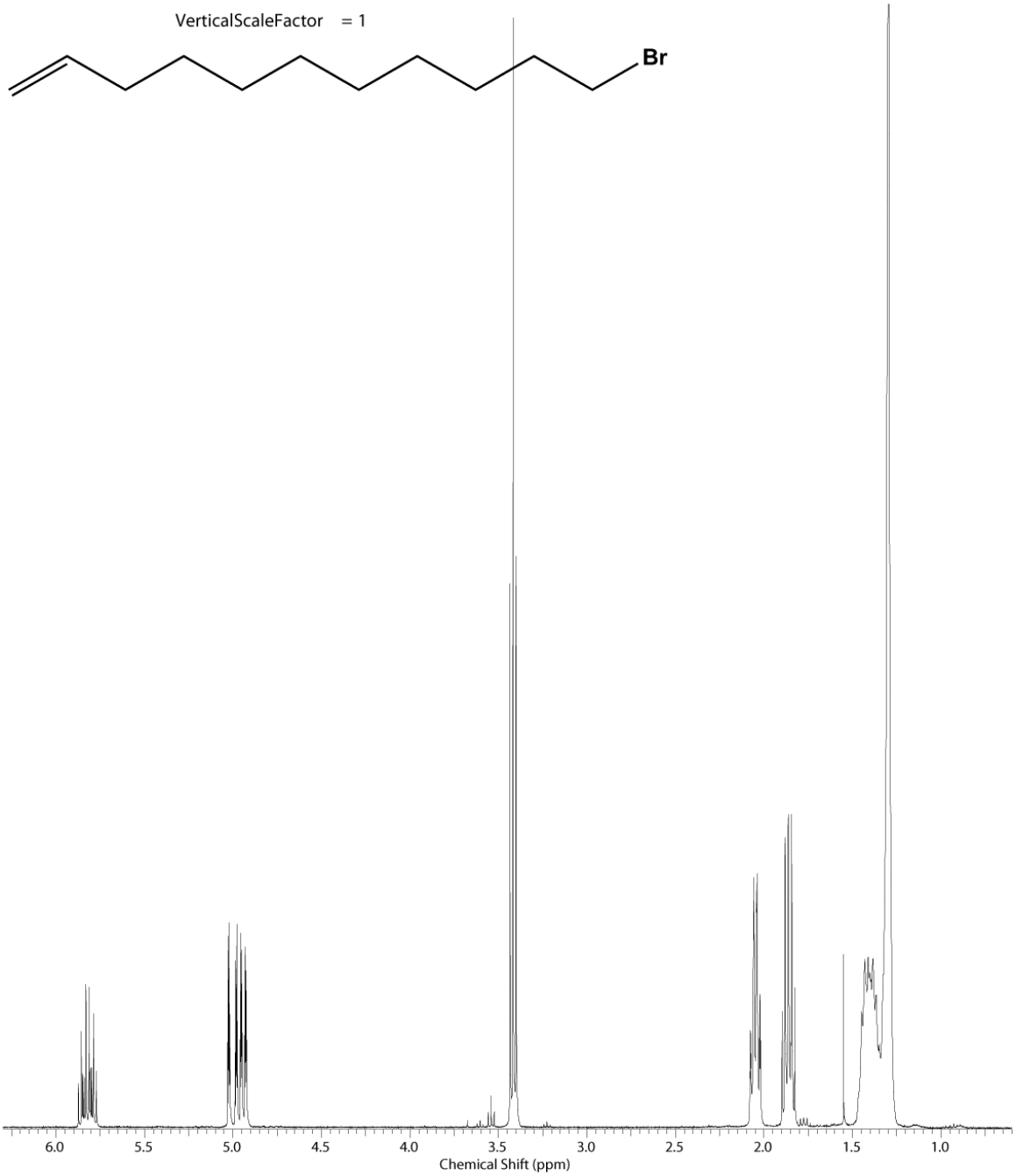

Figure A.3 - ^{1}H NMR of undec-1-en-11-yltri(ethylene glycol) in $CDCl_3$

Acquisition Time (sec)	3.7010	Comment	STANDARD 1H OBSERVE		
Date	Jan 12 2006	Date Stamp	Jan 12 2006		
File Name	C:\Documents and Settings\Leila Maurmann\Desktop\hoeman3				
Frequency (MHz)	399.78	Nucleus	1H	Number of Transients	16
Original Points Count	22208	Points Count	32768	Pulse Sequence	s2pul
Receiver Gain	48.00	Solvent	CHLOROFORM-d		
Spectrum Offset (Hz)	2007.3860	Sweep Width (Hz)	6000.60	Temperature (degree C)	29.000

VerticalScaleFactor = 1

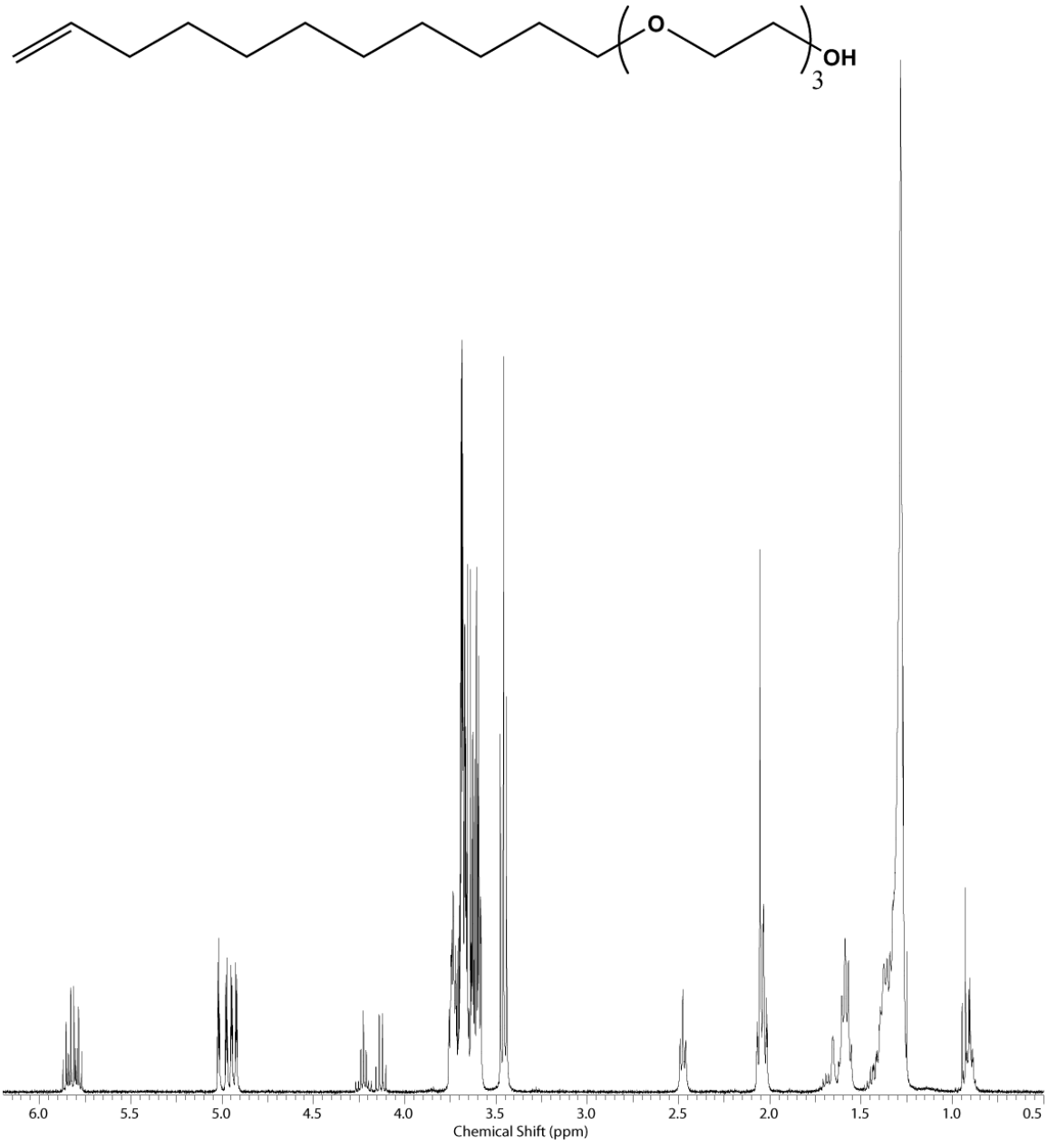

Figure A.4 - ^{1}H NMR of undec-1-en-11-yltri(ethylene glycol) in $CDCl_3$ after addition of D_2O

Acquisition Time (sec)	3.7010	Comment	STANDARD 1H OBSERVE		
Date	Jan 12 2006	Date Stamp	Jan 12 2006		
File Name	C:\Documents and Settings\Leila Maurmann\Desktop\hoeman3D2O				
Frequency (MHz)	399.78	Nucleus	1H	Number of Transients	16
Original Points Count	22208	Points Count	32768	Pulse Sequence	s2pul
Receiver Gain	48.00	Solvent	CHLOROFORM-d		
Spectrum Offset (Hz)	2007.3860	Sweep Width (Hz)	6000.60	Temperature (degree C)	29.000

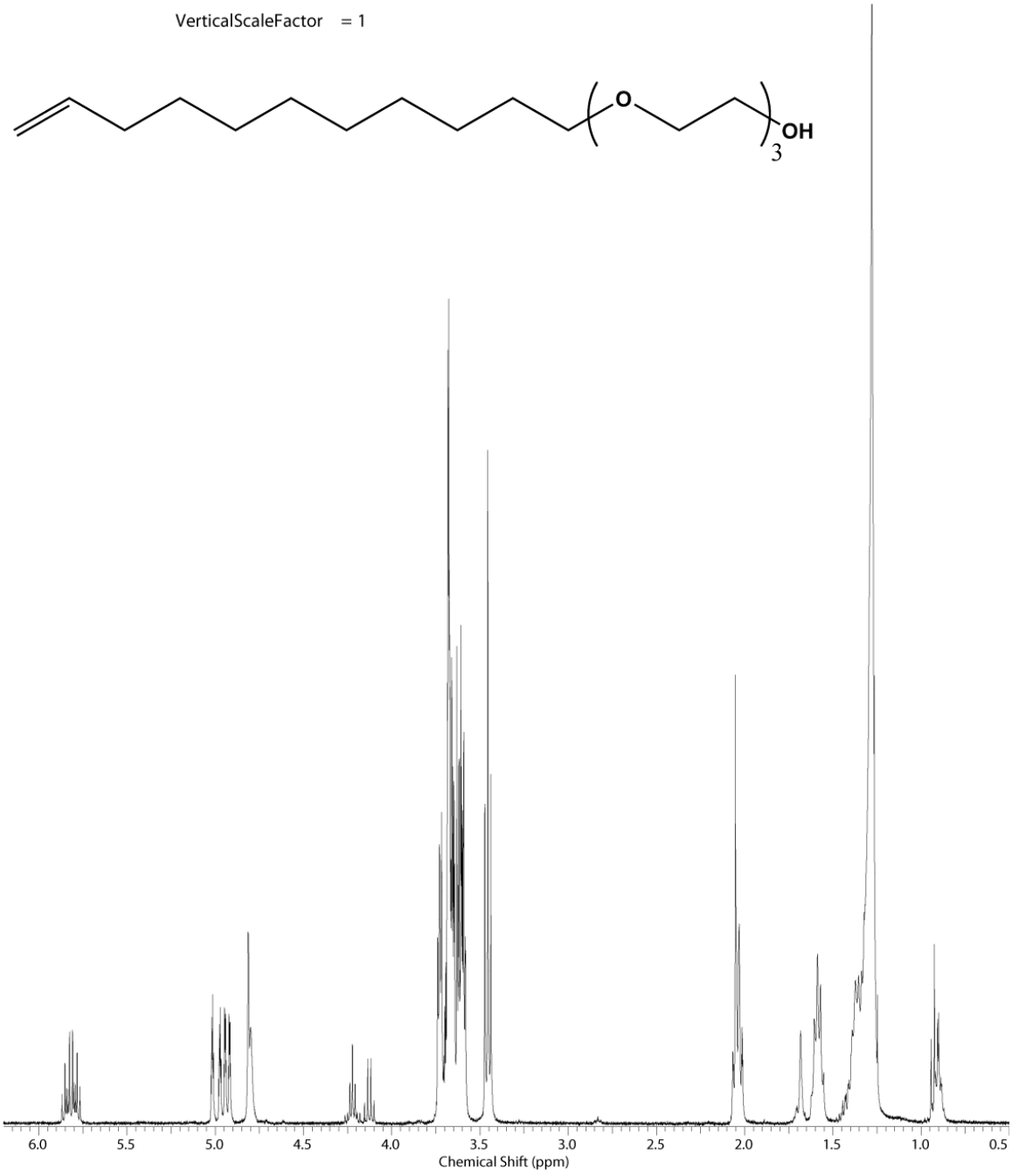

Figure A.5 - ^{1}H NMR of (1-mercaptoundec-11-yl)tri(ethylene glycol)

Acquisition Time (sec)	3.7010	Comment	STANDARD 1H OBSERVE		
Date	Feb 2 2006	Date Stamp	Feb 2 2006		
File Name	C:\Documents and Settings\Leila Maurmann\Desktop\hoemankh4-4				
Frequency (MHz)	399.78	Nucleus	1H	Number of Transients	32
Original Points Count	22208	Points Count	32768	Pulse Sequence	s2pul
Receiver Gain	50.00	Solvent	CHLOROFORM-d		
Spectrum Offset (Hz)	2007.7522	Sweep Width (Hz)	6000.60	Temperature (degree C)	29.000